THÈSE

Pour l'obtention du grade de
DOCTEUR DE L'UNIVERSITÉ DE POITIERS
UFR des sciences fondamentales et appliquées
Pôle poitevin de recherche pour l'ingénieur en mécanique, matériaux et énergétique - PPRIMME (Poitiers)
(Diplôme National - Arrêté du 25 mai 2016)

École doctorale : Sciences et ingénierie en matériaux, mécanique, énergétique et aéronautique - SIMMEA (Poitiers)
Secteur de recherche : Milieux denses, matériaux et composants

Présentée par :
Wei He

Mechanical and microstructural properties of thin metal films on compliant substrates

Directeur(s) de Thèse :
Philippe Goudeau, Eric Le Bourhis

Soutenue le 14 septembre 2016 devant le jury

Jury :

Président	**Vincent Ji**	Professeur des Universités, Université Paris-Sud 11
Rapporteur	**Lin-An Li**	Professor, Tianjin University, China
Rapporteur	**Damien Faurie**	Maître de conférences, Université Paris 13
Membre	**Philippe Goudeau**	Directeur de recherche CNRS, Poitiers
Membre	**Eric Le Bourhis**	Professeur des Universités, Université de Poitiers
Membre	**Pierre-Olivier Renault**	Professeur des Universités, Université de Poitiers

THÈSE

pour l'obtention du grade de

Docteur de l'Université de Poitiers

Faculté des Sciences Fondamentales et Appliquées

Diplôme National - Arrêté du 7 août 2006

École Doctorale : Sciences et Ingénierie
en Matériaux, Mécanique, Énergétique et Aéronautique

Domaine de Recherche : Milieux Denses, Matériaux et Composants

présentée par

Wei HE

Mechanical and Microstructural Properties of Thin Metal Films on Compliant Substrates

Directeurs de Thèse :

Ph. Goudeau, E. Le Bourhis et **P.-O. Renault**

Soutenance publique prévue le 14 September 2016

JURY

Lin-an Li	Professeur, Université de Tianjin, Chine	*Rapporteur*
Damien FAURIE	Maître de Conférences-HDR, Université Paris 13	*Rapporteur*
Vincent JI	Professeur, Université Paris-Sud 11	*Examinateur*
Philippe GOUDEAU	Directeur de Recherche CNRS	*Examinateur*
Eric LE BOURHIS	Professeur, Université de Poitiers	*Examinateur*
Pierre-Olivier RENAULT	Professeur, Université de Poitiers	*Examinateur*

ACKNOWLEDGMENTS

AS is well known, Ph.D. research is a long journey which often appears challenging and solitary. It is impossible for me to complete successfully without the support and encouragement of many people.

First and foremost, I would like to express my sincere acknowledgment of ***Philippe Goudeau*** for being my supervisor and mentor. He is not only my advisor but also my confidant who has given so much to help me succeed. I appreciate all his contributions of time, ideas and fundings to make me stimulating and creative. Certainly, I would also like to thank my co-advisors ***Eric Le Bourhis*** and ***Pierre-Olivier Renault*** for numerous highly beneficial discussions, such as X Ray Diffraction (XRD) and Digital Image Correlation (DIC). Their brilliant ideas and guidance provided me with the inspirations for theoretical and experimental work.

The research presented in this thesis was also supported by China Scholarship Council (CSC). The support of the sponsor is gratefully acknowledged.

Particularly, I am extremely grateful to professor ***Shibin Wang*** (Tianjin University, China) who provided me with constructive advice and kind encouragement. He is my master's thesis supervisor. It is with his recommendation, I become a Ph.D. candidate in Pprime Institute. I would also like to sincerely appreciate the group members who assist me enormously: professor ***Lin-an Li*** and ***Zhiyong Wang***.

For this dissertation I would like to greatly thank my jury members: ***Lin-an Li***, ***Damien Faurie*** and ***Vincent Ji*** for their time and interest. I'm looking forward to hear their insightful comments and suggestions.

This work would not have been possible without the support of members in Pprime Institute. Many thanks to ***Philippe Guérin***'s assistance for thin film de-

positions and ***Bruno Lamongie***'s valuable advice for the design of experimental systems. I am also very grateful to ***Patrick Tanguy***, ***Frédéric Gacioch***, ***Claude Veillon*** for putting their effort in fabricating all the stuff I need. I could hardly be successful without their professional skills. All the staff of this laboratory who assist me are appreciated too.

Especially, I have been very lucky to work with professor ***Jean-Christophe Dupré*** and ***Pascal Doumalin*** from Axis Photomechanics & Experimental Mechanics (PEM), Pprime Institute. They are so kind to give me the technical support of DIC measurements, such as the software "correla". With many discussions with them, we are confident about the measurements and some tricky problems have been solved. I am deeply indebted to both of them.

As long as I am writing names down, I can not neglect my good friends. ***Haikun Jia***, ***Meidong Han*** and ***Sami Hamade*** helped my numerical skills to flourish and thanks to their access to powerful workstation, the simulations are successful. Moreover, I would like to appreciate ***Firas Abed El Nabi*** and ***Tarik Sadat***. We have worked in the same office for more than 2 years. They are great guys who have provided me a lot of supports and beneficial discussions, such as skills of LaTeXand some tricky experiments. I would also like to acknowledge many other friends for their warm hearted help.

Last but not least, I would like to dedicate this work to my family: ***Haishui He*** and ***Meiqin Wu***. Without their love through my life, I would never have made it. They are always there helping me stay calm and serene even when things are tough. Thank you so much.

Wei He
Pprime Institute
July 2016

PREFACE

Thin film materials with thicknesses lower than one micron provoke great interest either for academic research: to better understand the size effect on physical properties and in particular the mechanical behavior of nanoscale materials, or for practical applications such as the stretchable devices.

Recently, flexible electronic devices play an increasing significant role in new applications which include paper-like electronic displays, electronic sensitive skins and solar cells. They have drawn more and more attention from academic and industrial points of view. As an elementary substructure among them, functional metallic thin films are often supported by a deformable polymer substrate. The lifetime of such systems is strongly dependent on their mechanical performance since they are submitted to complex thermo-mechanical loadings in use.

During their synthesis and fabrication, physical vapor deposition techniques, such as the ion sputtering, are used to bond adherent thin metal layers on different type of soft substrates thanks to the involved energetic particles in the deposition process. The obtained thin films can be dense, polycrystalline and often show in-plane compressive residual stresses up to several GPa. The grain size can be nanometric (less than 50 nm).

In such systems, residual stress is an important factor which affects the reliability and performance of advanced devices. These stresses may arise due to the presence of impurities or voids within the film, partial grain growth or thermo-mechanical differences between the film and the substrate. An excessive compressive or tensile stress can induce film buckling or cracks respectively leading to a loss of device functionality, or even the failure.

It is well known that the mechanical behavior of a metallic material depends not only on its residual stress state but also on its deformation history. In practical use, thin films are submitted to multiple strain cycles. This arises great interest to investigate the Bauschinger effect (related to tension/compression cycles) evidenced in bulk polycrystalline, where plastic deformation in one direction can affect subsequent plastic response in reverse direction. One consequence is the decrease of the yield strength when the direction of strain is changed. Furthermore, the microstructure and interface strength are also important contributing factors.

In order to study the mechanical properties of thin films, numerous techniques have been developed for twenty years thanks to the ingenuity of many research groups all over the word. Among them, the uniaxial tensile testing is the most direct method to get the typical stress-strain curves of freestanding thin films. However, when thin films are deposited on substrates, extracting their intrinsic properties will be a tricky task. On the other hand, it is uncomplicated to stretch thin films coated on a thin compliant substrate, while rather difficult to compress them due to the large lateral dimension/thickness ratio. Especially, to the best of our knowledge, no other groups have achieved to carry out a continuous uniaxial tensile/compressive test by applying positive and negative strains starting from the unloaded state.

It is these challenges that spur us to study the mechanical properties, especially the Young's modulus and the Bauschinger effect, of thin metal films on compliant substrates taking into account of their microstructures and interfacial adhesion. This dissertation is divided into four chapters:

I Chapter 1 is an introduction to thin film techniques and researches. The theoretical analyses and experimental methods to study the mechanical and microstructural properties of thin films are reviewed. In particular, the film-substrate interface and the Bauschinger effect are well described.

II Chapter 2 is devoted largely to the custom-design of various experimental setups including the specimen, grips, deposition masks *etc.*. Thin films are deposited on substrates in a special way, and the initial characterization of thin films are specified. Moreover, the main techniques, *i.e.* in situ tensile/compressive testing, DIC strain measurement, XRD strain/stress measurement, are introduced and discussed in detail.

III In Chapter 3, a new method is proposed to determine the in-plane elastic modulus of thin films. Based on the mechanical analysis of a model with films coated on both sides of a substrate along half of the gauge length, the Young's modulus can be obtained by measuring the strain difference between the films-substrate composite and the uncoated substrate simultaneously during the tensile testing. Numerical simulations (finite element method) are also performed.

IV Chapter 4 is dedicated to the cyclic deformation of thin films. Relying on the Deben MICROTEST tensile/compression stage, we propose a novel pre-stretching technique which allows stretching and compressing the as-deposited films on both sides of a Kapton® substrate. Thanks to the XRD stress/strain and DIC strain measurements at each step of the cyclic testing, the relationship between thin films' elastic stress/strain and true strain can be obtained within a relatively large applied strain domain, *i.e.* a positive or negative applied strain relative to the unloaded state. From these curves, the cyclic behavior and the Bauschinger effect are studied.

Subsequently, the general conclusions and perspectives are described with a French/English abstract at the end. It is hoped that this work could provide inspiration for other researchers and shed light on the Young's modulus determination and the Bauschinger effect study of thin metal films on soft substrates.

CONTENTS

1 CONTEXT OF STUDY

Contents

In general, a thin film is defined as a solid layer having thickness varying from fractions of a nanometer to several micrometers, although the definition could change depending on the physical properties of interest (Fewster 1996). Nanometer thin films are ubiquitous in numerous modern application fields, such as micro or nanoelectromechanical systems (MEMS/NEMS) and flexible electronics. It is imperative to study their mechanical properties and microstructures which are closely related to the performance, reliability and lifetime of those advanced devices. However, since the size of thin films is extremely small compared to their bulk counterparts at least in one dimension, dedicated characterization techniques are required. Some most common methods and the studies of thin films are described in this chapter.

1.1 THIN FILM TECHNIQUES AND APPLICATIONS

1.1.1 Background

As an emerging and promising field, flexible electronic has been developed for numerous applications including stretchable integrated circuits, thin film solar cells and deformable lighting systems (Crawford 2005; D.-H. Kim et al. 2010). It is aimed to bring about a revolution in design and implementation of electronics devices which will satisfy the various essential social needs and to create an amazing human life. In particular, some advanced technologies in optoelectronics, wearable health devices and paper-like displays are demonstrated as follows:

- Bio-inspired designs of digital imagers can achieve improved field of view, uniform illumination and higher precision compared to the conventional planer devices. Fig. 1.1(a) presents the magnified view of a hemispherical eye type camera: a curved focal array of silicon photodetectors (yellow pattern) for image capture is integrated with a printed circuit board (green) and a transparent hemispherical cap. The circuit is connected with a computer and the cap supports a planoconvex lens (Rogers, Someya, and Y. Huang 2010).
- It is necessary to monitor the state of human health in real time. Many sensors are integrated directly on the human body which requires them to be thin and flexible. Fig. 1.1(b) illustrates a stretchable wrist-based phototherapy device. It can follow the hand shape with a large deformation and high fatigue resistance. The blue LEDs are connected by stretchable meanders. Moreover, the complete sensor system is fitted into a textile wrap to enable easy fixation on the hand (Brand et al. 2015).

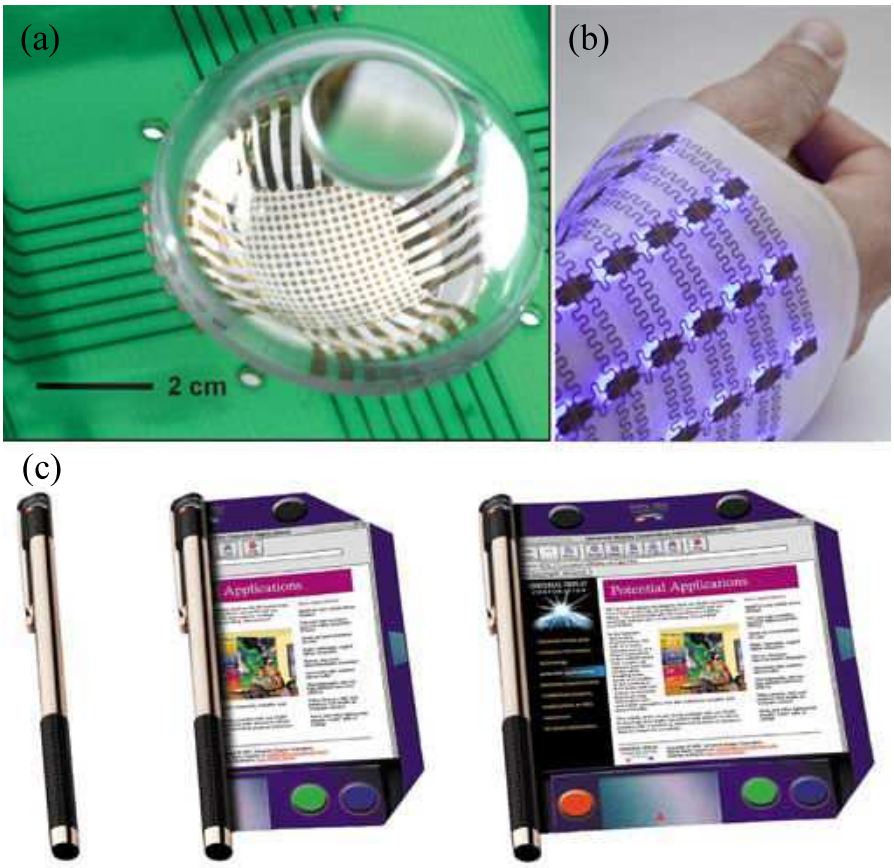

Figure 1.1: Flexible and stretchable electronics. (a) Electronic eyeball camera using a hemispherically curved array of silicon photodetectors. Reproduced from (Rogers, Someya, and Y. Huang 2010), copyright © American Association for the Advancement of Science. (b) A wrist-based phototherapy device made of the stretchable electronics which allows following the shape of the hand, Reproduced from (Brand et al. 2015), copyright © Elsevier Ltd. (c) A conceptual view of a future flexible smart display that can be rolled up into a pen-like device when not in use. Reproduced from (Forrest 2004), copyright © Nature Publishing Group.

- Flat-panel display has experienced an explosive development recently, and becomes immensely popular, such as iPad from Apple company. However, the displays are often made on glass substrates with a large screen which can cause problems of fragility and portability. Fig. 1.1(c) exhibits the conceptual view of a future smart display: the flexible screen with super processors inside that can be rolled up into a pen when not in use. You can easily access your data everywhere on the Internet (Forrest 2004).

Thin metallic films are ubiquitous in these attracting technologies serving as functional materials, such as electrodes and interconnects. In pursuit of being flexible and stretchable, thin films are usually deposited on compliant polymer substrates which allows undergoing large deformations (Lu, X. Wang, et al. 2007). Nonetheless, during the manufacturing and use, their reliability and maintainability will be strongly dependent on their mechanical properties which poses significant challenges, such as interfacial adhesion and ductility (Suo, J. J. Vlassak, and Wagner 2005). As shown in (D.-H Kim et al. 2008), diagonal stretching, twisting and bending of thin films can occur when the substrate is under free deformation. Furthermore, the elastic limit of thin metallic films, in many cases, is quite small ($< 1\%$), and cracks accompanied by delamination or buckling may appear early during stretching. It is well known that the intrinsic microstructure can also affect their mechanical behavior. In order to shed light on the development of flexible electronics and many other applications, further study of the mechanical properties and microstructures of thin films on soft substrates is imperative and necessary.

1.1.2 Thin film deposition processes

Thin film deposition allows to transfer material atom by atom from one or more sources to the growth surface of a film being deposited onto a substrate, and is usually divided into two broad categories: physical vapor deposition (PVD) and chemical vapor deposition (CVD) (Freund and Suresh 2004). One of the most common techniques of PVD is sputtering.

Sputtering involves the bombardment of a target material that is to be deposited on a substrate. The substrates are placed in a vacuum chamber containing an inert gas, usually argon, at a negative electric potential faced to the target material. Atoms are "Sputtered off" the target by collisions with the accelerated Ar gas atoms in the imposed electric field, carrying these particles across the vacuum chamber which are deposited as a thin film. Several different methods of sputtering are widely used, including magnetron sputtering and ion beam sputtering.

1.1.2.1 *Magnetron sputtering*

Magnetron sputtering uses magnets to trap electrons over the negatively charged target material so they are not free to bombard the substrate, preventing the object to be coated from overheating or being damaged, and allowing for a faster thin film deposition rate. Excellent layer uniformity and smooth sputtered coatings can be obtained. Recent developments and applications can be seen in a review of Kelly and Amell (Kelly and Arnell 2000).

1.1.2.2 *Ion beam sputtering*

Ion-beam sputtering consists in bombardment of a given target with high energy ion beams, and subsequent deposition of sputtered material on the substrate. Films obtained by ion-beam sputtering have high density and low roughness. One distinguishing advantage is the stable state of coatings during

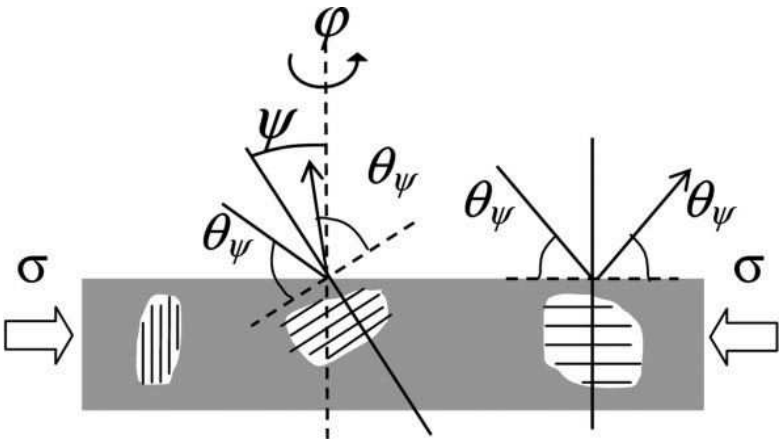

Figure 1.2: Concept of diffraction stress/strain analysis. When a polycrystal is subjected to a uniaxial compression parallel to the surface, the lattice spacing of {hkl} planes varies depending on their orientations with respect to the loading direction. This lattice strain can be measured by X-ray diffraction and its direction, i.e. the direction of the diffraction vector, is identified by the angles φ and ψ , where φ is the rotation angle of the specimen about the surface normal and ψ is the angle between the normal to the diffraction planes and the surface normal. Reproduced from (Welzel et al. 2005), copyright © International Union of Crystallography

exposure to atmospheric and various climatic conditions, which is one of the most crucial requirements of modern optical and functional coatings.

1.2 MICROSTRUCTURE AND MECHANICS

1.2.1 X-ray diffraction (XRD)

X-ray diffraction is a phase selective, non-contact and non-destructive method that allows determining the stress/strain data of thin metal films. When a polycrystalline thin film is irradiated with X-rays, the diffraction angle $2\vartheta_{hkl}$, at which the maximum or centroid diffracted intensity is determined, can be measured for each (hkl) diffraction planes. Due to the presence of stress, the

interplanar spacing d_{hkl} of the lattice planes {hkl} depends on the orientations of constituent crystallites with respect to the specimen frame of reference. For instance, if a polycrystalline material is subjected to a compressive stress parallel to the surface, as shown in Fig. 1.2, {hkl} planes parallel to the surface are extended, while planes normal to the surface are compressed (Welzel et al. 2005).

Thanks to the Bragg's law: $\lambda = 2d_{hkl}\sin\vartheta_{hkl}$, the spacing is obtained with the diffraction angle and X-ray wavelength λ. The principle of strain/stress measurement is to take the lattice spacing as a strain gauge:

$$\varepsilon_{hkl} = (d - d_0)_{hkl}/(d_0)_{hkl} \tag{1.1}$$

where $(d_0)_{hkl}$ is the stress-free spacing. The strain can be considered as uniform on the macroscopic scale, producing a shift of the diffraction peak, while the non-uniform microstrain due to the lattice distortion can cause a broadening of the diffraction peak. It is well known that the spacing difference at various elastic deformation state is proportional to the stress acting on the planes. After elasticity analysis, the residual or applied stresses can be determined (I. Noyan and Cohen 1987). Moreover, the microstructural characteristics such as crystallographic structure, texture and grain size can be also well scrutinized by X-ray diffraction.

1.2.2 Fiber texture and elastic anisotropy

FIBER TEXTURE Most thin films are polycrystalline materials constituted of numerous single crystals with different sizes and shapes. The distribution of crystal orientations with respect to the specimen system is an important parameter which can affect thin films' behavior. The materials are quasiisotropic or textured depending on the crystallographic orientations, i.e. randomly or

Table 1.1: Zener ratio $A = 2(s_{11} - s_{12})/s_{44}$ calculated from the single crystal elastic constants s_{ij} given in (Simmons and H. Wang 1971) at room temperature. The unit of Young's modulus E is GPa.

Materials	Cr	Mo	W	Al	Ni	Au	Ag	Cu
Zener ratio	0.71	0.71	1.01	1.22	2.58	2.86	3.01	3.21
E<111>	250	283	411	76	300	117	120	191
E<100>	328	381	408	63	130	43	44	67

preferably distributed (Hauk 1997). As a special case, the orientation distribution is independent of a rotation about one axis, and the pole figure is axially symmetric. Texture of this type is called fiber texture (Kocks, Tomé, and Wenk 2000), which is very common in sputtered thin films. It is noteworthy that face-centered cubic (fcc) and body-centered cubic (bcc) materials often have {111} and {110} fiber texture respectively. Fig. 1.3 shows pole figures obtained by XRD measurements which demonstrates a typical {111} fiber texture (Faurie, Renault, Le Bourhis, Chauveau, et al. 2011).

ELASTIC ANISOTROPY For a polycrystalline thin metal film (cubic system), the constituent crystallites usually show an anisotropic property which can be quantified by Zener ratio (Table 1.1).

The material is locally perfectly isotropic when the zener ratio equals to 1, such as W. If it is larger than 1, the Young's modulus in the <111> directions is larger than in <100>, while inverse situation appears when smaller than 1. The expression of Young's modulus in <hkl> directions is as follows:

$$\frac{1}{E<hkl>} = s_{11} - 2(s_{11} - s_{12} - \frac{1}{2}s_{44})\frac{h^2k^2 + k^2l^2 + h^2l^2}{(h^2 + k^2 + l^2)^2} \tag{1.2}$$

where s_{ij} is the compliance matrix of a single crystal. Obviously, when $A = 1$, the elastic modulus is a constant, and thus independent of directions as expected.

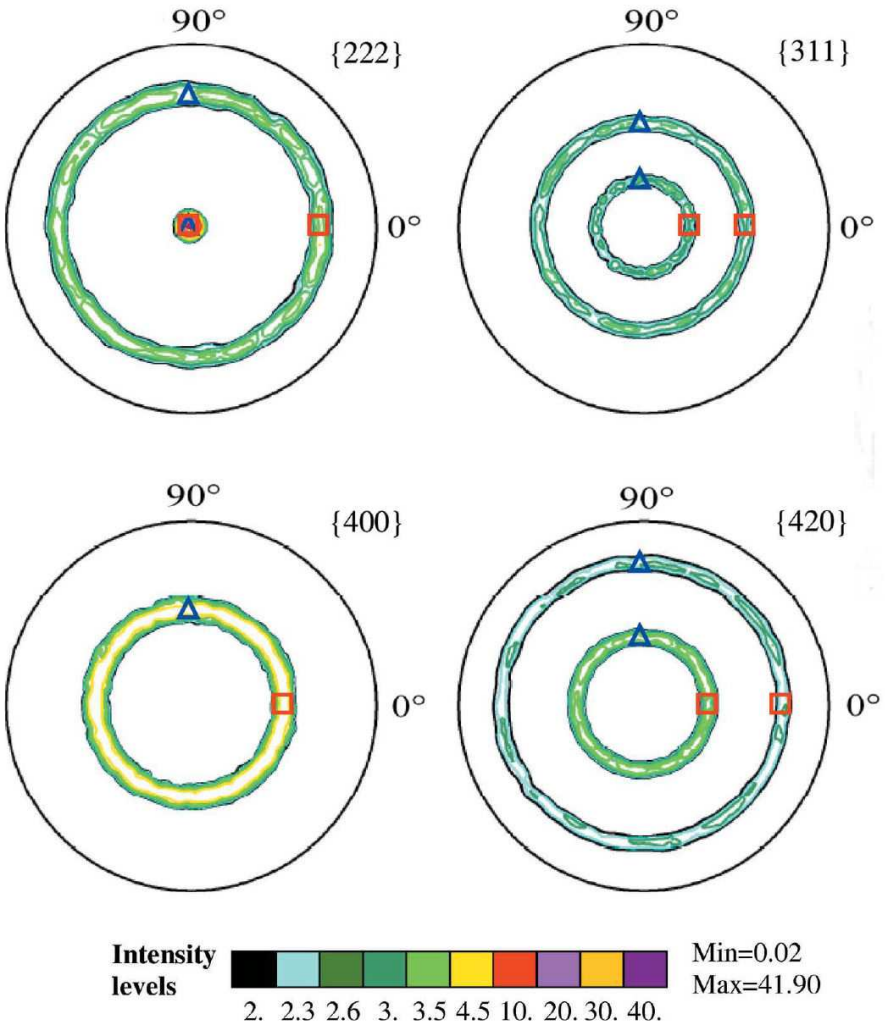

Figure 1.3: X-ray pole figures for the {222}, {311}, {400} and {420} plane families of the fcc gold film. The central peak of the {222} pole figure and the measured rings represent a typical {111} fiber texture. Reproduced from (Faurie, Renault, Le Bourhis, Chauveau, et al. 2011), copyright © International Union of Crystallography

Furthermore, the macroscopic elastic anisotropy depends not only on local anisotropy but also on the orientations of individual crystallites. If there is a random distribution of lattice directions, the thin films are quasiisotropic no matter what the local anisotropy. While, as previously mentioned, a thin metallic film usually exhibit a fiber texture with statistically uniform orientation distributions around the normal to the film surface. This can be considered as a hexagonal system or in-plane transversally isotropic, and the Young's modulus in <hkl> directions is:

$$\frac{1}{E<hkl>} = \left(\frac{h^2+k^2}{h^2+k^2+l^2}\right)^2 s^s_{11} + \left(\frac{l^2}{h^2+k^2+l^2}\right)^2 s^s_{33} + \frac{\left(h^2+k^2\right)l^2}{\left(h^2+k^2+l^2\right)^2}\left(2s^s_{13}+s^s_{44}\right) \tag{1.3}$$

Where s^s_{ij} is the macroscopic elastic compliance of thin films (specimen system). Apparently, the Young's modulus does not vary in the in-plane directions ($l = 0$).

1.3 MECHANICAL PROPERTIES AND RESEARCH APPROACHES OF THIN FILMS

1.3.1 Residual stresses

Residual stresses are almost always present in thin films deposited on substrates. From the definition "the self-equilibrating internal stresses existing in a free body at equilibrium with no externally imposed surface tractions", one should notice that residual stresses must be equilibrated and intrinsic to

the same body (I. Noyan, T. Huang, and York 1995). Residual stresses often arise during the deposition process due to the thermal expansion mismatch, defect incorporation, partial grain growth, etc., and can significantly affect the mechanical behavior and performance of film-substrate composites. For instance, the excessive compressive or tensile residual stresses can induce film buckling or cracks respectively (Freund and Suresh 2004). Consequently, it is imperative to develop the evaluation techniques, and they can be classified into non-destructive and destructive or semi-destructive methods.

1.3.1.1 *Non-destructive techniques*

CURVATURE METHOD (STONEY'S FORMULA) Thin films deposited on a flat substrate can lead to a curvature of the substrate related to the residual stresses. In 1909, Stoney (Stoney 1909) firstly derived an expression for the curvature of a steel strip caused by the stresses in a metallic coating, which is known as Stoney's formula. This equation is based on several assumptions, and has been extended and widely used for predicting stresses in a thin film from the curvature of the substrate, such as the extended Stoney's equation for thin substrate and the one in the case of spatially non-uniform curvature (Chou, S.-Y. Yang, and Chiang 2011). After assuming both film and substrate are elastically linear and isotropic, much smaller film thickness than the substrate thickness, equal-biaxial stress state, etc., the most basic Stoney's formula can be written as follows:

$$\sigma_f = \frac{E_s}{1-\nu_s}\frac{h_s^2}{6h_f}\left(\frac{1}{R_f}-\frac{1}{R_i}\right) \tag{1.4}$$

where $E_s/(1-\nu_s)$ is the biaxial modulus of the substrate, h_s and h_f are the thickness of substrate and film respectively, R_i and R_f the curvature radii before and after film deposition. However, in the majority of curvature methods, single crystalline Si wafers are used as the substrate. In this case, Si is elastically anisotropic, and a modified form of Stoney's formula may be used (Janssen et al. 2009).

It is important to note that if the substrate is relatively compliant and the film is highly deformed beyond the elastically linear range, the Stoney's formula is not directly applicable. For example, when a thin metal film is deposited on a polyimide substrate experiencing high compressive stresses, the common spherical shape would be transformed into a cylindrical shape, which is known as curvature bifurcation (C. Kim et al. 2015).

$Sin^2\psi$ METHOD (XRD) XRD technique uses the interplanar lattice spacing as an "atomic strain gauge" to measure strains; the residual elastic strains are determined as the relative change of this spacing with respect to the unstrained reference value. This allows the residual stress state to be readily calculated using the appropriate form of Hooke's law depending on the elastic properties (macroscopic isotropy or anisotropy) of thin films (Culity 1978; Hauk 1997; I. Noyan and Cohen 1987). The concrete process can be seen in Section 2.5.3. However, the calculated mechanical elastic constants should be carefully taken into consideration, since they are strongly dependent on the type and sharpness of texture, the number of randomly oriented crystallites in the polycrystalline aggregate and the assumed grain interaction model (Martinschitz et al. 2009; Faurie, Castelnau, et al. 2009; Clemens and Bain 1992).

1.3.1.2 *Destructive or semi-destructive methods*

There are many residual stress evaluation approaches involving material removal or machining (Krottenthaler et al. 2013; Sebastiani et al. 2011; Korsunsky, Sebastiani, and Bemporad 2009). All of these methods rely on the same principle: when new traction-free surfaces are created within the sample, a redistribution and re-equilibration of strains can be measured to obtain the pre-existing residual stress state in terms of a finite element (FE) or analytical model (Bemporad et al. 2014). For instance, as can be seen in Fig. 1.4 (Bemporad et al. 2014), an annular trench of 3 μm inner diameter was incrementally

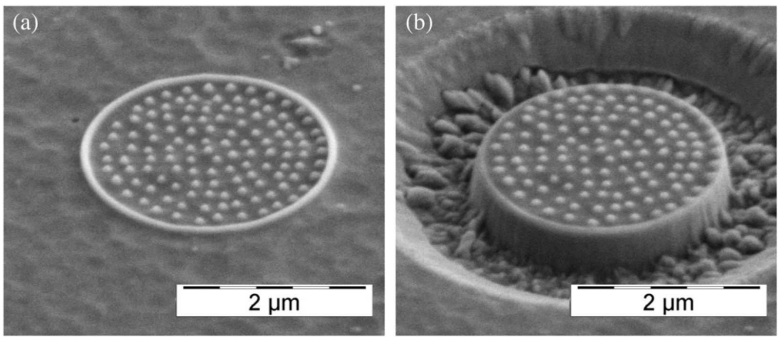

Figure 1.4: SEM images of the patterned area acquired before and after milling. The strain relief can be measured by means of DIC. Reproduced from (Bemporad et al. 2014), copyright © Elsevier B.V.

milled by focused ion beam (FIB) around the Pt-coated region (the central pillar with a patterned surface), and a sequence of scanning electron microscope (SEM) micrographs of the patterned area were acquired before and after each milling step. The average stress in the pillar volume can be calculated from the elastic modulus and Poisson's ratio by knowing the average strain at the maximum depth thanks to the digital image correlation (DIC) strain measurements. It is interesting to note that a significant stress gradient through the coating thickness can also be characterized.

1.3.2 Adhesion and characterization techniques of mechanical behavior

1.3.2.1 *Adhesion and stress/strain transfer*

When a thin film is deposited on a substrate, the interfacial adhesion, defined in terms of fracture mechanics as the minimum energy per unit area required to create new surfaces, becomes a key feature which can significantly affect the mechanical behavior of the film, and then the functionality and durability of advanced devices. For instance, well-bonded Cu films can sustain tensile strains up to 10% without appreciable cracks, while poor-bonded ones form

channel cracks at strains about 2% (Xiang, Li, et al. 2005). For a thin metal film on a polymer substrate, three types of tensile behavior can exist depending on the resistance of the interface to sliding (Li and Suo 2007). Therefore, it is important to measure the adhesion between thin films and substrates. Many methods have been developed, such as the indentation (Gerberich and Cordill 2006; J. Chen and Bull 2007), scratch test, the peel test and the time-of-flight secondary ion mass spectroscopy (Chapman 1974; Leterrier 2003). It is worth mentioning that the regular and parallel straight cracks are indicative of a good adhesion (Mittal 1976). In attempt to improve the adhesion of thin metallic films, an intermediate layer (Cr, Ti, etc.) is often used and a new energy balance model was proposed to determine the adhesion energy of Cr films on polyimide substrates by measuring the buckling geometry induced by the fragmentation test (Cordill et al. 2010). Furthermore, the influence of the brittle Cr interlayer on the deformation behavior of thin films was experimentally and numerically investigated (Marx, Toth, et al. 2015).

In many cases, the stress/strain of a thin film is only transfered from the substrate through the interface, since there is no direct force exerting on the film. It is often assumed that the interface is perfect and the deformation is continuous through the film-substrate interface, in other words, the strain of the film is indistinguishable compared to the strain of the substrate. This assumption is vital since it is the basis of many mechanical theories and methods, such as the rule of mixture (M. et al. 2016; Kirsch et al. 2005). Some insightful experiments have been done in an effort to clarify this hypothesis. Thanks to the X-ray diffraction and other strain measurement methods, a complete strain transfer through the film-substrate interface is observed in the elastic domain (Geandier et al. 2010; Hommel, Kraft, and Arzt 1999; Djaziri et al. 2014). However, it is not always true. In the case of a thin Ni/polyimide (PI)/Cu multilayer studied by X-ray tensile testing, it is concluded that only part of the elastic strain in the Ni is transferred to the Cu, and the PI has no effect on the

elastic stress transfer behavior (Schadler and I. C. Noyan 1991; Schadler and I. Noyan 1992). Furthermore, a general elastic solution for multi-layered materials is derived to predict the stress transfer through fully bonded interface (Yin and Prieto-Muñoz 2013).

For the stress transfer analysis, it is worth mentioning the well-known shear lag model. Considering a thin film coated on a strained substrate shown in Fig. 1.5, the ends of the film are not directly pulled in tension, *i.e.* free surfaces. Consequently, any stress the film experiences can only be transferred across the adhering interface. This implies the existence of an interfacial shear stress that accumulates from the ends of the film inward to cause an uniaxial tension, and the tensile stress in the film must be built from zero at the ends to an equilibrium value towards the middle (Wojciechowski and Mendolia 1991). When the applied load grows and the film stress near the center exceeds a critical value, a crack will appear and new free surfaces are introduced. The film is then split into two segments with smaller length. This causes a stress relief in the film. When the load keeps increasing, new cracks will occur midway in the same manner. As this process continues much further, the length of each new segments becomes tiny and the shear stresses at both ends of the segments begin to overlap which results in their partial balance, or in other words, the magnitude of the loading transferred across the shear lag region falls below the critical value, thereby limiting further crack generation which is known as the crack saturation. Moreover, a modification to the shear lag model is proposed to take into account the residual strains (Yanaka et al. 1998). It should be noted that even with numerous cracks, all the segments of the film are assumed to be adherent to the substrate everywhere. However, the substrate strain in the zone of the crack gaps is larger compared to the continuous composite, since only the substrate experience the load in the uncoated region.

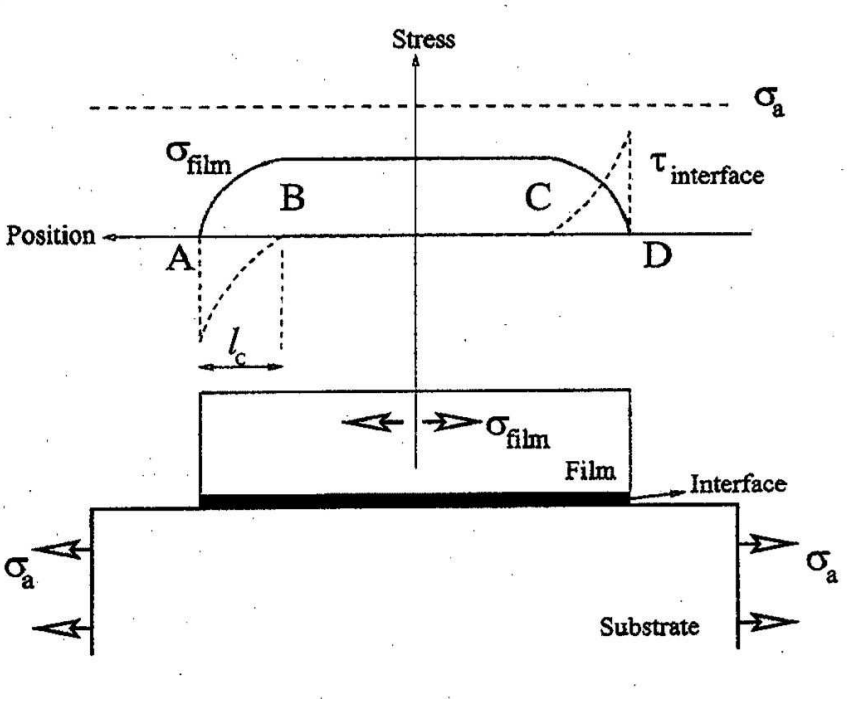

Figure 1.5: Schematic of the shear lag model: the film undergoes strain as a result of the substrate induced stresses that are transferred across the interface. The shear stress in the interface reaches a maximum at the ends of the film and zero closing to the center. From equilibrium, the tensile stress in the film, which is zero near the edges and increases to a maximum towards the center, can be determined from the accumulation (integration) of interfacial shear stress. Reproduced from (Jordan-Sweet et al. 2000), copyright © JCPDS

In summary, the interfacial adhesion is extremely important for the study of thin films' mechanical behavior and needs to be carefully taken into account.

1.3.2.2 *Mechanical characterization*

It is well known that many materials in thin film form can behave differently from their bulk counterparts (Eiper et al. 2007; Arzt et al. 2001). The mechanical characteristics of these varied materials are often influenced by fabrication and post-processing conditions such as deposition pressure (Freund and Suresh 2004), substrate temperature (Balakrishnan et al. 2013), and thermal annealing. Mechanical properties also depend strongly on the particular microstructure (grain size, texture and defects) (Faurie, Renault, Le Bourhis, and P. Goudeau 2006), and size effects (Lu, Suo, and J. J. Vlassak 2010; Misra, Hirth, and Hoagland 2005; Villain et al. 2004). As stated in (Cho et al. 2005), the tensile strain is as large as 2.2% for a MEMS-scale polycrystalline silicon, while macro-scale brittle materials typically reach 0.1-0.2% failure strains. In addition, some materials, for instance, obtained by means of PVD technology, do not exist in the bulk state. Consequently, although bulk properties provide valuable indications, it is necessary to characterize the mechanical properties of thin films which is vital from both industrial and academic viewpoints.

Unfortunately, most of the traditional and standardized techniques for bulk materials cannot be applied directly to thin films due to the small size and the fact that many thin films are supported by substrates. In order to scrutinize the mechanical behaviors of thin films or multi-layers, several specialized techniques were developed. For thin film/substrate composite, combined XRD and in situ tensile testing (Faurie, Renault, Le Bourhis, and Ph. Goudeau 2005; Böhm et al. 2004), nanoindentation (Oliver and Pharr 2004; Faurie, Djemia, et al. 2010), temperature-dependent substrate curvature (Eiper et al. 2007; Schmidt et al. 2004) are among the most common and suitable methods. Thanks to the support of substrates, they do not require complex

sample preparation. Nonetheless, all of these techniques have their own restrictions (Kraft and Volkert 2001). For instance, ordinary XRD measurements are time-consuming and the sample alignments in tensile testing is always a tricky task. In the nanoindentation method, the influence of the substrate can be non-negligible. In the case of measuring the mechanical behavior of freestanding thin films, plane-strain bulge test (J. J. Vlassak and Nix 1992; Xiang, X. Chen, and J. J. Vlassak 2005) and microtensile testing based on MEMS-type devices (Mompiou, Legros, Boé, et al. 2013; Chasiotis 2004) were well established. They can provide information in both elastic and plastic regimes, such as Young's modulus and dislocation interactions. However, sophisticated setup and extensive sample preparation are required which usually involves lithography and etching.

In order to study the surface morphology (*e.g.* cracks and buckling) and the intrinsic microstructure (*e.g.* grain size and grain structure) of thin films, in-situ microscopy techniques, such as transmission electron microscopy (TEM), scanning electron microscope (SEM) and atomic force microscope (AFM) were widely used (Mompiou, Legros, Radetic, et al. 2012; Akogwu et al. 2010). Furthermore, an in situ electrical resistance measurement can be applied to determine the failure strain (Lu, Suo, and J. J. Vlassak 2010). On the other hand, since thin films are often subject to repeated loads in practical applications, it is necessary to investigate their fatigue behavior. Wang *et al.* (D. Wang et al. 2014) studied the influences of Ta passivation layers on the fatigue life of thin Cu films on polyimide substrates using cyclic tensile testing, and the high cycle fatigue tests were periodically interrupted to address the damage evolution with SEM and focused ion beam (FIB). Several other fatigue testing methods are summarized in (Zhang et al. 2007), where a more complicated case, coupled mechanical and thermal loading, was considered.

As previously mentioned, numerous studies based on microtensile testing have addressed the mechanical behavior of thin film/substrate composite. In

an attempt to obtain the thin film's intrinsic mechanical behavior, one can subtract the substrate's contribution from the overall measurement which is known as the rule of mixture (Macionczyk et al. 1998; Denis and Spaepen 2004; Choi and Lee 2010). Chen *et al.* (X. Chen et al. 2009) examined its validity for different sample geometries and loading configurations. The 1-D approach is a great and simple way to extract the elastic characteristics, however, several factors should be considered, such as the strain transfer through interface and the effects of films' microstructure. Additionally, accurate and precise strain measurement is necessary in a small elastic regime. This can be achieved by an immensely popular optical technique, digital image correlation, to obtain full-field strain (Gianola and Eberl 2009; Hild and Roux 2006; Besnard, Hild, and Roux 2006). Meanwhile, lateral strain can be measured to get Poisson's ratio of the substrate. It is also non-destructive without any special environmental requirements which is imperative for thin films.

1.3.3 Bauschinger effect (BE)

The mechanical behavior of a metallic material depends not only on its residual stress state but also on its deformation history. The plastic deformation in one direction can affect subsequent plastic response in the reverse direction. One consequence is the decrease of the yield strength of a metal when the direction of strain is changed. This specific mechanical response evidenced in bulk polycrystalline materials is known as the Bauschinger effect (Bauschinger 1881).

Fig. 1.6 schematically shows this effect on a typical stress-strain curve. The stress σ_y is the yield stress, σ_f the forward flow stress and σ_r corresponding to the yield stress on the reverse loading. The material is firstly loaded in tension and yields at point A. After stretching to point B, the loading direction

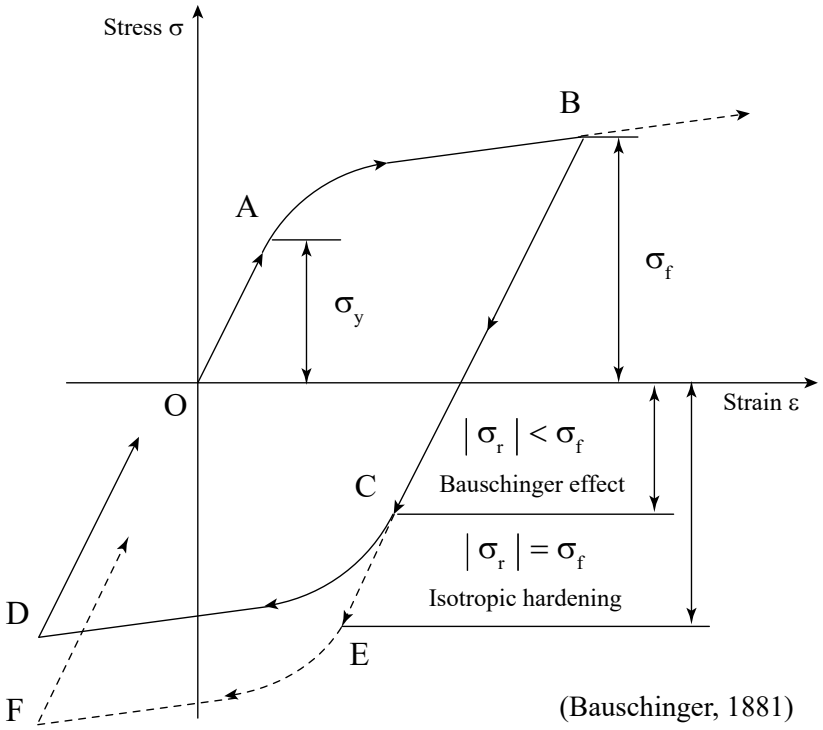

Figure 1.6: Schematic illustration of the Bauschinger effect existing in many metallic materials with coarse grains.

is reversed. Unloading occurs along the elastic line until yielding. If there is no directionality effect, *i.e.* isotropic hardening, the material will start flowing plastically at a stress equal to σ_f (point E), then reload along a linear line starting from point F. The idealized curve is shown in dashed lines (the sequence O-A-B-E-F). However, the material exhibiting the Bauschinger effect will have a lower reverse yield stress ($\sigma_r < \sigma_f$), and the loading path follows O-A-B-C-D. It should be noted that the loss of the reverse yield stress may be equal to the growth of the forward yield stress ($|\sigma_r| + \sigma_f = 2\sigma_y$), which is referred to as the kinematic hardening. The Bauschinger effect is generally ascribed to either short-range effects or to long-range effects which assist inhomogeneous plastic deformation in the reverse direction (Davoudi, Nicola, and J. J. Vlassak 2014). It is then important to verify whether this effect appears also in thin metallic films since these systems are subject to multiple strain cycles, and the loss of strength in the reverse direction may cause serious failure. Moreover, the nanometric length scale in such systems could influence their plastic responses.

It is straightforward to scrutinize the Bauschinger effect using cyclic testing in tension and in compression, which has been well established for bulk materials. However, this is much more difficult for both freestanding thin films and film-substrate composites. Taking a thin composite as an example, the compressive stress will be challenging to apply in a relatively large strain regime, since the tiny thickness/lateral dimension ratio can lead to a specimen curvature, and to obtain the intrinsic stress-strain curves of thin films in such a strain range is even more tricky.

Although there are many experimental techniques, as mentioned above, on the plasticity of thin metal films, only a very few were successfully exploited to address the Bauschinger effect. Based on the substrate curvature method, Baker *et al.* (Baker, Keller-Flaig, and Shu 2003) studied the thermomechanical behavior of passivated thin Cu films on Si substrates. In this technique, the changes in substrate curvature during thermal cycles with varying tempera-

ture endpoints were used to calculate the film stresses. When small amounts of oxygen were added to a Cu film in the deposition process, a Bauschinger-like effect was observed. Nevertheless, it is difficult to interpret due to the change of temperature. Xiang and Vlassak (Xiang and J. Vlassak 2005) reported the direct experimental evidence of a strong Bauschinger effect in thin metal films under isothermal condition. They developed a new technique to measure the cyclic stress-strain curve based on the plane-strain bulge test method. It is concluded that passivated films exhibit a significant Bauschinger effect even when the applied stress is still in tension, while unpassivated or freestanding films show little or no reverse flows. This was explained as follows: for the film-passivation composites, a boundary layer with high dislocation density forms at the interface causing a high back stress which facilitates the earlier reverse plastic flow; for a freestanding film, many dislocations can exit the film because of the free surfaces, and no back stresses are generated. Since the interface is an obstacle to the motion of dislocations, it is believed to introduce a plastic strain gradient nearby. Strain-gradient plasticity theory was successfully used to describe the effects of film thickness on the plasticity of passivated Cu films, but failed to describe the Bauschinger effect (Xiang and J. J. Vlassak 2006). It is interesting to point out that Brugger et al. (Brugger et al. 2010) presented a two-dimensional (2D) strain gradient plasticity finite-element model involving grain boundaries which agrees well with the experimental results obtained by Xiang and Vlassak (Xiang and J. J. Vlassak 2006). Unfortunately, the Bauschinger effect was not taken into account.

To the best of our knowledge, only Xiang and Vlassak (Xiang and J. Vlassak 2005; Xiang and J. J. Vlassak 2006) experimentally investigated the Bauschinger effect in passivated thin films. Some theories and simulations were proposed to describe this experimental phenomenon. A three-dimensional (3D) dislocation dynamics simulation was used by Zhou and LeSar (Zhou and LeSar 2012). They found in an excellent agreement that the passivated films exhibit

a significant Bauschinger effect, and either an increased prestrain or a smaller film aspect ratio can promote a stronger Bauschinger effect. Their analysis shows that the reverse motion of dislocation pile-ups and the collapse of misfit dislocations are responsible for this effect. However, recent experiments by Rajagopalan *et al.* (Rajagopalan, Rentenberger, et al. 2010; Rajagopalan, Han, and Saif 2008) have shown that the substantial Bauschinger effect also exists in unpassivated thin metal films. It should be noted that the films tested by Xiang and Vlassak (Xiang and J. Vlassak 2005; Xiang and J. J. Vlassak 2006) and Rajagopalan *et al.* (Rajagopalan, Rentenberger, et al. 2010; Rajagopalan, Han, and Saif 2008) are different in terms of material, film thickness, microstructural size and heterogeneity. For instance, in the former case, the average grain size is 0.3-1.5 μm and the Cu film thickness is 0.3-4.2 μm, whereas in the latter case, the mean grain size is 70-140 nm of 150-250 nm thick Al films. They demonstrated that in microstructurally heterogeneous (non-epitaxial growth with a wide distribution of grain sizes) films, dislocation activities are confined to relatively larger grains with smaller grains deforming elastically. This microplasticity leads to the build-up of internal stresses and then the BE. By contrast, the microstructurally homogeneous (epitaxial growth with a limited distribution of grain sizes) films show minimal BE. In order to compare with their experimental data and to investigate the mechanism stated above, a two-dimensional discrete dislocation plasticity simulation was carried out by Shishvan *et al.* (Shishvan, Nicola, and Van der Giessen 2010). In their simulations, the BE can originate from different mechanisms, such as grain orientations and disperse grain sizes. It is the stress inhomogeneity caused by these mechanisms that gives rise to the BE in freestanding thin films. In addition, some other numerical models (Guruprasad, Carter, and Benzerga 2008; Liu et al. 2011; Davoudi, Nicola, and J. J. Vlassak 2014) may also shed light on the Bauschinger and size effects in thin films.

1.4 STRATEGY

From the above literature review, we decided to address two major subjects in this thesis:

- Determination of thin films' Young's modulus based on uniaxial tensile testing and digital image correlation (DIC) strain measurements.
- Study of Bauschinger effect in ductile metal films under uniaxial tensile/-compressive testing. Pre-stretching technique combining XRD stress/strain measurements with DIC strain measurements are applied.

ELASTIC MODULUS DETERMINATION If thin films are deposited on both sides of a substrate along half of the gauge length, based on our mechanical analysis, the macroscopic strain difference between coated and uncoated section will allow extracting the elastic constants of thin films with high precision. Accordingly, we will develop a dual digital image correlation (DIC) system to measure the time-resolved strain of film-substrate composite and virgin substrate simultaneously during a tensile testing. The feasibility will be demonstrated in some thin metallic films and finite element method (FEM) will be performed to compare with the theoretical analysis and experimental determination.

EXPERIMENTAL STUDY OF BAUSCHINGER EFFECT Due to the compliance of substrate and tiny thickness compared to the lateral dimension of film-substrate composite, low compressive stress could cause buckling. A new pre-stretching technology will be developed that the thin films can be deformed alternately in tension and compression within a large strain domain. The elastic stress/strain and true strain of thin films will be measured in situ by XRD and DIC respectively. From the lattice stress/strain-true strain curve which in-

cludes both elastic and plastic deformation, the Bauschinger effect of thin films can be studied and the residual stress and texture will be also considered.

All these strategies and other relative research will be discussed in detail in the following chapters. In summary, several novel approaches from theoretical, numerical and experimental points of view have been proposed, and X-ray diffraction, digital image correlation and controlled tensile/compressive testing are the main powerful tools we used to address both mechanical properties and microstructures of thin metallic films on compliant substrates.

BIBLIOGRAPHY

Akogwu, O. et al. "Large strain deformation and cracking of nano-scale gold films on PDMS substrate". In: *Materials Science and Engineering: B* 170.1 (2010), pp. 32–40 (cit. on p. 18).

Arzt, E. et al. "Interface controlled plasticity in metals: dispersion hardening and thin film deformation". In: *Progress in Materials science* 46.3 (2001), pp. 283–307 (cit. on p. 17).

Baker, S.P., R.-M. Keller-Flaig, and J.B. Shu. "Bauschinger effect and anomalous thermomechanical deformation induced by oxygen in passivated thin Cu films on substrates". In: *Acta materialia* 51.10 (2003), pp. 3019–3036 (cit. on pp. 21, 99).

Balakrishnan, G. et al. "Effect of substrate temperature on microstructure and optical properties of nanocrystalline alumina thin films". In: *Ceramics International* 39.8 (2013), pp. 9017–9023 (cit. on p. 17).

Bauschinger, J. "Ueber die Veranderung der Elasticitatagrenze und dea Elasticitatamoduls verschiadener Metalle". In: *zivilingenieur* 27 (1881), pp. 289–348 (cit. on p. 19).

Bemporad, E. et al. "A critical comparison between XRD and FIB residual stress measurement techniques in thin films". In: *Thin Solid Films* 572 (2014), pp. 224–231 (cit. on pp. 12, 13).

Besnard, G., F. Hild, and S. Roux. ""Finite-element" displacement fields analysis from digital images: application to Portevin–Le Châtelier bands". In: *Experimental Mechanics* 46.6 (2006), pp. 789–803 (cit. on pp. 19, 72).

Böhm, J. et al. "Tensile testing of ultrathin polycrystalline films: a synchrotron-based technique". In: *Review of Scientific Instruments* 75.4 (2004), pp. 1110–1119 (cit. on p. 17).

Brand, J. van den et al. "Flexible and stretchable electronics for wearable health devices". In: *Solid-State Electronics* 113 (2015), pp. 116–120 (cit. on pp. 2, 3).

Brugger, C. et al. "Strain gradient plasticity analysis of the strength and ductility of thin metallic films using an enriched interface model". In: *Acta materialia* 58.15 (2010), pp. 4940–4949 (cit. on p. 22).

Chapman, B.N. "Thin-film adhesion". In: *Journal of Vacuum Science & Technology* 11.1 (1974), pp. 106–113 (cit. on p. 14).

Chasiotis, I. "Mechanics of thin films and microdevices". In: *Device and Materials Reliability, IEEE Transactions on* 4.2 (2004), pp. 176–188 (cit. on p. 18).

Chen, J. and S.J. Bull. "Indentation fracture and toughness assessment for thin optical coatings on glass". In: *Journal of Physics D: Applied Physics* 40.18 (2007), p. 5401 (cit. on p. 14).

Chen, X. et al. "Tensile testing of thin films supported on compliant substrates". In: *Mechanics of Materials* 41.7 (2009), pp. 839–848 (cit. on p. 19).

Cho, S. et al. "Young's modulus, Poisson's ratio and failure properties of tetrahedral amorphous diamond-like carbon for MEMS devices". In: *Journal of Micromechanics and Microengineering* 15.4 (2005), p. 728 (cit. on p. 17).

Choi, Y.J. and Y.-K. Lee. "Elastic modulus of amorphous Ge2Sb2Te5 thin film measured by uniaxial microtensile test". In: *Electronic Materials Letters* 6.1 (2010), pp. 23–26 (cit. on p. 19).

Chou, T.-L., S.-Y. Yang, and K.-N. Chiang. "Overview and applicability of residual stress estimation of film–substrate structure". In: *Thin Solid Films* 519.22 (2011), pp. 7883–7894 (cit. on p. 11).

Clemens, B.M. and J.A. Bain. "Stress determination in textured thin films using X-ray diffraction". In: *MRS bulletin* 17.07 (1992), pp. 46–51 (cit. on p. 12).

Cordill, M.J. et al. "Adhesion energies of Cr thin films on polyimide determined from buckling: Experiment and model". In: *Acta Materialia* 58.16 (2010), pp. 5520–5531 (cit. on p. 14).

Crawford, G. *Flexible flat panel displays*. John Wiley & Sons, 2005 (cit. on p. 2).

Culity, B.D. "Elements of X-ray Diffraction". In: *2nd, Addition-Wesley, MA, London* (1978) (cit. on pp. 12, 58).

Davoudi, K.M., L. Nicola, and Joost J. Vlassak. "Bauschinger effect in thin metal films: Discrete dislocation dynamics study". In: *Journal of Applied Physics* 115.1 (2014), p. 013507 (cit. on pp. 21, 23).

Denis, Y.W. and F. Spaepen. "The yield strength of thin copper films on Kapton". In: *Journal of Applied Physics* 95.6 (2004), pp. 2991–2997 (cit. on p. 19).

Djaziri, S. et al. "Comparative study of the mechanical properties of nanostructured thin films on stretchable substrates". In: *Journal of Applied Physics* 116.9 (2014), p. 093504 (cit. on pp. 14, 66, 68, 80).

Eiper, E. et al. "Size-independent stresses in Al thin films thermally strained down to- 100 C". In: *Acta materialia* 55.6 (2007), pp. 1941–1946 (cit. on p. 17).

Faurie, D., O. Castelnau, et al. "In situ diffraction strain analysis of elastically deformed polycrystalline thin films, and micromechanical interpretation". In: *Journal of Applied Crystallography* 42.6 (2009), pp. 1073–1084 (cit. on p. 12).

Faurie, D., P. Djemia, et al. "Elastic anisotropy of polycrystalline Au films: Modeling and respective contributions of X-ray diffraction, nanoindentation and

Brillouin light scattering". In: *Acta Materialia* 58.15 (2010), pp. 4998–5008 (cit. on p. 17).

Faurie, D., P.-O. Renault, E. Le Bourhis, T. Chauveau, et al. "X-ray strain analysis of 111 fiber-textured thin films independent of grain-interaction models". In: *Journal of Applied Crystallography* 44.2 (2011), pp. 409–413 (cit. on pp. 8, 9).

Faurie, D., P.-O. Renault, E. Le Bourhis, and P. Goudeau. "Study of texture effect on elastic properties of Au thin films by X-ray diffraction and in situ tensile testing". In: *Acta Materialia* 54.17 (2006), pp. 4503–4513 (cit. on pp. 17, 89, 125).

Faurie, D., P.-O. Renault, E. Le Bourhis, and Ph. Goudeau. "Determination of elastic constants of a fiber-textured gold film by combining synchrotron x-ray diffraction and in situ tensile testing". In: *Journal of applied physics* 98.9 (2005), p. 093511 (cit. on pp. 17, 66, 69).

Fewster, P.F. "X-ray analysis of thin films and multilayers". In: *Reports on Progress in Physics* 59.11 (1996), p. 1339 (cit. on p. 1).

Forrest, S.R. "The path to ubiquitous and low-cost organic electronic appliances on plastic". In: *Nature* 428.6986 (2004), pp. 911–918 (cit. on pp. 3, 4).

Freund, L.B. and S. Suresh. *Thin film materials: stress, defect formation and surface evolution*. Cambridge University Press, 2004 (cit. on pp. 5, 11, 17).

Geandier, G. et al. "Elastic-strain distribution in metallic film-polymer substrate composites". In: *Applied Physics Letters* 96.4 (2010), p. 041905 (cit. on pp. 14, 66).

Gerberich, W.W. and M.J. Cordill. "Physics of adhesion". In: *Reports on Progress in Physics* 69.7 (2006), p. 2157 (cit. on p. 14).

Gianola, D.S. and C. Eberl. "Micro-and nanoscale tensile testing of materials". In: *JOM* 61.3 (2009), pp. 24–35 (cit. on p. 19).

Guruprasad, P.J., W.J. Carter, and A.A. Benzerga. "A discrete dislocation analysis of the Bauschinger effect in microcrystals". In: *Acta Materialia* 56.19 (2008), pp. 5477–5491 (cit. on p. 23).

Hauk, V. *Structural and residual stress analysis by nondestructive methods: Evaluation-Application-Assessment*. Elsevier, 1997 (cit. on pp. 8, 12, 58, 61, 125).

Hild, F. and S. Roux. "Digital image correlation: from displacement measurement to identification of elastic properties–a review". In: *Strain* 42.2 (2006), pp. 69–80 (cit. on pp. 19, 52, 55, 72).

Hommel, M., O. Kraft, and E. Arzt. "A new method to study cyclic deformation of thin films in tension and compression". In: *Journal of materials research* 14.06 (1999), pp. 2373–2376 (cit. on pp. 14, 98, 108, 110).

Janssen, G.C.A.M. et al. "Celebrating the 100th anniversary of the Stoney equation for film stress: Developments from polycrystalline steel strips to single

crystal silicon wafers". In: *Thin Solid Films* 517.6 (2009), pp. 1858–1867 (cit. on p. 11).
Jordan-Sweet, J.L. et al. "Characterization of strain in thin-film structures with microdiffraction". In: *Adv. X-Ray Anal* 42 (2000) (cit. on p. 16).
Kelly, P.J. and R.D. Arnell. "Magnetron sputtering: a review of recent developments and applications". In: *Vacuum* 56.3 (2000), pp. 159–172 (cit. on p. 5).
Kim, C. et al. "Warpage Analysis of Electroplated Cu Films on Fiber-Reinforced Polymer Packaging Substrates". In: *Polymers* 7.6 (2015), pp. 985–1004 (cit. on p. 12).
Kim, D.-H et al. "Materials and noncoplanar mesh designs for integrated circuits with linear elastic responses to extreme mechanical deformations". In: *Proceedings of the National Academy of Sciences* 105.48 (2008), pp. 18675–18680 (cit. on p. 4).
Kim, D.-H. et al. "Stretchable, curvilinear electronics based on inorganic materials". In: *Advanced Materials* 22.19 (2010), pp. 2108–2124 (cit. on p. 2).
Kirsch, B.L. et al. "Probing the effects of nanoscale architecture on the mechanical properties of hexagonal silica/polymer composite thin films". In: *Advanced Functional Materials* 15.8 (2005), pp. 1319–1327 (cit. on p. 14).
Kocks, U.F., C.N. Tomé, and H.-R. Wenk. *Texture and anisotropy: preferred orientations in polycrystals and their effect on materials properties*. Cambridge university press, 2000 (cit. on p. 8).
Korsunsky, A.M., M. Sebastiani, and E. Bemporad. "Focused ion beam ring drilling for residual stress evaluation". In: *Materials Letters* 63.22 (2009), pp. 1961–1963 (cit. on p. 12).
Kraft, O. and C.A. Volkert. "Mechanical testing of thin films and small structures". In: *Advanced Engineering Materials* 3.3 (2001), pp. 99–110 (cit. on p. 18).
Krottenthaler, M. et al. "A simple method for residual stress measurements in thin films by means of focused ion beam milling and digital image correlation". In: *Surface and Coatings Technology* 215 (2013), pp. 247–252 (cit. on p. 12).
Leterrier, Y. "Durability of nanosized oxygen-barrier coatings on polymers". In: *Progress in Materials Science* 48.1 (2003), pp. 1–55 (cit. on p. 14).
Li, T. and Z.G. Suo. "Ductility of thin metal films on polymer substrates modulated by interfacial adhesion". In: *International Journal of Solids and Structures* 44.6 (2007), pp. 1696–1705 (cit. on p. 14).
Liu, Z.-L. et al. "Bauschinger and size effects in thin-film plasticity due to defect-energy of geometrical necessary dislocations". In: *Acta Mechanica Sinica* 27.2 (2011), pp. 266–276 (cit. on p. 23).

Lu, N.S., Z.G. Suo, and Joost J. Vlassak. "The effect of film thickness on the failure strain of polymer-supported metal films". In: *Acta Materialia* 58.5 (2010), pp. 1679–1687 (cit. on pp. 17, 18).

Lu, N.S., X. Wang, et al. "Metal films on polymer substrates stretched beyond 50%". In: *Applied Physics Letters* 91.22 (2007), p. 221909 (cit. on p. 4).

M., Maryam et al. "Evaluation of structure and mechanical properties of Ni-rich NiTi/Kapton composite film". In: *Materials Science and Engineering: A* 668 (2016), pp. 13–19 (cit. on p. 14).

Macionczyk, F. et al. "Young's modulus and tensile strength of CuNi (Mn) thin films on polyimide foils by tensile testing". In: *Journal of materials research* 13.10 (1998), pp. 2852–2858 (cit. on p. 19).

Martinschitz, K.J. et al. "Elastic constants of fibre-textured thin films determined by X-ray diffraction". In: *Journal of applied crystallography* 42.3 (2009), pp. 416–428 (cit. on p. 12).

Marx, V.M., F. Toth, et al. "The influence of a brittle Cr interlayer on the deformation behavior of thin Cu films on flexible substrates: Experiment and model". In: *Acta materialia* 89 (2015), pp. 278–289 (cit. on p. 14).

Misra, A., J.P. Hirth, and R.G. Hoagland. "Length-scale-dependent deformation mechanisms in incoherent metallic multilayered composites". In: *Acta materialia* 53.18 (2005), pp. 4817–4824 (cit. on p. 17).

Mittal, K.L. "Adhesion measurement of thin films". In: *Active and Passive Electronic Components* 3.1 (1976), pp. 21–42 (cit. on p. 14).

Mompiou, F., M. Legros, A. Boé, et al. "Inter-and intragranular plasticity mechanisms in ultrafine-grained Al thin films: an in situ TEM study". In: *Acta Materialia* 61.1 (2013), pp. 205–216 (cit. on p. 18).

Mompiou, F., M. Legros, T. Radetic, et al. "In situ TEM observation of grain annihilation in tricrystalline aluminum films". In: *Acta Materialia* 60.5 (2012), pp. 2209–2218 (cit. on p. 18).

Noyan, I.C. and J.B. Cohen. *Residual stress: measurement by diffraction and interpretation*. Springer, 1987 (cit. on pp. 7, 12).

Noyan, I.C., T.C. Huang, and B.R. York. "Residual stress/strain analysis in thin films by X-ray diffraction". In: *Critical Reviews in Solid State and Material Sciences* 20.2 (1995), pp. 125–177 (cit. on pp. 11, 60, 66, 108).

Oliver, W.C. and G.M. Pharr. "Measurement of hardness and elastic modulus by instrumented indentation: Advances in understanding and refinements to methodology". In: *Journal of materials research* 19.01 (2004), pp. 3–20 (cit. on p. 17).

Rajagopalan, J., J.H. Han, and M.T.A. Saif. "Bauschinger effect in unpassivated freestanding nanoscale metal films". In: *Scripta Materialia* 59.7 (2008), pp. 734–737 (cit. on pp. 23, 98).

Rajagopalan, J., C. Rentenberger, et al. "In situ TEM study of microplasticity and Bauschinger effect in nanocrystalline metals". In: *Acta Materialia* 58.14 (2010), pp. 4772–4782 (cit. on pp. 23, 98).

Rogers, J.A., T. Someya, and Y.G. Huang. "Materials and mechanics for stretchable electronics". In: *Science* 327.5973 (2010), pp. 1603–1607 (cit. on pp. 2, 3).

Schadler, L.S. and I. Cevdet Noyan. "Experimental Determination of the Strain Transfer Across a Flexible Intermediate Layer in Thin Film Structures as a Function of Flexible Layer Thickness". In: *MRS Proceedings*. Vol. 239. Cambridge Univ Press. 1991, p. 151 (cit. on p. 15).

Schadler, L.S. and I.C. Noyan. "Experimental determination of the strain transfer across a flexible intermediate layer in thin-film structures". In: *Journal of Materials Science Letters* 11.15 (1992), pp. 1067–1069. ISSN: 1573-4811 (cit. on p. 15).

Schmidt, T.K. et al. "Influence of tantalum and silver interlayers on thermal stress evolution in copper thin films on silicon substrates". In: *Scripta materialia* 50.6 (2004), pp. 733–737 (cit. on p. 17).

Sebastiani, M. et al. "Depth-resolved residual stress analysis of thin coatings by a new FIB–DIC method". In: *Materials Science and Engineering: A* 528.27 (2011), pp. 7901–7908 (cit. on p. 12).

Shishvan, S.S., L. Nicola, and E. Van der Giessen. "Bauschinger effect in unpassivated freestanding thin films". In: *Journal of Applied Physics* 107.9 (2010), p. 093529 (cit. on p. 23).

Simmons, G. and H. Wang. *Single crystal elastic constants and calculated aggregate properties: a handbook*. Tech. rep. The M.I.T.press, 1971 (cit. on pp. 8, 127).

Stoney, G.G. "The tension of metallic films deposited by electrolysis". In: *Proceedings of the Royal Society of London. Series A, Containing Papers of a Mathematical and Physical Character* 82.553 (1909), pp. 172–175 (cit. on p. 11).

Suo, Z.G., Joost J. Vlassak, and S. Wagner. "Micromechanics of macroelectronics". In: *China Particuology* 3.06 (2005), pp. 321–328 (cit. on p. 4).

Villain, P. et al. "Atomistic calculation of size effects on elastic coefficients in nanometre-sized tungsten layers and wires". In: *Scripta materialia* 50.9 (2004), pp. 1247–1251 (cit. on p. 17).

Vlassak, Joost J. and W.D. Nix. "A new bulge test technique for the determination of Young's modulus and Poisson's ratio of thin films". In: *Journal of Materials Research* 7.12 (1992), pp. 3242–3249 (cit. on p. 18).

Wang, D. et al. "Influences of Ta passivation layers on the fatigue behavior of thin Cu films". In: *Materials Science and Engineering: A* 610 (2014), pp. 33–38 (cit. on p. 18).

Welzel, U. et al. "Stress analysis of polycrystalline thin films and surface regions by X-ray diffraction". In: *Journal of Applied Crystallography* 38.1 (2005), pp. 1–29 (cit. on pp. 6, 7).

Wojciechowski, P.H. and M.S. Mendolia. "Fracture and cracking phenomena in thin films adhering to high-elongation substrates". In: *Physics of thin films* 16 (1991), pp. 271–340 (cit. on pp. 15, 80).

Xiang, Y., X. Chen, and Joost J. Vlassak. "Plane-strain bulge test for thin films". In: *Journal of materials research* 20.09 (2005), pp. 2360–2370 (cit. on p. 18).

Xiang, Y., T. Li, et al. "High ductility of a metal film adherent on a polymer substrate". In: *Applied Physics Letters* 87.16 (2005), p. 161910 (cit. on p. 14).

Xiang, Y. and J.J. Vlassak. "Bauschinger effect in thin metal films". In: *Scripta Materialia* 53.2 (2005), pp. 177–182. ISSN: 1359-6462 (cit. on pp. 22, 23, 99, 110).

Xiang, Y. and Joost J. Vlassak. "Bauschinger and size effects in thin-film plasticity". In: *Acta Materialia* 54.20 (2006), pp. 5449–5460. ISSN: 1359-6454 (cit. on pp. 22, 23, 99, 110).

Yanaka, M. et al. "Cracking phenomena of brittle films in nanostructure composites analysed by a modified shear lag model with residual strain". In: *Journal of Materials Science* 33.8 (1998), pp. 2111–2119 (cit. on p. 15).

Yin, H.M. and P.A. Prieto-Muñoz. "Stress transfer through fully bonded interface of layered materials". In: *Mechanics of Materials* 62 (2013), pp. 69–79 (cit. on pp. 15, 66).

Zhang, G.P. et al. "Fatigue and thermal fatigue damage analysis of thin metal films". In: *Microelectronics Reliability* 47.12 (2007) (cit. on p. 18).

Zhou, C.Z. and R. LeSar. "Dislocation dynamics simulations of the Bauschinger effect in metallic thin films". In: *Computational Materials Science* 54 (2012), pp. 350–355 (cit. on p. 22).

2 EXPERIMENTAL DESIGN AND RESEARCH METHODS

Contents

According to the objects of this dissertation, various experimental setups including the specimen, grips, deposition masks etc. are custom-designed. All the systems were designed by Catia V5 (Dassault Systèmes). Thin films will be deposited on substrates in a special way, and the initial characterization of thin films are specified. Moreover, the main techniques, i.e. in situ tensile/compressive testing, DIC strain measurement, XRD strain/stress measurement, are introduced and discussed in detail.

2.1 SUBSTRATES DESIGN FOR MECHANICAL TESTING

As previously mentioned, thin films deposited on Kapton® are widely used in a large amount of promising fields. Many of these applications are based on the flexibility and the excellent balance of Kapton®'s superior properties over a wide range of temperatures, such as electrical, thermal, mechanical and chemical properties. In this study, Kapton® HN from DuPont™ with a thickness of 125 µm was chosen as a substrate to be coated with thin metal films. It is a compliant polyimide film which can be stretched beyond 70% with an elastic range of 4-5%, a Young's modulus of ~4 GPa and a Poisson's ratio of 0.34 at room temperature.

It is necessary to design two kinds of substrate geometry considering different requirements which will be described later in detail. Both of them were fabricated in dogbone shape, while one has smaller strain gauge or homogeneous strain field (Fig. 2.1(a)). It should be noted that the full lengths are the same due to the size limitation of specimen holder in the sputtering chamber. Owing to the compliance and tiny thickness of polyimide film, it is unattainable to clamp in a traditional way. Herein, we rely on the holes in Kapton® to maintain a given force. It may be noticed that the two holes are quite close to the edges, and Kapton® is a low strength material so that a failure can appear at the stress concentrations around the holes (Fig. 2.1(b)). However, it can be solved thanks to the flat metal washers sticked around the holes with cyanoacrylate glues. In this way, the specimens are reinforced and can be stretched up to more than 120 N without any damages.

It is well known that, as-deposited film-substrate composite could bend due to the large residual stresses present in the film especially when the substrate is compliant. In order to keep the soft specimen flat even under small forces

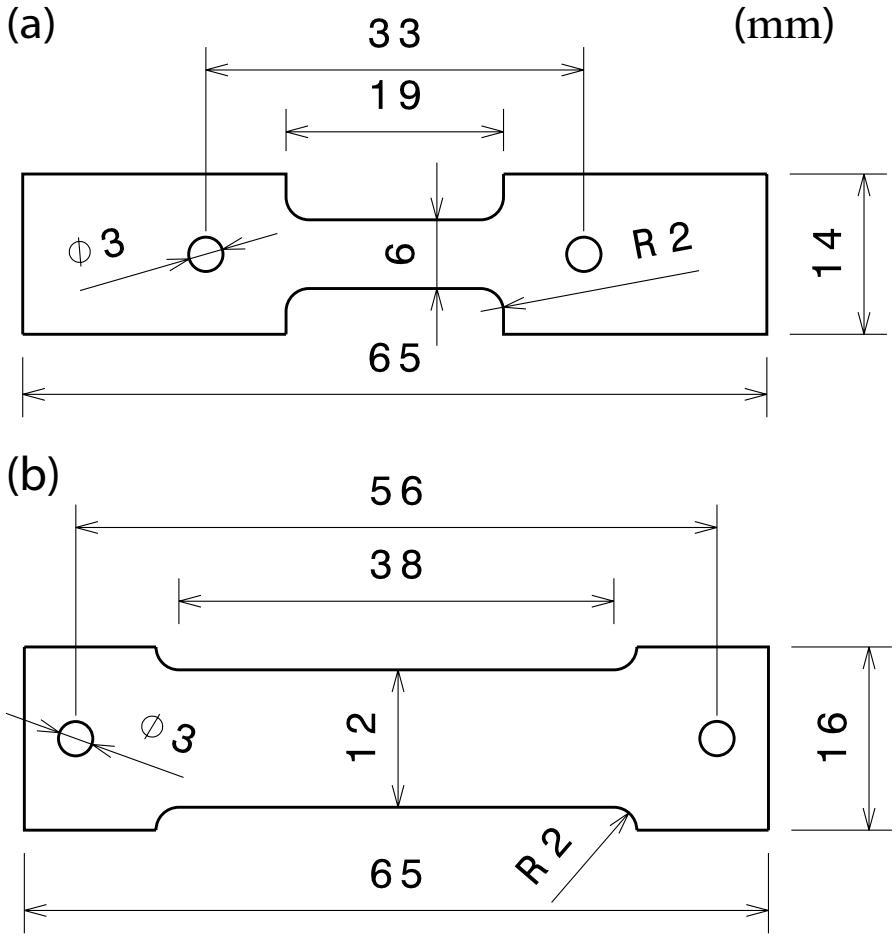

Figure 2.1: Geometry design of the dogbone-shaped Kapton® substrates.

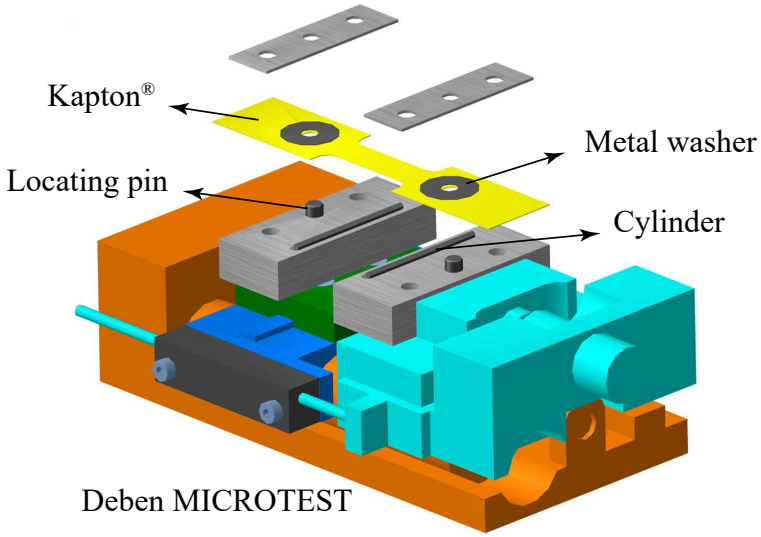

Figure 2.2: Schematic illustration of one Kapton® substrate mounted on the Deben MICROTEST. By virtue of the metal washers and cylinders, precise uniaxial tensile/compression testing within a large strain domain can be achieved.

and to facilitate the XRD measurements, two slender metal cylinders are put inside the V-shaped notch of the grips. For clarity, Deben MICROTEST tensile/-compression stage with a dogbone shaped Kapton® for mechanical testing is shown in Fig. 2.2.

The force is transferred to Kapton® mainly through two locating pins. As well known, the alignment of a specimen in the tensile tester is critical, because if the specimen is misaligned, either at an angle or offset to one side, a bending force will exist and the results can be skewed from the theoretical predictions. In this study, all the screws are not fixed firmly so as to assure excellent automatic alignment of the specimen during tensile testing. Hence, all the specimens are pre-strained to ~5 N before further testing except the ones for cyclic testing. With the support of cylinders, the central zone of the specimen is 0.45 mm higher than the surface level of other parts which will be important for XRD measurements, since a part of the X-ray scans can not

penetrate in the interesting specimen zone. Furthermore, a black paper under the translucent polyimide film is used to reduce the effects of light reflection on the uncertainties of DIC strain measurements.

2.2 DEVELOPMENT OF SETUPS ADAPTED TO DEBEN MICROTEST AND X-RAY DIFFRACTOMETER

For the purpose of performing different kinds of measurements, it is necessary to design specific setups adapted to the Deben MICROTEST stage and the X-ray diffractometer. There are two main requirements in this work:

- Young's modulus determination of thin films deposited on both sides of a substrate over half of the gauge length, in other words, only half of the top and bottom surfaces are coated with thin films (Fig. 2.8). This method is grounded in the strain difference between the film-substrate composite and the uncoated Kapton®. A dual DIC system combined with the Deben MICROTEST is necessary to monitor the strains simultaneously during the tensile testing.
- Bauschinger effect of thin metal films deposited on both sides of a pre-stretched Kapton® over the full gauge length: combining the cyclic tensile/compressive testing, XRD stress/strain analysis and DIC strain measurements. All the measurements must be performed step by step with the Deben MICROTEST and one DIC system being inside the X-ray diffractometer.

Since thin films are deposited on a very soft substrate, many techniques which require good flatness would suffer from the curvature of film-substrate composite if the residual stresses are too large. This effect can be avoided by

depositing thin films on both sides of a substrate under the same deposition condition. Because of the geometric symmetry, the warpage arising during the first deposition on one side will disappear after the second deposition on the opposite side. In this work, all the substrates will be coated on both sides, not only to have an excellent flatness but also to increase the contribution of thin films on XRD measurements and Young's modulus determination to have better precision (please refer to later chapters for more details).

In the first subject, since films are coated on half surface of the substrate and only the center of each section is of interest for DIC measurements, it is reasonable to use the substrate (Fig. 2.1(b)) with a long strain gauge to get rid of the edge effect, and from the shear lag model (Section 1.3.2.1), an uniform stress distribution in the central section can be expected in elastic regime which is imperative for theoretical analysis. It should be noted that the width in Fig. 2.1(b) is much larger compared to Fig. 2.1(a). The key consideration is to reach a stable state speedily and keeping flat in the longitudinal direction at the very beginning of tensile testing, i.e. at a small strain of the specimen. In order to stretch the long specimen in a relatively large strain domain, it is necessary to design a new grip considering the limited working distance of Deben MICROTEST [1]. Moreover, in the interest of measuring the strains on each side of the specimen simultaneously, it is impossible to keep it horizontal if the configuration of Deben MICROTEST is taken into account. Consequently, a vertical arrangement is selected so that both sides of the specimen can be captured by a horizontally located camera (Fig. 2.3). Similar to the design in Fig. 2.2, cylinders and locating pins are used to strain the specimen and its plane is exactly aligned with the center of a ballscrew underneath, so as to minimize yaw-induced Abbe errors at the load sensor (Bamberg et al. 2006). Unfortunately, the moment created by the ballscrew force being below the plane of the specimen causes a relatively large deflection making the force values ques-

1 Maximum 35 mm, about half of the specimen length.

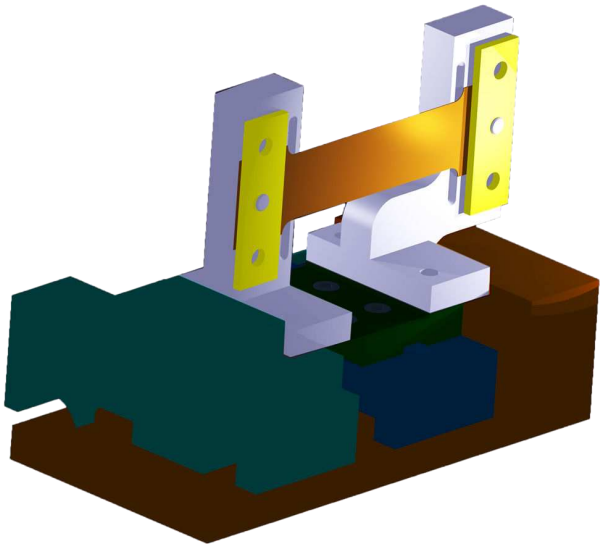

Figure 2.3: Vertical grips with elongated specimen for dual DIC strain measurements. The Deben MICROTEST is darkened to highlight the design of new grips.

tionable. However, this is not true in the case of strain measurements since DIC technique is tracking directly the deformation of the sample surface, and flexible locating pins allow an automatic perfect specimen alignment during a tensile testing.

In the second subject, thin films are deposited on both sides and the whole surfaces of a substrate differing from the first subject. Since the virgin or uncoated section is useless here, and in view of the size limitation of specimen holder in the deposition chamber, the substrate in Fig. 2.1(a) with a short strain gauge is used. In this study, the technique, named as pre-stretching technique, to deposit thin films on a pre-strained substrate plays a crucial role. Recently, we demonstrated a novel pre-stretching technique in which the substrate was firstly pulled up to 50 N using Deben MICROTEST inside our home-made vacuum sputtering chamber, and then kept at the constant strain during both the pumping and deposition processes (Renault et al. 2012). However, this is

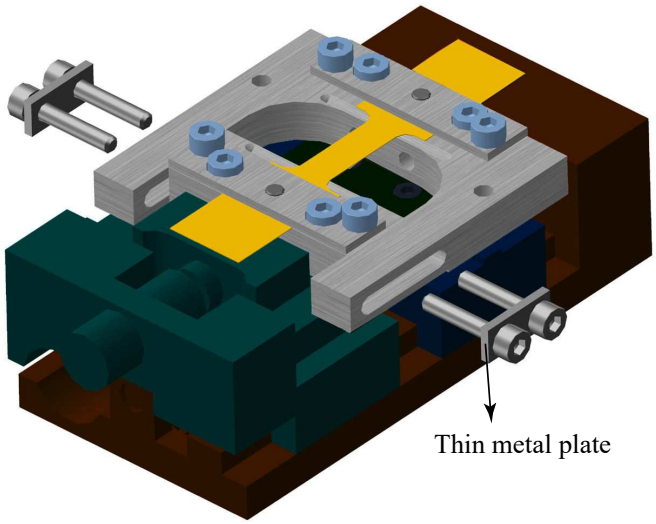

Figure 2.4: Grips for substrate pre-stretching and cyclic testing of films coated on both sides of the Kapton® with a shorter strain gauge. The Deben MICROTEST is darkened to highlight the design of new grips.

harmful to both the tensile tester and the deposition machine, especially the electrical parts even with the extra protection. Furthermore, only one sample was obtained at each deposition. In order to be efficient and to ensure consistency and repeatability, a new method is in demand.

It is not difficult to pre-strain a substrate in tension while tricky to maintain the pre-strain for film deposition after removing from the Deben MICROTEST. Thanks to our self-built grips, the substrate can be pre-stretched and then the grips are fixed with four screws and cyanoacrylate glues adding to both sides of two thin metal plates (Fig. 2.4). In that way, the whole grips together with the pre-strained substrate can be taken away from the Deben MICROTEST, and kept stable during the film deposition. The detail of this newly developed pre-stretching technique will be discussed in Chapter 4.

After preparing the specimens, the Deben MICROTEST and one DIC system need to be put inside the X-ray diffractometer. Accordingly, we develop a new setup combining the tensile tester and the DIC system which is adapted to

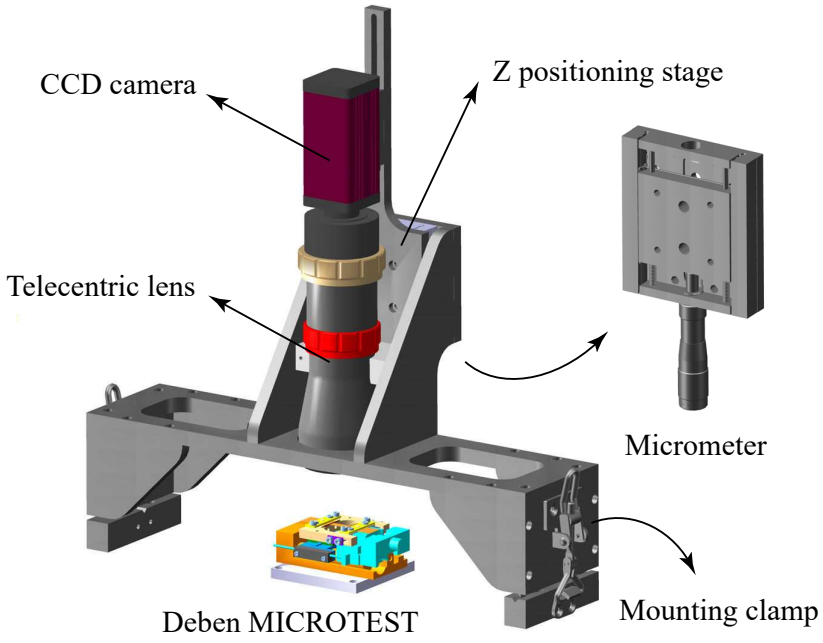

Figure 2.5: Home-made setup adapted to the X-ray diffractometer: a CCD camera is equipped with a 1.0X gold series telecentric lens used for DIC strain measurements; the camera can be translated along Z direction (normal to the surface of a specimen stretched on the Deben MICROTEST) to have the right focus. This setup can be fixed inside the goniometer chamber thanks to the mounting clamps.

the goniometer (Fig. 2.5). One CCD camera equipped with a 1.0X gold series telecentric lens (Edmund Optics) is attached firmly to the Z positioning stage. The working distance of the telecentric lens can be adjusted by a micrometer closely behind. Thanks to the mounting clamps, the setup can be fixed inside the goniometer chamber, the Deben MICROTEST being located beneath the telecentric lens. It is worth mentioning that this setup (except the Deben MICROTEST) must be removed to have the next XRD measurement due to its size and weight which will destroy the collimator and internal XYZ positioning stage during the measurement.

2.3 SPUTTERING METHODS AND CONDITIONS

2.3.1 Residual stress control of thin metal films in PUMA

In this study, magnetron sputtering and ion-beam sputtering, both physical vapor deposition (PVD) methods, were employed to deposit thin metal films on compliant substrates. The sputter depositions were carried out in a vacuum chamber to enable control of the vapor composition. For magnetron sputtering, with the availability of many parameters, one device named PUMA allows flexible control over the growth, microstructure and residual stresses of thin films. An approximately stress-free specimen is important in our case, since large compressive residual stress can cause film delamination. In order to determine the right parameters, five depositions for 300 nm W have been done, and the macroscopic biaxial residual stresses were calculated based on Stoney's formula. As can be seen in Fig. 2.6, the magnitude and sign of the residual stresses change when adjusting the flow rate and vapor pressure of argon. The zero stress is between 22 SCCM and 22.5 SCCM which is very difficult to determine exactly and to reproduce at different deposition sessions. Consequently, depositing thin films on both sides of a substrate is important to get a specimen as flat as possible.

2.3.2 Film deposition for pre-tensile specimens in NORDIKO

For film deposition on pre-tensile specimens, a machine named NORDIKO (ion-beam sputtering method) was used considering the fact that its pumping system is very powerful which allows to get a good vacuum even with many pre-stretching setups. Furthermore, the high energy of the ion beam sputtering process results in extremely uniform, high density films with excellent

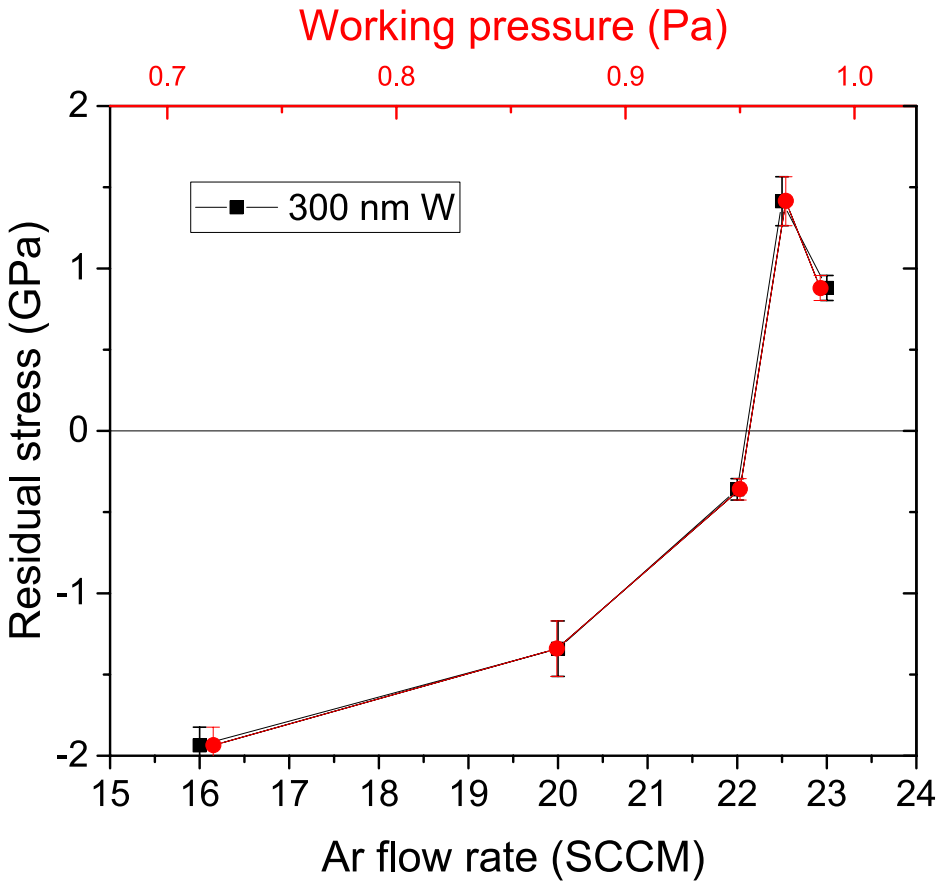

Figure 2.6: Residual stress (Stoney's formula) as a function of flow rate (black) and working pressure (red). The residual stress increases sharply from compressive to tensile.

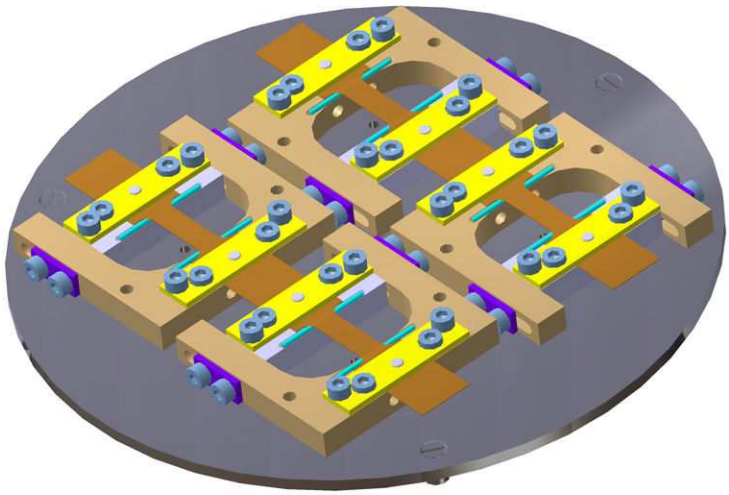

Figure 2.7: Four pre-tensile specimens mounted on the carriage plate for ion-beam sputtering (NORDIKO). Top or back side of the grips can be attached to the plate thanks to the holes, i.e. the ones without showing the screws. Each side of the specimen corresponds to one deposition. For the purpose of better illustration, different parts are represented by various colors.

adhesion to the substrate despite the presence of high compressive residual stresses (W, Cr and Ni). This translates into high environmental stability and mechanical durability with low surface roughness.

All the sputtering depositions for thin metal films with different materials in NORDIKO were achieved with an argon ion gun (energy: 1.2 keV): the base pressure in the chamber was 7×10^{-5} Pa and the working pressure during the film growth was 1×10^{-2} Pa. For 300 nm Ni and Cu films coated on both sides of the pre-tensile substrates, the deposition rate is 0.93 Å/sec. and 1.45 Å/sec. respectively.

Thanks to our new pre-stretching technique, one Kapton® substrate was pre-stretched to 50 N, and then the whole entity of Kapton® and grips was removed from Deben MICROTEST. After pre-stretching four times, the specimens were installed on the carriage plate to put inside the sputtering chamber (Fig. 2.7).

2.3.3 Film deposition on both sides of a substrate over half of the gauge length

As a means to control film microstructure and residual stresses, the films have been deposited using magnetron sputtering machine (PUMA). For instance, the pressure was fixed at 9.54×10^{-1} Pa (gas flow of 22 SCCM) during deposition to reduce the residual stress level in W films. A sputtering power of 300 W on the tungsten target has been used to get a deposition speed of 0.22 nm/s. The Kapton® was coated on both sides over half of the gauge length under the same condition. Thanks to the high symmetry, a flat specimen was obtained. The concrete process is as follows: immediately prior to the film deposition, the substrates were cleaned with acetone and ethanol ultrasonically; then two specimens were mounted with specially designed masks as shown in Fig. 2.8. Two additional silicon substrates were used for thickness and residual stress measurements. One is a 650 μm thick and (100) oriented Si wafer, supporting a 5×5 mm^2 mask which is made of 200 μm thick silicon wafer. Removing the small mask after deposition gives rise to a step from where the thickness can be measured using the DEKTAK IIa profilometer. The other one is a Si strip of 200 μm thick to measure the curvature induced by the in-plane residual stresses of as-deposited films using the same profilometer.

It is worth pointing out that after two depositions (each deposition corresponds to one side of the Kapton® substrate), the as-deposited specimen becomes flat although the residual stresses still exist. Moreover, the compressive residual stresses could be beneficial for the study of thin films' mechanical behavior by increasing their elastic range in the tensile testing.

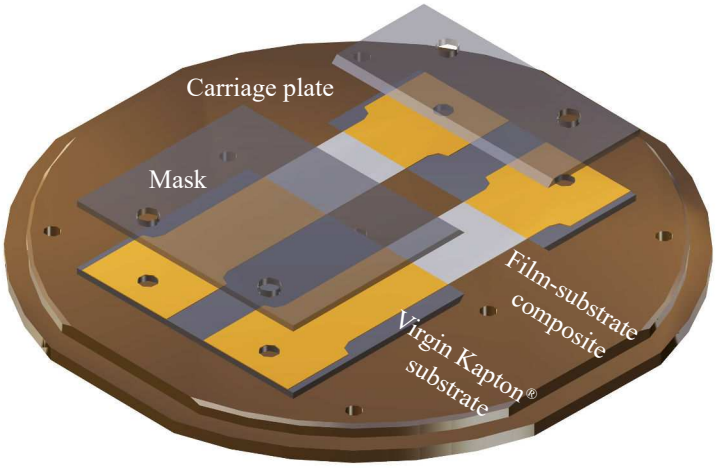

Figure 2.8: Film deposition on both sides of Kapton® over half of the gauge length with specific masks (PUMA).

2.4 INITIAL CHARACTERIZATIONS OF AS-DEPOSITED THIN FILMS

X-ray diffraction has been used for phase identification and texture analysis. The 4-circles x-ray diffractometer is provided by the Seifert Company and works with a Cu- K_α X-ray tube and a punctual detector. The obtained diffraction diagrams (Fig. 2.9) show the presence of α and β cubic phases of 300 nm tungsten films under different chamber pressures. The diffraction peaks are large indicating the presence of nanometric grain sizes and the reference diffraction angles (powder diffraction files N° 4-806 and N° 47-1319 from the International Center for Diffraction Data) are indicated by the vertical lines. As can be seen, the position of the α-W {110} diffraction peak is shifted towards small diffraction angles with respect to the reference data. This is mainly due to the presence of auto-interstitials and residual stresses in the cubic lattice. Most of the specimens are mainly α-W, while the sample prepared under 0.97 Pa is mainly β-W. Such phase is generally associated with the tensile resid-

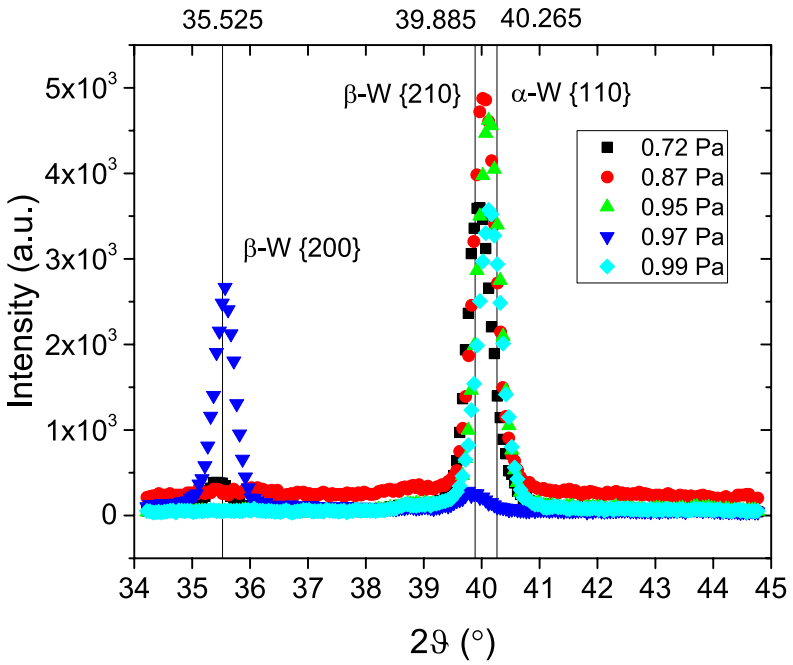

Figure 2.9: X-ray diffraction patterns of 300 nm W films under different chamber pressures. They are measured by the 4-circles Seifert diffractometer working with Cu- K_α lines. (Step size: 0.05°/ recording time: 1 second). The vertical lines show the positions of the main diffraction peaks of the two possible phases of tungsten which are taken from the ICDD-PDF files N° 47-1319 for β-W (cubic) and N°4-806 for α-W (body-centered cubic).

ual stresses, while α-W phase is related to the compressive residual stresses (Girault, Eyidi, Ph. Goudeau, et al. 2013).

Diffraction angles extracted from the analysis of the diffraction peaks are summarized in Table 2.1, as well as the information of rocking curves (Fig. 2.10) performing to get the texture of thin films. Obviously, all these curves present a strong {110} texture.

Table 2.1: Diffraction angles and the characteristics of rocking curves extracted from the XRD measurements. The "×" denotes non-measurement. Moreover, a software Analyze from Seifert has been used to get the $K\alpha_1$ contribution ($\lambda = 1.5408\,\mathring{A}$).

W (PUMA)		α-W {110}	β-W {200}	Rocking curve	
Pressure (Pa)	Flow rate (SCCM)	2ϑ (°)	2ϑ (°)	FWHM (°)	Intensity (a.u.)
0.72	16.0	39.939 [a]	35.427	25.64	3147
0.87	20.0	40.025 [a]	×	25.80	4213
0.95	22.0	40.090 [a]	×	27.08	3974
0.97	22.5	39.835	35.562 [a]	26.23	2896
0.99	23.0	40.112 [a]	×	31.24	2880

[a] The diffraction angles fixed for texture analysis.

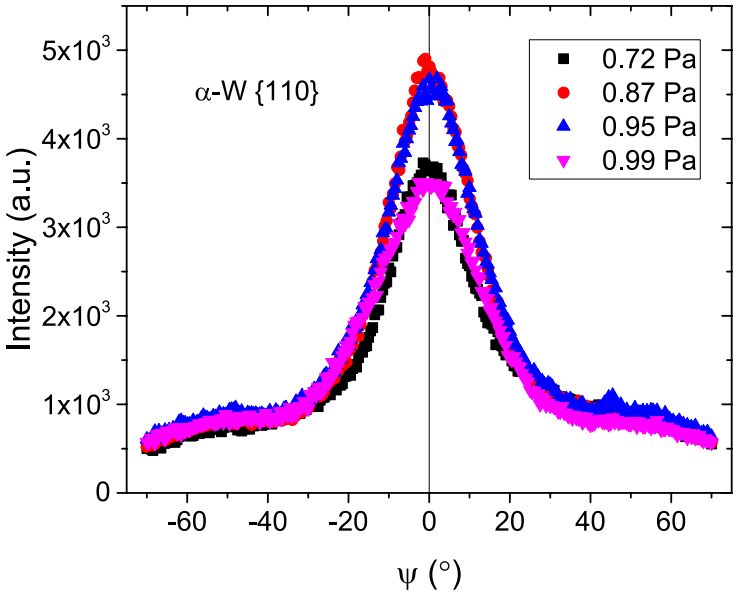

Figure 2.10: Rocking curves of the α-W {110} diffracting planes measured with the same diffractometer. The diffraction angles are fixed to the values given in Table 2.1, and the ψ angle is varied between -70° and +70°. The step size is 0.5° and the recording time is 1 second.

2.5 MECHANICAL TESTING AND STRESS/STRAIN MEASUREMENTS

2.5.1 In situ uniaxial tensile and compressive testing

Deben MICROTEST tensile/compression stage is primarily designed for use within a confined space, such as the SEM and X-ray diffractometer chambers. A 200 N tensile stage is selected using exchangeable load cells (5 N, 20 N and 200 N). Samples are mounted by our custom-designed grips clamped to a pair of jaws which are 25-35 mm apart. A dual threaded (left- and right hand thread) leadscrew drives the jaws symmetrically in opposite directions, keeping the sample centered in the field of view. This in-situ tensile/compressive tester is communicated with a software which allows the control of loading speed (0.1 mm/min to 1.5 mm/min), force and displacement (minimum step: 10 μm, maximum value: 10 mm).

In this study, 200 N load cell is used with an accuracy readout $\pm 1\%$, and the loading speed is fixed at 0.2 mm/min. Since the resolution of this displacement control cannot satisfy our much more precise requirements, we only use force control for loading continuously or step by step. Consequently, it is a pity that a constant strain step, which is very interesting for the Bauschinger effect study, cannot be achieved.

2.5.2 True strain measurements (DIC)

Digital image correlation is a 2D/3D, full-field, non-contact optical technique which allows measuring the deformation and strains of materials. It is an extremely precise method which can be used for many tests, especially the micro-

and nano-scale tensile/compressive testing for both static and dynamic applications. This technique consists in acquiring digital images of the interested specimen surfaces during mechanical testing, which is eminently suitable for the study of thin films, since many images from various microscopes can be used, such as the optical microscope (OM) and scanning tunneling microscope (STM). In this thesis, only two dimensional DIC is introduced and employed considering the tiny film thickness and the predominant in-plane deformation during tensile/compressive testing.

2.5.2.1 *Principle of digital image correlation*

DIC (Belrhiti et al. 2012; Hild and Roux 2006; J. Dupré et al. 2015; Barranger et al. 2012; Bornert et al. 2009) is an optical technique based on the analysis of successive digital images of a specimen surface during the mechanical testing. Many subsets (D) are defined in the zone of interest (ZOI) of an image (Fig. 2.11). A virtual grid forms with the intersecting points at the center of each subset. The goal is to determine the displacement of each node which constitutes the discrete displacement field of the specimen. After assuming a conservation of the optical flow, this can be achieved by measuring the similarity degree [2] of all the corresponding subsets between various images, which is given by the minimization of the correlation coefficient C (Belrhiti et al. 2012). A random distribution of gray levels is important for the determination of similarity degree, and artificial speckle pattern is usually made by spraying paints on the sample to increase the surface contrast.

Since the position and shape of the subsets can change after deformation, it is necessary to introduce a function (shape function ϕ) which links the coordinates of the reference state ($\underline{X}$) to the deformed state ($\underline{x}$):

$$\underline{x} = \phi(\underline{X}) = \underline{X} + \underline{u}(\underline{X}) \approx \underline{X} + \underline{u}(\underline{X}_0) + \frac{\partial \underline{u}}{\partial \underline{X}}(\underline{X}_0) \cdot (\underline{X} - \underline{X}_0) \tag{2.1}$$

2 Gray levels of the reference and deformed state.

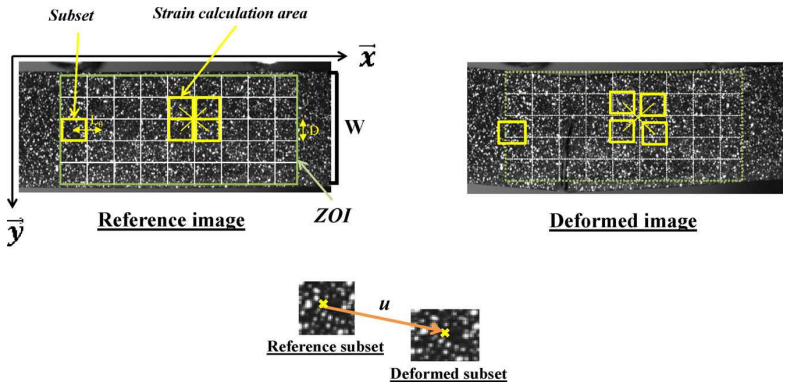

Figure 2.11: Principle of digital image correlation: the discrete displacement field (center of the subsets) is determined by measuring the similarity degree of the subsets between different states. Reproduced from (Belrhiti et al. 2012), copyright © Elsevier Ltd.

where $\underline{X}_0$ is the center of D, $\underline{u}(\underline{X}_0)$ defines the rigid body translation and $\frac{\partial \underline{u}}{\partial \underline{X}}(\underline{X}_0)$ describes the rigid body rotation and the local deformation of the subset. It should be noted that the gray levels in C will be a function of $\underline{X}$ and $\phi(\underline{X})$, i.e. $f(\underline{X})$ is the gray level of the reference state, $g(\phi(\underline{X}))$ corresponds to the gray level of the deformed state:

$$C = 1 - \frac{\sum_{\underline{X}\in D}(f(\underline{X}) - \overline{f_D}) \cdot (g(\phi(\underline{X})) - \overline{g_D})}{\sqrt{\sum_{\underline{X}\in D}(f(\underline{X}) - \overline{f_D})^2} \cdot \sqrt{\sum_{\underline{X}\in D}(g(\phi(\underline{X})) - \overline{g_D})^2}} \tag{2.2}$$

where $\overline{f_D}$ and $\overline{g_D}$ are the averages of gray levels on D and $\phi(D)$.

After obtaining the discrete displacement field, it is necessary to calculate the strains which are more interesting in the mechanical analysis. Then the gradient of the plane transformation $\underline{\underline{F}}$ is defined by:

$$\underline{\underline{F}} = \frac{\partial \underline{x}}{\partial \underline{X}} = \underline{\underline{I}} + \frac{\partial \underline{u}}{\partial \underline{X}} \tag{2.3}$$

From four contiguous subsets, two vectors $(\underline{dX_1}, \underline{dX_2})$ diagonally connecting their center points (yellow cross in Fig. 2.11) define a quadrilateral where $\underline{\underline{F}}$ is

considered to be homogeneous. With these vectors and their homologous ones in the deformed state noted $(\underline{dx_1}, \underline{dx_2})$, it is not difficult to get $\underline{\underline{F}}$ (Barranger et al. 2012). Ultimately, the Green-Lagrange strain tensor $\underline{\underline{E}}$ can be achieved:

$$\underline{\underline{E}} = \frac{1}{2}(\underline{\underline{F}}^T \cdot \underline{\underline{F}} - \underline{\underline{I}}) \tag{2.4}$$

2.5.2.2 *Accuracy and precision*

A DIC system is usually composed of a CCD camera connected to a computer, a telecentric lens and a stable illumination. After the development of this system, it is necessary to assess its precision and reliability, and several experimental tests have to be performed.

Above all, we tested a motionless specimen with a 1 µm W film coated on the long dogbone substrate (Fig. 2.1(a)). Speckles were sprayed directly on the film surface, and a 0.5X gold series telecentric lens from Edmund was used. After capturing 200 images (1 image/sec.), the strains were calculated by a software named Correla (J. Dupré et al. 2015; Barranger et al. 2012). In this case, we are only concerned with the macroscopic strains rather than with the full-field strains. Accordingly, only four subsets (64×64 pixels) were used in order to increase the gauge length. The distance between two neighboring subsets are 1200 pixels in the horizontal direction and 1000 pixels in the vertical direction. The calculated strains as a function of image number are shown in Fig. 2.12, and the average strains are: $\varepsilon_{11} = -1.21 \times 10^{-6} \pm 1.93 \times 10^{-5}$, $\varepsilon_{12} = 1.86 \times 10^{-7} \pm 1.59 \times 10^{-5}$, $\varepsilon_{22} = 2.75 \times 10^{-6} \pm 1.56 \times 10^{-5}$. As can be seen, the measurements are highly precise, however, a more reasonable way to assess the accuracy is to perform several translation tests with subpixel displacement increments in the range equal to 1 pixel which have already done by Dupré using the same technique (J. Dupré et al. 2015). With these tests, one can evaluate the effects of rigid body motion on displacement measurements, and the small translation during our tensile/compressive testing is negligible. It

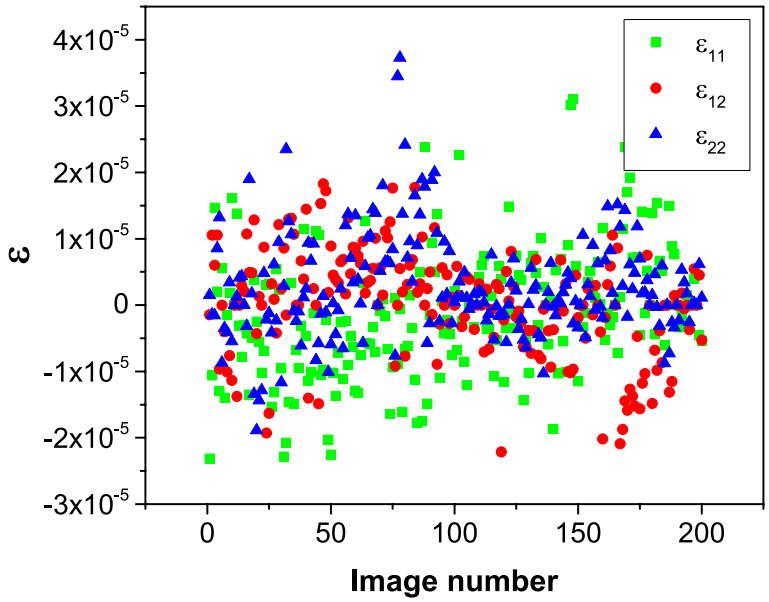

Figure 2.12: Strain measurement of a completely still 1 μm W film-substrate composite lasting for 200 seconds. The uncertainty of ε_{11} is $\pm 1.93 \times 10^{-5}$ at the 95% confidence level.

should be noted that this technique will be used throughout this dissertation, but the full-field measurements are also shown below.

Herein, we demonstrate the full-field displacement and strain measurements when stretching the virgin or uncoated substrates elastically. For the displacement field measurement, the specimen surface (Fig. 2.1(a)) was acquired with a CCD camera (1392 × 1040) combined with 1.0X lens. The image size is about 9×7 mm^2 with a resolution of about 6.6 μm/pixel. In order to demonstrate the speckle pattern and to compare with Correla, a Correli Q4-procedure (Hild and Roux 2006) was used. The size of subsets is 64 × 64 pixels and the step of the uniform grid is also 64 pixels. Fig. 2.13 shows the displacement field in the direction of tension under a certain force. The vertical contour lines indicate a uniform displacement field that is expected for a perfect uniaxial tensile testing of Kapton®. Furthermore, the displacement field agrees well with the one obtained from Correla.

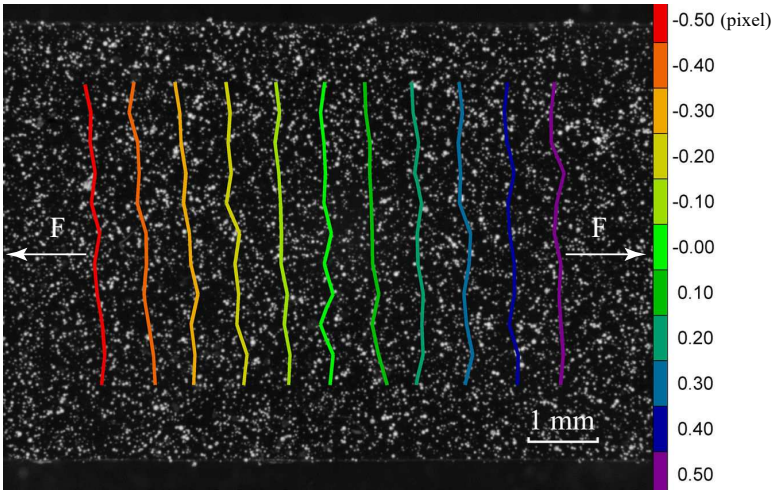

Figure 2.13: Displacement field at a given force. A randon speckle pattern was created by spraying the white paints on the specimen surface. The uniform displacement distribution is clear from the uniform vertical contour lines.

For the strain field measurement, the specimen surface (Fig. 2.1(b)) was acquired with a digital CMOS camera (2560 × 1920 pixels) combined with 0.5X lens. The image size is nearly the same as the one above, i.e. about 9×7 mm^2. Correla was used with the size of subsets being 64×64 pixels and the step of the uniform grid being 16 pixels. The Kapton® was stretched up to 12 N with an image capturing rate of 1 image/sec., and the strain field at each step is shown in Fig. 2.14. As expected, the strain field is uniform as indicated by the homogeneous contour bands under each force.

2.5.2.3 *Effects on precision of strain measurements*

It is well known that there are several essential prerequisites and requirements for the two dimensional DIC displacement/strain measurements:

- The specimen surface should be perfectly or nearly flat, i.e. not sloping in any direction, so that every part is at the same height approximately.
- The specimen mainly experiences in-plane deformation. Even an extremely small out-of-plane displacement can result in an alteration of lens

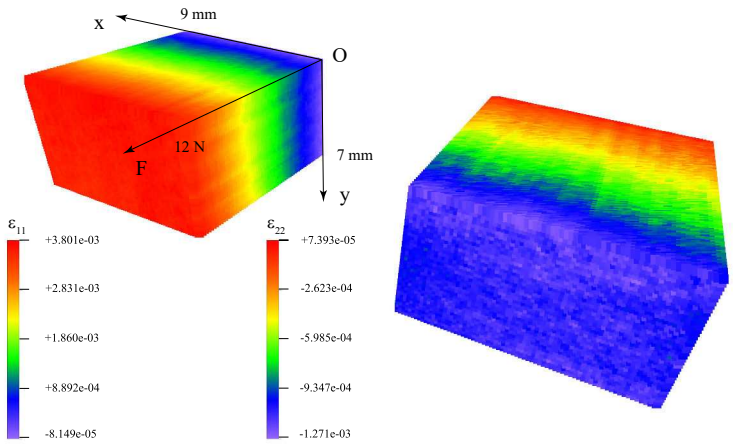

Figure 2.14: Strain field in the longitudinal and transverse direction during the tensile testing. XY plane corresponds to the specimen surface. The contour bands represent the strain values at different loading level, and a uniform strain field is evidenced in both directions.

magnification which will significantly affect the measurement of in-plane displacements. Herein, we use a telecentric lens to achieve magnification constancy.

- The optical axis of a lens is normal to the measured specimen plane, and the lens distortion is negligible [3]. If the off-axis angle is very small (usually $< 5°$), the effects can be disregarded, otherwise a calibration process must be proposed (Helm and Deanner 2004).

After ensuring the basic conditions stated above, various factors should be considered to reduce or avoid the complex influences on DIC measurements and calculations in practical applications. The effects can be classified mainly into two categories, hardware and software, in addition to the external environments as shown in Table 2.2. To go much further, some practical rules for users have been given, and the evaluation of the DIC performance has been done thanks to a collaborative work (Bornert et al. 2009). All these effects

3 Telecentric lens with an extremely low distortion is strongly recommended.

Table 2.2: Factors influencing the precision of DIC measurements

Hardware	Lens depth of field[a], speckle pattern, illumination[b]...
Software	Correlation criteria, shape function, size of subsets...

[a] With telecentric lenses, the image size is left unchanged when the object stays within the depth of field.
[b] Bright and homogeneous illumination is imperative to improve the image contrast and to reduce the statistical noise.

should be carefully taken into account to avoid suffering from the accuracy and precision of DIC measurements.

2.5.3 Applied lattice strain and residual stress measurements

Most thin metal films are polycrystalline with one phase, which consists of single crystals having given orientations with respect to the specimen coordinate system. If the orientations are randomly distributed, the polycrystalline material is quasi-isotropic, in other words, although the constituent crystals usually show an anisotropic behavior on a microscopic scale, the properties are the same in any directions from a macroscopic point of view. If some orientations are preferred, the material is textured and the macroscopic behavior can be anisotropic (Hauk 1997).

APPLIED LATTICE STRAIN The principle of applied strain analysis is based on the measurement of the interplanar spacings of any selected (h k l) set of planes in different directions (Culity 1978). If the specimen is unstressed, the plane spacing is independent of plane orientation. However, this is not true when stress is present. The applied strain along the normal of (h k l) planes can be considered as uniform on the macroscopic scale, producing a shift of the corresponding diffraction peak. Furthermore, the applied strain can also be

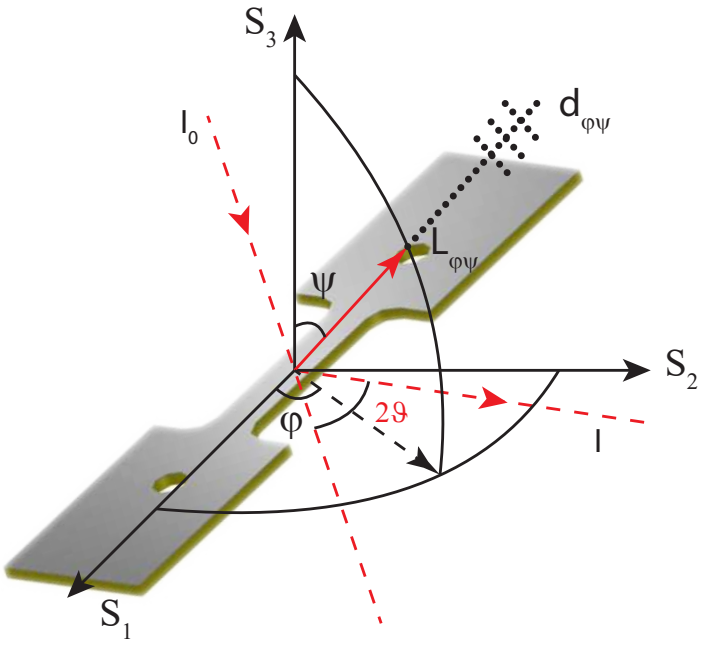

Figure 2.15: Description of the coordinate system for the specimen S_i and the diffraction direction $L_{\varphi\psi}$. The incident beam I_0, diffracted beam I at the diffraction angle 2ϑ, and the diffracting plane normal $L_{\varphi\psi}$ are in the same plane. The sample can be rotated in the diffractometer with φ and ψ.

considered as inhomogeneous on the microscopic scale (microstrain), inducing a broadening of the diffraction peak (Maeder 1986).

For any reflection (h k l) plane, the lattice spacing ($d_{\varphi\psi} = d_{hkl}$) is determined from the angular position ϑ of the diffraction peak thanks to Bragg's law: $\lambda = 2d_{hkl}\sin\vartheta$. These planes are normal to the diffraction vector $L_{\varphi\psi}$ which bisects the incident and diffracted beams (Fig. 2.15). Therefore, the applied strain measured in this direction can be represented by the angles φ and ψ:

$$\varepsilon_{\varphi\psi}^{\text{Appl.}} = \frac{d_{\varphi\psi} - d_0}{d_0} = \ln\left(\frac{d_{hkl}}{d_0}\right) = \ln\left(\frac{\sin\theta_0}{\sin\theta}\right) \tag{2.5}$$

where "Appl." is the written abbreviation of "applied", and d_0 represents the stress-free lattice spacing or any reference interplanar spacing.

On the other hand, $\varepsilon_{\varphi\psi}^{Appl.}$ can be expressed in terms of applied strains $\varepsilon_{ij}^{Appl.}$ $(i,j=1,2,3)$ in the specimen coordinate system S (I. Noyan, T. Huang, and York 1995):

$$\varepsilon_{\varphi\psi}^{Appl.} = \left(\varepsilon_{11}^{Appl.}\cos^2\varphi + \varepsilon_{12}^{Appl.}\sin 2\varphi + \varepsilon_{22}^{Appl.}\sin^2\varphi - \varepsilon_{33}^{Appl.}\right)\sin^2\psi + \varepsilon_{33}^{Appl.} + \varepsilon_{13}^{Appl.}\cos\varphi\sin 2\psi + \varepsilon_{23}^{Appl.}\sin\varphi\sin 2\psi \tag{2.6}$$

Assuming $\varepsilon_{\varphi\psi}^{Appl.}$ to be homogeneous within the penetration depth of the X-rays, $\varphi = 0$ (S_1 corresponds to the loading direction) and $\varepsilon_{i3}^{Appl.} = 0$ $(i = 1,2)$. Combined with Eq. (2.5), the general lattice strain expression Eq. (2.6) becomes:

$$\ln\left(\frac{\sin\theta_0}{\sin\theta_{hkl}}\right) = \left(\varepsilon_{11}^{Appl.} - \varepsilon_{33}^{Appl.}\right)\sin^2\psi + \varepsilon_{33}^{Appl.} \tag{2.7}$$

In this study, Eq. (2.7) was used to measure the applied lattice strain, and the applied stress determination can be achieved applying Hooke's law (Appendix A).

RESIDUAL STRESS If the polycrystalline film experiences in-plane equi-biaxial residual stresses ($\sigma_{11}^{Res.} = \sigma_{22}^{Res.}, \sigma_{33}^{Res.} = 0$) is non-textured or quasi-isotropic, one can substitute the isotropic Hooke's law in Eq. (2.7) and obtain the film residual stresses from the linear "$\varepsilon_{\varphi\psi}^{Res.} - \sin^2\psi$" plot:

$$\ln\left(\frac{\sin\theta_0}{\sin\theta_{hkl}}\right) = \frac{1}{2}S_2(hkl)\,\sigma^{Res.}\sin^2\psi + S_1(hkl)\,2\sigma^{Res.} \tag{2.8}$$

where "Res." is the written abbreviation of "residual", $\frac{1}{2}S_2(hkl)$ and $S_1(hkl)$ are the X-ray elastic constants, and $2\vartheta_0$ denotes the diffraction angle in stress-free state. It should be emphasized that the measurements using XRD always pick up only a small part of all crystallites, i.e. diffracting grains. If the elastic anisotropy of these crystallites is taken into account, this collective may

have different elastic behavior from the macroscopic one. Therefore, the hkl-dependent X-ray elastic constants are utilized rather than bulk ones (Hauk 1997).

On the other hand, if a perfect {111} fiber texture exists in polycrystalline thin films, Neerfeld-Hill model based on Eq. (A.5) and Eq. (A.11) in Appendix A would be preferred:

$$\ln\left(\frac{\sin\theta_0}{\sin\theta_{hkl}}\right) = \frac{s_{44}}{2}\sigma^{Res.}\sin^2\psi + \frac{2s_{11}+4s_{12}-s_{44}}{3}\sigma^{Res.} \tag{2.9}$$

However, the approaches listed above may not be applicable in other textured films, such as a mixture, the use of experimentally measured elastic constants could be the best choice at the present time. You may notice that the stresses and strains are distinguished as "applied" and "residual". Actually, residual stress is a kind of "applied stress" when both using stress-free state as a reference, to put it differently, the reference for residual stress determination corresponds to the stress-free state, while various stress state can be used as a reference for applied stress analysis depending on your object.

2.6 SUMMARY

The uniaxial tensile/compressive testing, DIC true strain measurement and XRD elastic stress/strain determination, which run through this study, are of crucial importance. These techniques have been introduced and discussed in detail in this chapter. Adapting to the Deben MICROTEST, the substrate geometry and the grips for (pre-) stretching have been custom-designed. Meanwhile, the masks for a new form of film deposition, and a setup combining the X-ray diffractometer, one DIC system and the Deben MICROTEST are also developed. Thanks to all these new designs, a large amount of mechanical

properties and microstructures can be studied. Moreover, the residual stresses, texture, α and β phases of W films, can be controlled thanks to our sputtering system, are well described as well as the deposition processes.

BIBLIOGRAPHY

Bamberg, E. et al. "A tensile test device for in situ atomic force microscope mechanical testing". In: *Precision engineering* 30.1 (2006), pp. 71–84 (cit. on p. 40).

Barranger, Y. et al. "Strain measurement by digital image correlation: influence of two types of speckle patterns made from rigid or deformable marks". In: *Strain* 48.5 (2012), pp. 357–365 (cit. on pp. 52, 54, 72).

Belrhiti, Y. et al. "Application of optical methods to investigate the non-linear asymmetric behavior of ceramics exhibiting large strain to rupture by four-points bending test". In: *Journal of the European Ceramic Society* 32.16 (2012), pp. 4073–4081 (cit. on pp. 52, 53, 73).

Bornert, M. et al. "Assessment of digital image correlation measurement errors: methodology and results". In: *Experimental mechanics* 49.3 (2009), pp. 353–370 (cit. on pp. 52, 57).

Culity, B.D. "Elements of X-ray Diffraction". In: *2nd, Addition-Wesley, MA, London* (1978) (cit. on pp. 12, 58).

Dupré, J.C. et al. "Displacement Discontinuity or Complex Shape of Sample: Assessment of Accuracy and Adaptation of Local DIC Approach". In: *Strain* 51.5 (2015), pp. 391–404 (cit. on pp. 52, 54).

Girault, B., D. Eyidi, Ph. Goudeau, et al. "Controlled nanostructuration of polycrystalline tungsten thin films". In: *Journal of Applied Physics* 113.17 (2013), p. 174310 (cit. on p. 49).

Hauk, V. *Structural and residual stress analysis by nondestructive methods: Evaluation-Application-Assessment*. Elsevier, 1997 (cit. on pp. 8, 12, 58, 61, 125).

Helm, J.D. and J.R. Deanner. "Off-axis two-dimensional digital image correlation". In: *Proceedings of 2004 SEM X international congress & exposition on experimental and applied mechanics, Costa Mesa*. 2004, pp. 06–01 (cit. on p. 57).

Hild, F. and S. Roux. "Digital image correlation: from displacement measurement to identification of elastic properties–a review". In: *Strain* 42.2 (2006), pp. 69–80 (cit. on pp. 19, 52, 55, 72).

Maeder, G. "X-Ray Diffraction and Stress Measurement". In: *Chemica Scripta* 26A (1986), pp. 23–31 (cit. on p. 59).

Noyan, I.C., T.C. Huang, and B.R. York. "Residual stress/strain analysis in thin films by X-ray diffraction". In: *Critical Reviews in Solid State and Material Sciences* 20.2 (1995), pp. 125–177 (cit. on pp. 11, 60, 66, 108).

Renault, P.-O. et al. "Deposition of ultra-thin gold film on in situ loaded polymeric substrate for compression tests". In: *Materials Letters* 73 (2012), pp. 99–102 (cit. on pp. 41, 100).

3 DETERMINING THE YOUNG'S MODULUS OF THIN FILMS BY A DUAL DIC SYSTEM

Contents

A new method is proposed to determine the in-plane elastic modulus of thin films. Based on the mechanical analysis of a model with films coated on both sides of a substrate along half of the gauge length, the Young's modulus can be obtained: measuring the strain difference between the films-substrate composite and the uncoated substrate simultaneously during the tensile testing. This agrees well with our numerical simulations (finite element method), and has been verified by the experiments for different film materials thanks to our custom-designed dual DIC system.

3.1 MECHANICAL ANALYSIS

For freestanding films, uniaxial microtensile testing is the most attractive method to obtain mechanical properties (H. Huang and Spaepen 2000; Y. Yang et al. 2008), since the output is interpretable directly without recourse to complicated models. Nevertheless, it is much more challenging for film/substrate structure due to the role of substrate. In this case, thin film is usually deposited on the whole surface of a substrate and several stress/strain analyses have been done (Faurie, Renault, Le Bourhis, and Ph. Goudeau 2005; I. Noyan, T. Huang, and York 1995). In the present work, thin films will be deposited on both sides of a substrate under the same experimental condition to obtain a flat surface regardless of the residual stresses and to increase the contribution of thin films. For multi-layered materials, Yin and Prieto-Muñoz (Yin and Prieto-Muñoz 2013) derived the displacement field for both coatings and substrate using plane strain elastic theory. Nonetheless, it is quite complex to apply in practice.

Herein, we propose a simple approach to extract the elastic constants and stress field. Fig. 3.1 schematically shows our model that includes films coated on both sides and half surface of the substrate. The composite is subjected to a uniaxial tension along S_1 axis. ε_c and ε_v are the strains of films/substrate composite and virgin (uncoated) substrate respectively, and are considered uniform in sections far away from edges. It is assumed that all points of a given plane remain in the same plane during the tensile testing. It should be noted that in the elastic regime, a complete strain transfer through a film/substrate interface is experimentally observed (Geandier et al. 2010; Djaziri et al. 2014). In other words, the film and substrate do not slip each other and the strain in the film is consistent with the one in the substrate. This will be also inspected using our custom-designed apparatus. Furthermore, both films and substrate are under plane stress condition considering the tiny thickness compared with

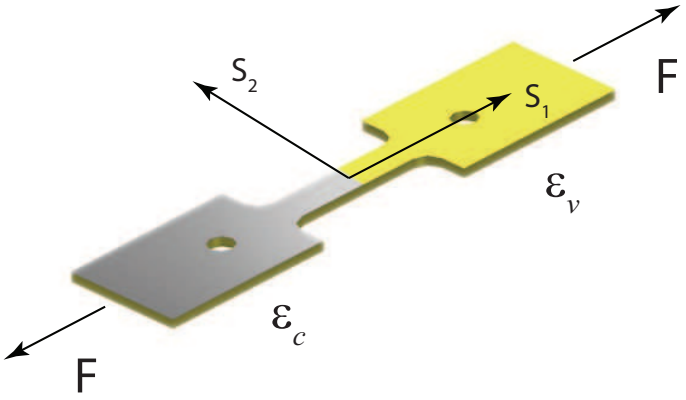

Figure 3.1: Schematic illustration of one dogbone shaped specimen with films coated on both sides and half surface of a substrate. The left section is film/substrate composite, and the right part is the virgin substrate. S_1 and S_2 axis corresponding to loading and transversal direction respectively. ε_c and ε_v represent the applied strain of each section.

the other dimensions. For multilayer section, the resultant force along longitudinal or transversal direction is the sum of the forces exerted on thin films and substrate in the same direction. If both thin films and substrate are homogeneous and isotropic or transversally isotropic materials, after applying the Hooke's law, the mechanical behavior in the elastic domain can be expressed as follows:

$$\begin{cases} (\varepsilon_c)^s_{11} = \dfrac{(\sigma_c)^s_{11} - \nu_s\,(\sigma_c)^s_{22}}{E_s} \\ (\varepsilon_c)^s_{22} = \dfrac{(\sigma_c)^s_{22} - \nu_s\,(\sigma_c)^s_{11}}{E_s} \\ (\varepsilon_c)^s_{11} = (\varepsilon_c)^f_{11} = \dfrac{(\sigma_c)^f_{11} - \nu_f\,(\sigma_c)^f_{22}}{E_f} \\ (\varepsilon_c)^s_{22} = (\varepsilon_c)^f_{22} = \dfrac{(\sigma_c)^f_{22} - \nu_f\,(\sigma_c)^f_{11}}{E_f} \\ 0 = (\sigma_c)^s_{22}\,t_s + (\sigma_c)^f_{22}\,t_f \\ (\sigma_v)^s_{11}\,t_s = E_s\,(\varepsilon_v)^s_{11}\,t_s = (\sigma_c)^s_{11}\,t_s + (\sigma_c)^f_{11}\,t_f \end{cases} \tag{3.1}$$

where the subscripts c and ν correspond respectively to the films/substrate composite and the virgin substrate, superscripts f and s denote films and substrate respectively. The subscripts 11 and 22 are related to the longitudinal and transversal directions, σ and ε denote applied stresses and strains, t the thickness and E, ν the Young's modulus and Poisson's ratio respectively. Solving these equations, the elastic constants of thin films and applied stresses on films and substrate are found to be:

$$\begin{cases} E_f = \dfrac{[(\nu_s-1)(\varepsilon_\nu)^s_{11}+(\varepsilon_c)^s_{11}+(\varepsilon_c)^s_{22}][(\nu_s+1)(\varepsilon_\nu)^s_{11}-(\varepsilon_c)^s_{11}+(\varepsilon_c)^s_{22}]E_s t_s}{\left[((\varepsilon_c)^s_{11})^2-((\varepsilon_c)^s_{22})^2+\left((\nu_s)^2-1\right)(\varepsilon_\nu)^s_{11}(\varepsilon_c)^s_{11}\right]t_f} \\ \nu_f = \dfrac{\nu_s\left[((\varepsilon_c)^s_{11})^2-((\varepsilon_c)^s_{22})^2\right]+\left(1-(\nu_s)^2\right)(\varepsilon_\nu)^s_{11}(\varepsilon_c)^s_{22}}{((\varepsilon_c)^s_{11})^2-((\varepsilon_c)^s_{22})^2+\left((\nu_s)^2-1\right)(\varepsilon_\nu)^s_{11}(\varepsilon_c)^s_{11}} \\ (\sigma_c)^f_{11} = \dfrac{E_s t_s}{t_f}\left[(\varepsilon_\nu)^s_{11}-\dfrac{(\varepsilon_c)^s_{11}+\nu_s(\varepsilon_c)^s_{22}}{1-(\nu_s)^2}\right] \\ (\sigma_c)^f_{22} = \dfrac{-E_s t_s(\nu_s(\varepsilon_c)^s_{11}+(\varepsilon_c)^s_{22})}{t_f\left(1-(\nu_s)^2\right)} \\ (\sigma_c)^s_{11} = \dfrac{E_s((\varepsilon_c)^s_{11}+\nu_s(\varepsilon_c)^s_{22})}{1-(\nu_s)^2} \\ (\sigma_c)^s_{22} = \dfrac{E_s(\nu_s(\varepsilon_c)^s_{11}+(\varepsilon_c)^s_{22})}{1-(\nu_s)^2} \end{cases} \tag{3.2}$$

However, these formulas are tricky to apply in practice, since the elastic limit (ε_{11}) of thin metal films on polymer substrates are rather small ($< 0.5\%$) in many cases (Djaziri et al. 2014). Furthermore, large accumulation of errors will be introduced in the calculation of elastic constants. While, from another point of view, it is interesting to know not only the difference between $(\varepsilon_c)^f_{11}$ and $(\varepsilon_\nu)^s_{11}$, but also its relationships with other important quantities, such as

the stresses in films. In order to obtain the elastic modulus precisely, another way is proposed based on Eq. (3.1):

$$\frac{E_f t_f}{E_s t_s} = \frac{(\varepsilon_v)^s_{11}}{(\varepsilon_c)^f_{11}} + \frac{\nu_f - \nu_s}{1-(\nu_s)^2}\frac{(\varepsilon_c)^f_{22}}{(\varepsilon_c)^f_{11}} - \frac{1-\nu_f\nu_s}{1-(\nu_s)^2} \tag{3.3}$$

If $\nu_f = \nu_s$, Eq. (3.3) is simplified to

$$\frac{E_f t_f}{E_s t_s} = \frac{(\varepsilon_v)^s_{11}}{(\varepsilon_c)^f_{11}} - 1 \tag{3.4}$$

It is straightforward that $(\varepsilon_c)^f_{22}/(\varepsilon_c)^f_{11}$ is linear in the elastic domain (Faurie, Renault, Le Bourhis, and Ph. Goudeau 2005), so as $(\varepsilon_v)^s_{11}/(\varepsilon_c)^f_{11}$. In general, on the basis of Eq. (3.3), the Young's modulus of thin films can be easily extracted knowing the thickness and Poisson's ratio of the films and substrate, and also the substrate's elastic constants. However, we will show that the difference of Poisson's ratio does not play a significant role and Eq. (3.4) can be used to get elastic modulus in many practical cases.

3.2 FINITE ELEMENT METHOD (FEM)

To demonstrate the feasibility of Eq. (3.4) and to examine the role of Poisson's ratio mismatch, finite element method was used in ABAQUS to mimic the tensile testing in the elastic regime. In the case of isotropic thin films, 500 nm W films were coated on both sides of a substrate over half of the gauge length. The substrate was also regarded as isotropic, and the polycrystalline characters of thin films were not taken into account. The Young's modulus and Poisson's ratio of the substrate were 4.0 GPa and 0.34 respectively as measured in the experiments. For thin films, bulk values (396 GPa and 0.29) were taken.

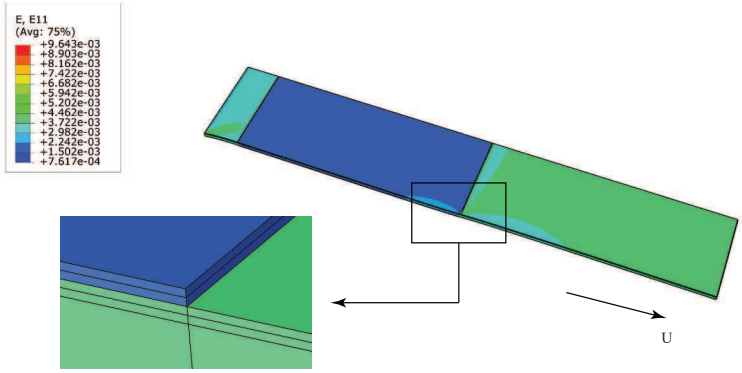

Figure 3.2: Applied longitudinal strain distribution of films and substrate. The structure is fixed at one end with displacement U (45 μm) applying at the other end. The mesh through thickness direction is also shown. Evidently, the strain in virgin substrate is larger than in composite as expected.

In this model, 3D brick elements (C3D8R) were used for films and substrate. Due to the tiny thickness, the films were discretized with only two elements along thickness direction. While for substrate, there are ten layers of elements with the first two being the same as films (Fig. 3.2). Films and substrate were bonded together at their coincident nodes using a tie constraint to obtain strong adhesion. In order to reduce the amount of elements, only half of the entire structure was modeled considering the symmetry, and the in-plane film size was 7×3 mm^2. The model was fixed at one end, and displacement (45 μm) was applied at the other end. After the calculations, the average strains of the elements in central section of thin films were $(\varepsilon_c)^f_{11} = 2.12 \times 10^{-3}$, $(\varepsilon_c)^f_{22} = -6.74 \times 10^{-4}$; and $(\varepsilon_v)^s_{11} = 3.82 \times 10^{-3}$, $(\varepsilon_v)^s_{22} = -1.31 \times 10^{-3}$ for the virgin substrate. Referring to Eq. (3.4), Young's modulus was obtained to be 401 GPa which is quite close to the bulk value (2% difference).

To examine the role of Poisson's ratio mismatch, it is necessary to use Eq. (3.3). A value of 400.5 GPa was obtained which is in accordance with the value obtained using Eq. (3.4). This indicates that Eq. (3.4) can be used to extract the Young's modulus of thin films even if the difference of Poisson's ratio between

Table 3.1: Nickel elastic constants used for Lamina options in ABAQUS. The unit of the Young's modulus and the shear moduli is MPa.

E1	E2	Nu12	G12	G13	G23
242917	242917	0.38	88019	65456	65456

films and substrate (~15%) is large. This will be also checked by experimental measurements.

In the case of transverse isotropy, we take the perfect {111} fiber-textured nickel film as an example. The procedure is akin to the isotropic case stated above, but the "type of elastic" in ABAQUS must be changed to "Lamina", and the 3D-shell elements are set for the film since "Lamina" can be only used with plane stress elements. Furthermore, the elastic constants are selected from the inverse of Eq. (A.12), i.e. the compliance matrix, and with a simple transformation[1], the parameters in ABAQUS can be obtained as shown in Table 3.1.

Similarly, the average strains of the elements in central section of thin films can be calculated as $(\varepsilon_c)^f_{11} = 2.40 \times 10^{-3}$, $(\varepsilon_c)^f_{22} = -8.52 \times 10^{-4}$; and $(\varepsilon_v)^s_{11} = 3.56 \times 10^{-3}$, $(\varepsilon_v)^s_{22} = -1.22 \times 10^{-3}$ for the virgin substrate. After applying the simplified formula (Eq. (3.4)), the in-plane Young's modulus is 241.7 GPa which agrees well with the input value. If Eq. (3.3) was used, the elastic modulus will be 241.3 GPa. Obviously, the Poisson's ratio mismatch does not play a role.

In short, the feasibility of our new approach based on the longitudinal strain difference to get the in-plane Young's modulus of thin films is demonstrated from both theoretical and numerical points of view. The effect of the Poisson's ratio mismatch is verified to be negligible by the finite element method.

1 In-plane Young's modulus: $1/\tilde{s}^p_{11}$, Poisson's ratio: $-\tilde{s}^p_{12}/\tilde{s}^p_{11}$.

3.3 DEVELOPMENT OF A DUAL DIC SYSTEM COMBINED WITH THE TENSILE TESTING

3.3.1 Experimental approach and true strain measurements

As previously stated, in the case of microtensile testing, DIC is an efficient method for strain measurement. It is a full-field, non-contact optical technique which allows imaging deformation heterogeneities during a testing. The displacement fields are obtained by measuring the similarity degree of subset series between the images corresponding to an unloaded state and the deformed state (Hild and Roux 2006; Besnard, Hild, and Roux 2006; Barranger et al. 2012). To track changes in images, good surface contrast is essential. Sometimes, the natural contrast is enough, while in most cases, an artificial pattern with a random distribution of speckles is necessary by spraying paints on the sample surface. In this study, both films and substrate were stretched with speckle patterns on the surfaces.

In order to measure the strains of the composite and the virgin substrate simultaneously, a dual DIC system is developed as shown in Fig. 3.3. One DIC system is mainly composed of a telecentric lens, a camera and illumination. To acquire better digital images and to reduce measurement errors, a stable and uniform light source is necessary and a telecentric lens is preferred to have constant magnification and geometry. 1.0X and 0.5X gold series telecentric lenses with large depth of field from Edmund were utilized. The light system for 1.0X lens is a standard working distance LED ring light from Edmund, while the one for 0.5X lens is a flexible fiber optic light called model 21 dc from TechniQuip. It is noteworthy that Kapton® is translucent which can cause significant light interplay between the two DIC systems. Thanks to the polarizers and the flexible fiber light with a low incidence angle relative to

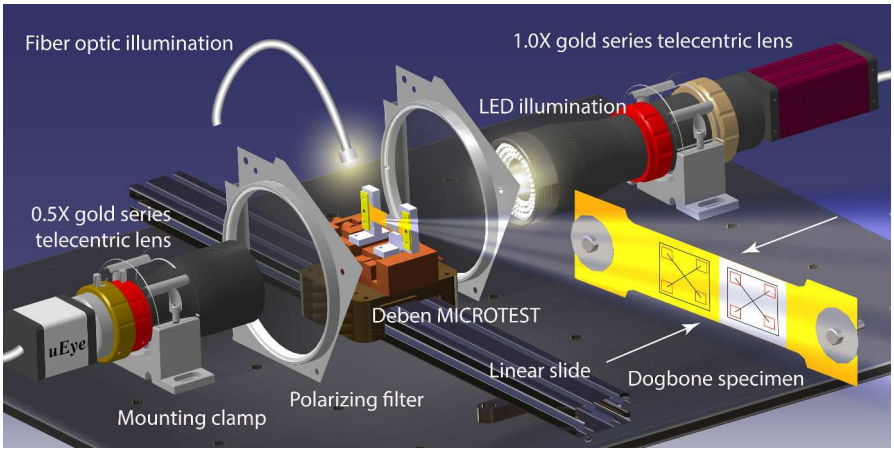

Figure 3.3: The experimental setup which combines a dual DIC system with the Deben MICROTEST: the 0.5X lens is focusing on the films/substrate composite, while 1.0X lens on the virgin Kapton®. The four subsets for calculations in each section are shown in the enlarged view of the dogbone specimen.

the specimen surface, the interaction between respective DIC systems can be neglected. We also employ two cameras with different resolutions to record images. One is a digital 8-bit CMOS camera (2560×1920 pixels) combined with 0.5X lens, the other one has 1392×1040 pixels with 1.0X lens. Importantly, the captured in-plane size of the specimen by them is similar which is about 9×7 mm^2 . Moreover, the acquisition frequency is 1 image every 2 seconds using the software Deftac (Belrhiti et al. 2012).

During the tensile testing, DIC system with 0.5X lens is monitoring the center of films/substrate composite and the other one the virgin substrate to measure their strains. Meanwhile, this allows direct measurement of the stress-strain characteristics of Kapton® instead of relying on the manufacturer's data. However, the force value is not reliable as mentioned in Section 2.2, a new design would be interesting in the future. After capturing the images simultaneously, the DIC software Correla was used to calculate the displacements and strains. This method can achieve a resolution up to $\Delta\varepsilon = 0.5 \times 10^{-4}$. For composite, four subsets with a size of 64×64 pixels were used. The distance

between subsets are 1200 pixels in the horizontal direction and 1000 pixels in the vertical direction, while for virgin Kapton®, it is 700 pixels in the horizontal direction, 550 pixels in the vertical direction (Fig. 3.3).

It is important to point out that, the dual DIC system is flexible that the position of each telecentric lens can be translated. In this mode, it is possible to study the strain transfer along the thickness direction when simultaneously monitoring the same zone in each specimen plane.

3.3.2 Validation of the home-made system

Before going further, it is crucially necessary to check the validity of the new experimental setup. As a standard specimen, a Kapton® substrate (Fig. 2.1(b)) is coated with continuous black paints on both sides, and then white speckles were sprayed to have a good surface contrast. Initially, the specimen was stretched up to 5 N to keep itself flat and to decrease the experimental errors due to the sample manipulation. Then the tensile testing was started to synchronize with the optical image acquisitions. The grips in Fig. 2.3 was used, and the tensile speed was fixed to 0.2 mm/min which corresponds to a strain rate value of 4.1×10^{-5} s^{-1}. 0.5X telecentric lens was used for monitoring one side of the specimen, and 1.0X lens for the other side. As can be seen in Fig. 3.4, the position of lenses are different and the strains captured by the DIC systems are identical (Fig. 3.4). This indicates a high reliability of the dual DIC system considering the fact that the strain is homogeneous along the gauge length. It should be noted that the thirtieth image was selected as a reference for strain calculations to further decrease the experimental errors (see Section 3.4.3). The experimental results in Fig. 3.4(a) and Fig. 3.4(b) are, respectively, the basis of Young's modulus measurements and strain transfer investigations which will be discussed in later sections.

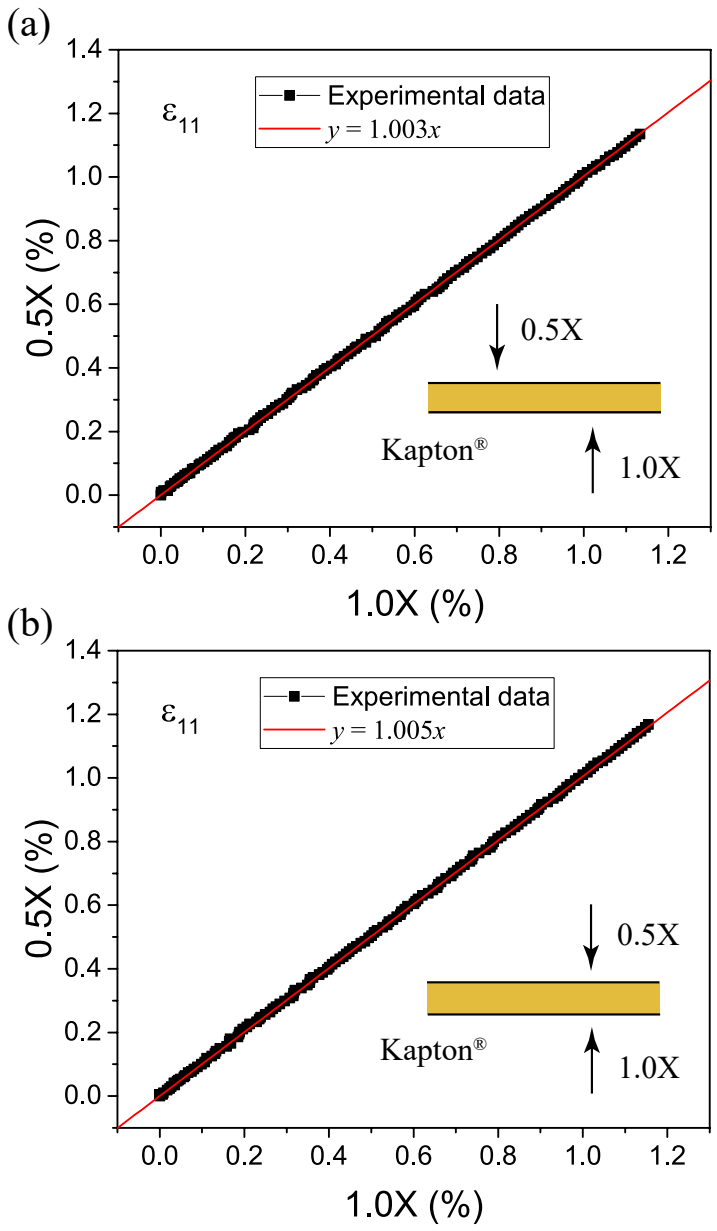

Figure 3.4: Validity of the dual DIC system: longitudinal applied strains ε_{11} measured by DIC technique on the two sides of a virgin Kapton® substrate, i.e. 0.5X telecentric lens for one side versus 1.0X lens for the opposite side. The red straight line is the linear fit.

Table 3.2: Overview of the investigated films.

Element	Ar flow (SCCM)	Expected thickness (nm)	Measured thickness (nm)	Residual stress (GPa)	texture
W[a]	22	50	38.6 ± 0.3[c]	1.04 ± 0.05	α-W {110}
	22	100	77.2 ± 0.6	0.79 ± 0.05	β-W {200}/α-W {110}
	22	200	154 ± 1	1.7 ± 0.1	β-W {200}
	22	400	309 ± 2	1.1 ± 0.1	α-W {110}
	25	500	405 ± 5	1.2 ± 0.2	β-W {200}
	22	800	619 ± 5	1.8 ± 0.1	β-W {200}
	22	1000	774 ± 6	0.47 ± 0.01	α-W {110}/β-W {200}
Cu[b]	10 & 5	1000	899 ± 29	-0.11 ± 0.04	{111}
Ni[b]	10 & 5	500	447 ± 1	-1.04 ± 0.04	{111}

[a] Magnetron sputtered in PUMA.
[b] Ion-beam sputtered in NORDIKO: gun & neutralizer gas flow
[c] Measured by a reflectometry, and others are determined by the DEKTAK IIa profilometer.

3.4 STRAIN TRANSFER THROUGH INTERFACE AND THE CURVATURE EVOLUTION DURING A TENSILE TESTING

3.4.1 Characteristics of as-deposited thin films

There may be many factors which could affect the strain transfer from a substrate to a thin film, such as the interfacial adhesion, film thickness and residual stresses. Therefore, thin films with different materials and thicknesses have been prepared. As can be seen in Table 3.2, the measured film thickness is always smaller than the expected value since the deposition rate values are overestimated. For conciseness, the expected values are used for illustrations while the measured thickness for experimental analysis.

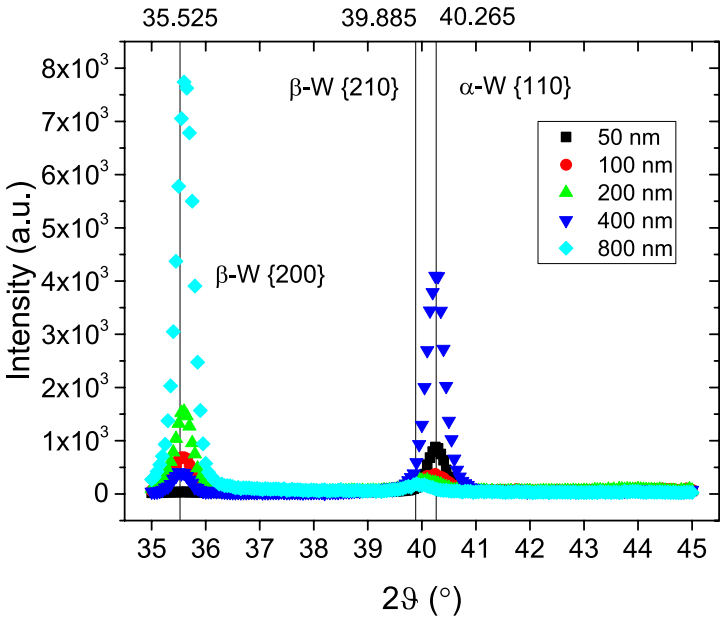

Figure 3.5: Evolution of tungsten phase with various deposition time or thickness under the same Ar gas flow of 22 SCCM.

Similar to the characterization in Section 2.4, the X-ray diffraction patterns of W films with various thicknesses are plotted in Fig. 3.5. The film depositions were performed under the same pressure (0.95 Pa) with a gas flow rate of 22 SCCM. Obviously, both α-W and β-W phase exist.

3.4.2 Strain transfer from the substrate to films with various materials and thicknesses

In this study, complete strain transfer from substrate to film is absolutely vital for the experimental determination of Young's modulus and the cyclic testing. Herein we will investigate the strain transfer mechanism using various thin metallic films. Moreover, considering the small strain range, the film-substrate

composite will be perceived as fully bonded when the strain difference is less than 5%.

For the brittle W films with thickness varying from 50 nm to 1 μm deposited on one side of the Kapton® substrate, the applied strains on the thin films and substrates are measured simultaneously by our dual DIC system. The 0.5X telecentric lens is monitoring the surface of thin films, and 1.0X lens for substrates. The central zone of interest for strain calculation is indicated by the arrows in the inserts (Fig. 3.6). Before starting the image acquisition, all the specimens were pre-strained up to 5 N. Then the tensile speed was set to be 0.2 mm/min, image acquisition rate being 1 image/2 seconds. The tensile testing and image capture are synchronous throughout each experiment.

As can be seen in Fig. 3.6(a)-(e), the longitudinal applied strain of thin films are measured as a function of that of the substrates, and all curves are plotted to the same scale. A continuous and consistent deformation (the slope of each linear fit is ~ 1, difference: < 4%) through the film/substrate interface is clear for applied strain smaller than 1.2%. In order to see whether this strain transfer behavior still exists in a thicker film within larger strain domain, a 1 μm W film coated on the Kapton® substrate was stretched up to ~ 1.7% (Fig. 3.6(f)). Similarly, the strain is identical on both sides of the film-substrate composite. Noteworthy, these observations hold in the complete applied strain range regardless of the thin films' thickness, residual stress and microstructure.

It is also interesting to verify this behavior when the material properties of thin films are different, such as the ductile and brittle materials. For 1 μm Cu, 500 nm Ni and 500 nm Cr, the same phenomenon, i.e. a complete strain transfer through the film-substrate interface, is observed as shown in Fig. 3.7(a)-(c). On the other hand, if films are coated on both sides of a substrate as done in this study to measure the thin films' Young's modulus and to perform the cyclic testing, it is also needed to examine the strain difference in respective

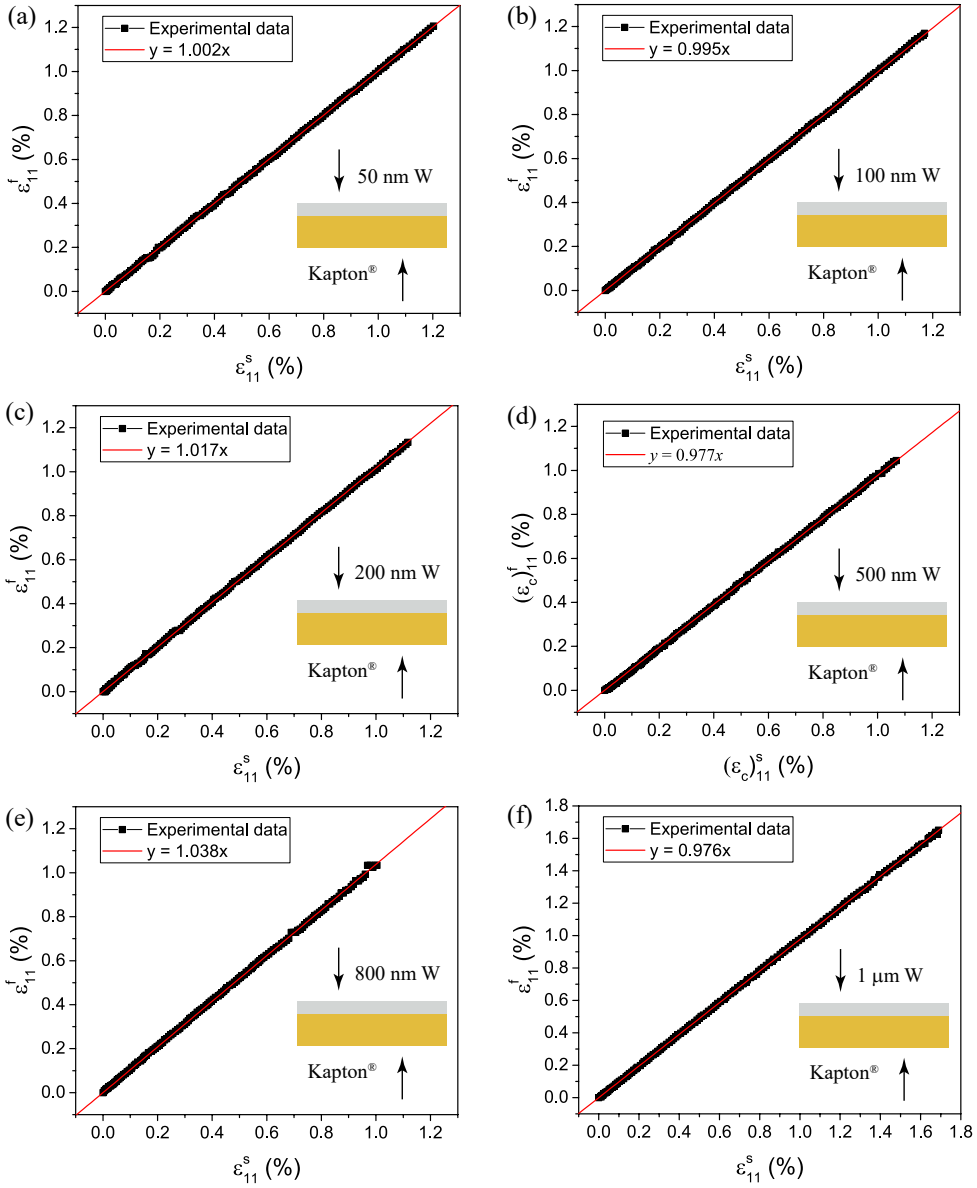

Figure 3.6: Applied strain transfer through interface for thin W films of different thickness deposited on one side of Kapton®: longitudinal applied strain measured in thin films versus longitudinal applied strain measured in the substrates. All curves are plotted to the same scale except the last one for 1 µm W film. The continuous red lines correspond to the linear regression.

films. As shown in Fig. 3.7(d), 400 nm W films are deposited on both sides of a substrate, and the strains are still consistent with each other.

From all these experiments, we can consider that the strain distribution through the thickness of film-substrate composite is uniform even in a relatively large strain domain ($\sim 1.9\%$) which is far beyond the elastic limit (Djaziri et al. 2014). It is evident that channel cracks appear in 1 μm W and 500 nm Cr from the digital images, indicating a cohesive failure (Wojciechowski and Mendolia 1991). However, for W ($\leqslant$ 200 nm), Ni (500 nm) and Cu (1 μm) films, no cracks can be seen. This may be due to the size effect in W films and the ductility of Ni and Cu films, or owing to the insufficient magnification of the telecentric lens and camera. Indeed, the evolution of damages such as cracks in thin films can be captured by DIC analysis if the image resolution is much better than the present one (Roland et al. 2011). Further study on the various cracking behavior may be interesting. Moreover, we conclude that the central sample surface is kept practically flat during the tensile testing, otherwise the strains of the films and substrate should be entirely distinct (Section 3.4.3).

In summary, the macroscopic applied strain transfer through interface is only controlled by the interfacial adhesion in our case. When the interface is perfect, no slipping exists and the film deforms in accordance with the substrate whatever the film thickness ($\leqslant$ 1 μm), inelastic properties, microstructure and residual stresses.

3.4.3 Curvature evolution measurements by an optical three-dimensional profiler

As stated above, many techniques based on the tensile testing assume a flat specimen surface. However, this may not be true if the setup configuration and the biaxial stress state of thin films (Poisson's ratio mismatch) are consid-

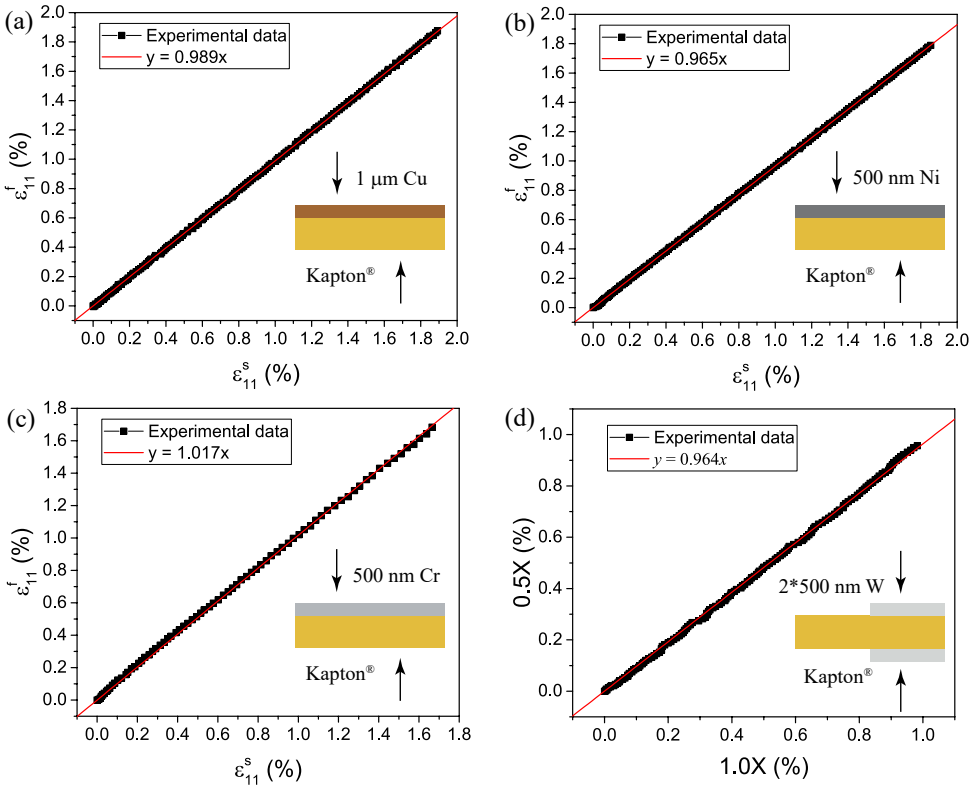

Figure 3.7: Applied strain transfer. (a) Longitudinal applied strain measured in thin film versus longitudinal applied strain measured in the substrate for 1 µm Cu deposited on one side of Kapton®. (b) 500 nm Ni on one side of Kapton®. (c) 500 nm Cr on one side of Kapton®. (d) Longitudinal applied strain in thin film on one side (labeled 0.5X) versus longitudinal applied strain in thin film on the other side (labeled 1.0X) for 400 nm W films coated on both sides of Kapton®. The continuous red lines correspond to the linear regression.

ered, especially when the substrate is pretty soft as Kapton®. Herein, we will investigate the curvature evolution of film-substrate composite by means of Talysurf CCI 6000, one of the world's highest resolution automated optical 3D profiler.

The Talysurf CCI is an advanced non-contact tool combining the surface imaging quality of a microscope with the high accuracy measuring capability of a surface profiler. Taylor Hobson's patented coherence correlation interferometry (CCI) technology provides ultra high resolution interferometric measurements (Conroy and Armstrong 2005). In this study, 10X lens with a measurement area of 1.8×1.8 mm^2 is selected. This configuration has the ability to offer a true topographical representation of a surface with 0.01 nm vertical resolution and 1.75 µm lateral resolution.

In order to observe the 3D surface evolution of thin films' full central section under biaxial stress state, and to reduce the optical scanning time, 500 nm W film deposited on one side of the Kapton® substrate (Fig. 2.1(a), width: 6 mm) was used. The tensile testing was performed step by step (9 steps in total) with a strain rate of $\sim 2.2 \times 10^{-4}$ s^{-1}. Thanks to the advanced data stitching technique, the specimen surface topography ($\sim 11 \times 6$ mm^2) with over 1,000,000 data points can be obtained between each loading step.

Six successive 3D surfaces are shown in Fig. 3.8: the specimen was pre-stretched to 3 N, and finally strained to 65 N. However, the force cannot be used for a precise analysis due to the stress relaxation of the Kapton® substrate. From this intuitive and vivid demonstration, we can see that the surface in the longitudinal direction is becoming flat. While in the transverse direction, the surface is changing gradually from concave to convex. To have a more accurate investigation, the mean profiles at each given load are necessary in both directions.

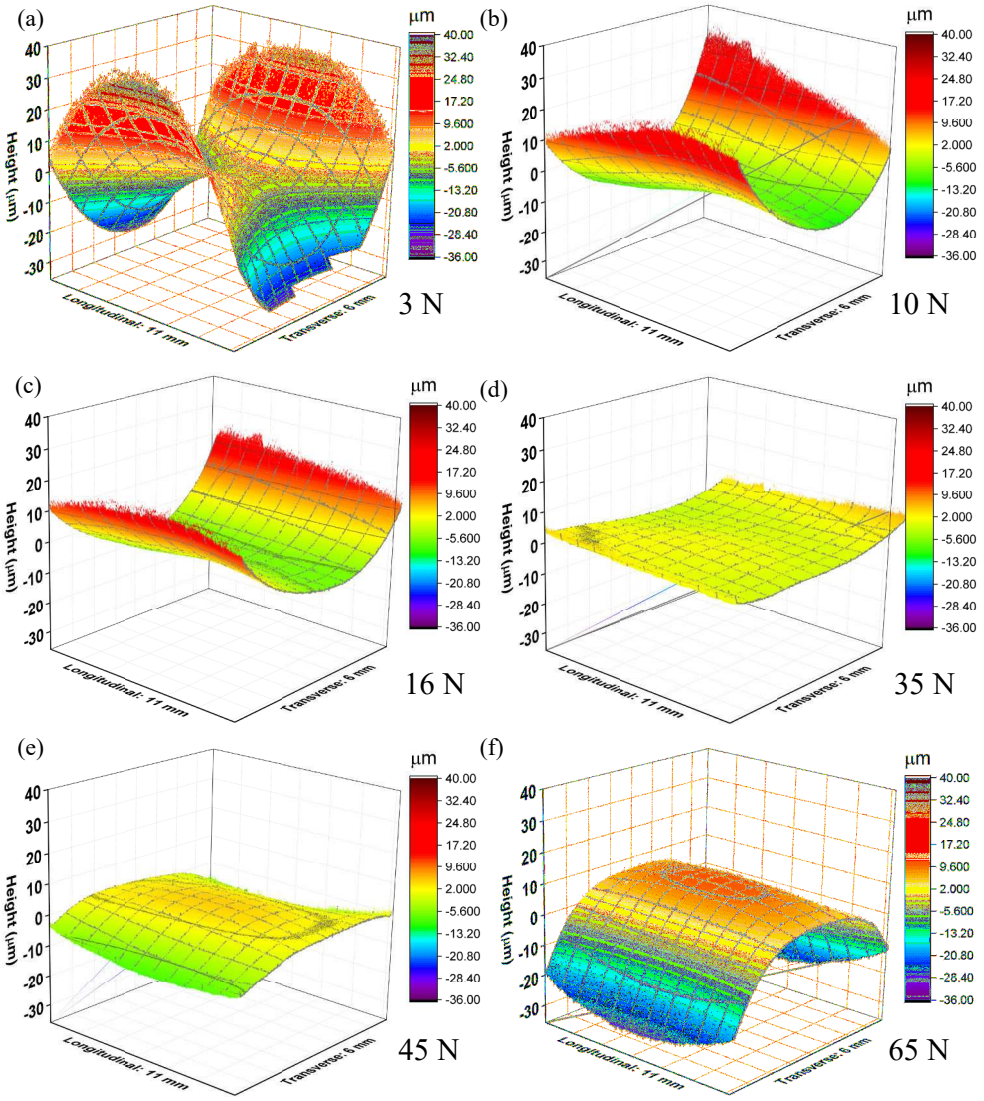

Figure 3.8: The progressive development of 500 nm W film's 3D surface during a tensile testing. All the color map surfaces are plotted to the same scale.

In Fig. 3.9, the longitudinal and transverse profiles at each load are plotted as the average in the surface center of $\sim 10 \times 2$ mm^2 and $\sim 6 \times 3$ mm^2 respectively. It is clear that all the curves except the initial one (Fig. 3.9(a)) are extremely flat especially in the central length (~ 7mm). This is not surprising if the slender cylinders and the setup configuration (Section 2.1) are considered. It is based on this observation that we always pre-stretch the specimen up to 5 N and monitor the center of film-substrate composite. In this way, the effects of height alteration on DIC measurements will be minimized and negligible.

However, this will not be the case in the transverse direction: as a result of Poisson's ratio mismatch (W film: 0.28, Kapton® substrate: 0.34), a compressive transverse film stress is introduced. As can be seen in Fig. 3.9(b), the profile is initially concave due to the tensile residual stress. After loading up to 35 N, it becomes completely flat, and transforms to the inverse shape (convex) when continuing the tensile testing. It is interesting to notice that all the curves cross at points A and B. Moreover, the curvature evolution is the sign of stress evolvement, the achievement of stress based on the curvature would be attractive. Evidently, even in the sample center, the height difference is more than 20 µm which may affect the precision of XRD measurements, since it is very sensitive to the out-of-plane displacement. But this is insignificant for DIC measurements because the telecentric lens' depth of focus is as large as 500 µm. On the other hand, the existence of curvature could make the experimental data deviate from the theoretical analysis. Accordingly, thin films are deposited on both sides of a substrate to maintain it flat during the tensile testing.

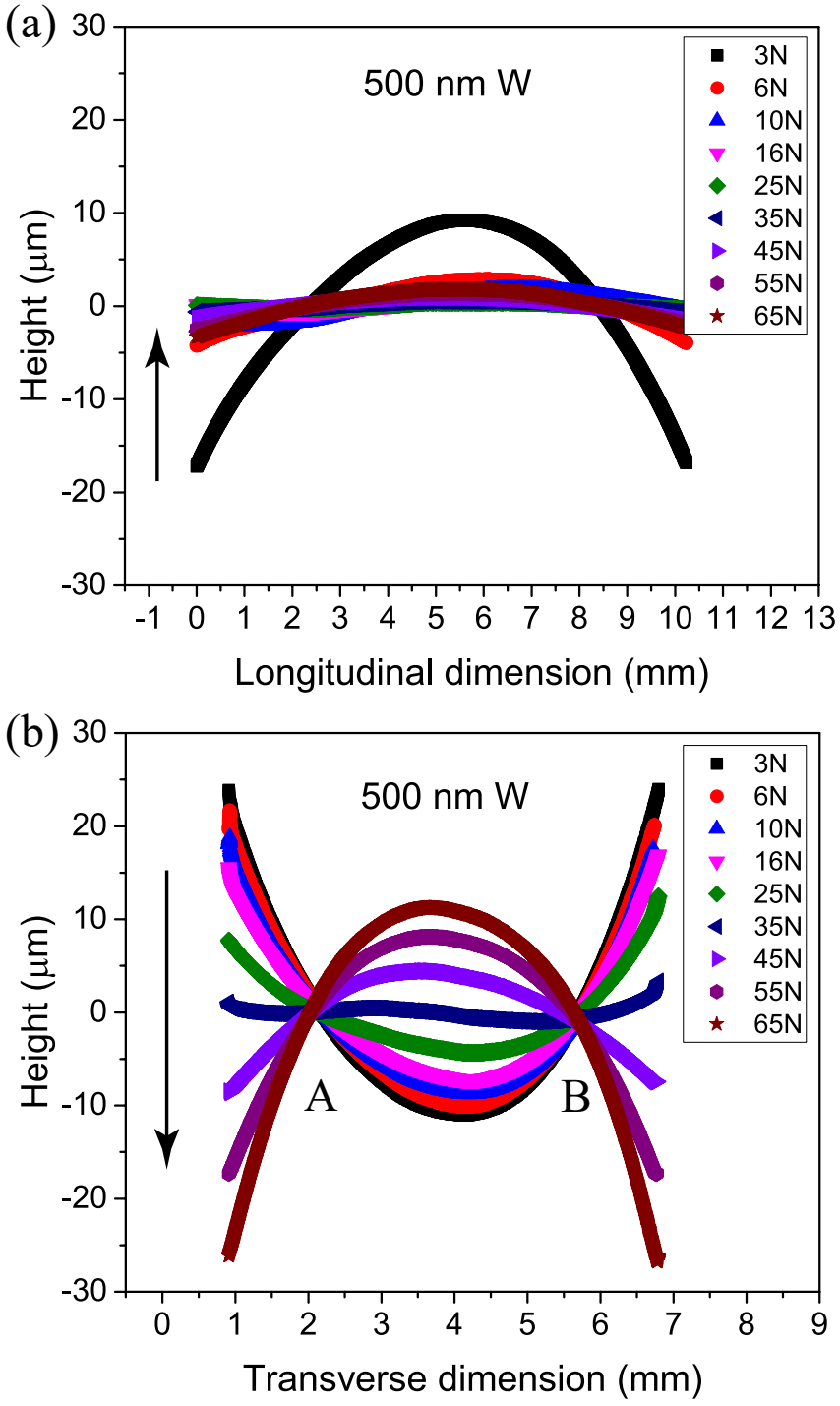

Figure 3.9: Curvature evolution for 500 nm W deposited on one side of the Kapton® substrate during the tensile testing. (a) Profiles in longitudinal direction (~ 10 mm). (b) Profiles in transverse direction (~ 6 mm). Each curve corresponds to a mean profile in the center region of ~ 10×2 mm^2, ~ 6×3 mm^2 at a given load.

3.5 YOUNG'S MODULUS DETERMINATION OF VARIOUS THIN METAL FILMS COATED ON BOTH SIDES OF KAPTON®

Thick W films (measured thickness: 405 ± 5) have been deposited on both sides of Kapton® over half of the gauge length. The applied strain of virgin kapton® along the loading direction and the transversal applied strain in the films as a function of longitudinal films strain are plotted in Fig. 3.10. The experimental data of the two plots may be separated into two regimes: a linear behavior for smaller applied strains, and then after a transition domain, another linear behavior at larger applied strains. The two plots clearly show that the presented measurements may help to capture the elastic limit. Linear regressions have been performed in the elastic domain of W films which is $\sim 0.2\%$ in the present case. It should be pointed out that the load cell and electrical parts do not work well in this experiment which leads to a smaller force output compared with other measurements, i.e. about half of the given load. Accordingly, all the elastic limits stated in this study correspond to an applied strain regime. However, the true elastic limit can be obtained easily since all the measurements were started at 5 N, and all present a linear elastic behavior.

As verified by the numerical analysis in Section 3.2, the effect of Poisson's ratio mismatch can be investigated. Assuming the Poisson's ratio of W films is 0.29, and using the slope value of -0.37 in Fig. 3.10(b), the sum of the second and third items in Eq. (3.3) is -0.999. Obviously, the effect of Poisson's ratio mismatch can be neglected, although the difference of Poisson's ratio of films and substrate is relatively large in the present study (0.29 for the films and 0.34 for a substrate).

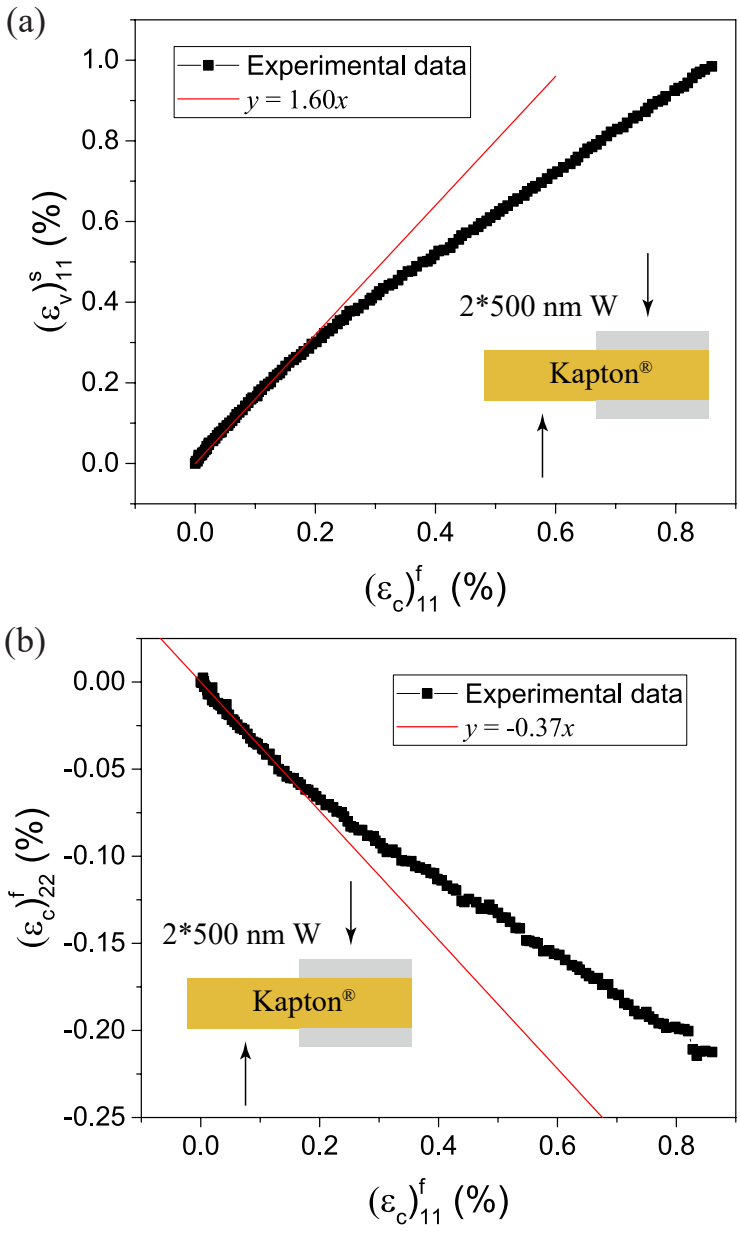

Figure 3.10: Determination of Young's modulus. (a) Longitudinal applied strain on virgin Kapton® as a function of the longitudinal applied strain on W-Kapton®-W composite. (b) Transversal applied strain versus longitudinal applied strain on W-Kapton®-W composite. Both red straight lines are the linear fits when longitudinal applied strain of film-substrate-film composite is ~ 0.2%.

Hence Eq. (3.4) can be used, and with the slope value of 1.60 ± 0.02 (Fig. 3.10(a)) and substrate's elastic characteristics of 4.0 ± 0.2 GPa and 0.34 (obtained from other measurements on Kapton® due to the unreliable force value here, please see Section 2.2), the Young's modulus is found to be 370 ± 20 GPa. This experimental value for the W films agrees well with the bulk value of 396 GPa. The difference may be explained by grain boundaries' contribution related to the presence of nanometric grain sizes and also to the presence of β-W phase.

Moreover, it is interesting to notice that after a transition from elastic to inelastic state of films, the curve becomes linear and the slope is about 1. In other words, the applied strain on the composite is almost equal to the applied strain on the virgin Kapton®, which means the films do not affect the mechanical behavior of substrate any more. This may be due to the channel cracks in the longitudinal direction and the buckling in the transverse direction which separate the continuous film to numerous isolated islands like the speckles on the film, and the interfacial adhesion could play a role (Marx, Kirchlechner, et al. 2015).

To the best of our knowledge, the exact Young's modulus of the β-W phase has never been determined since the synthesis of pure β-W phase is nearly impossible. Most studies use the Young's modulus of α-W phase and assume no significant effect of the crystallographic structure on the elastic constants since both phases are cubic, namely A2 and A15. This hypothesis is supported by the case of Fe-Cr thin films. Indeed, these two different cubic phases exist in this material and the authors have reported that the indentation reduced modulus $E_r = E/(1-\nu^2)$ is the same whatever the cubic phase structure (Le Bourhis et al. 2005).

Since W films are brittle with high Young's modulus, it is fascinating to study the mechanical behavior of ductile films with smaller elastic modulus using this new technique. Then 500 nm Ni films (measured thickness: 447 ± 1) and 1 µm Cu films (measured thickness: 899 ± 29) were deposited on both

sides of the Kapton® substrate along half of the gauge length. As can be seen in Fig. 3.11, the elastic limit of Ni (~ 0.7%) and Cu (~ 0.8%) films is much larger than W films indicating a significant resistance to brittleness. Moreover, they behave in the opposite direction in the inelastic domain. Similar to the analysis above, the Young's modulus of Ni and Cu films are 213 ± 12 GPa and 109 ± 7 GPa respectively, while the bulk values are 205 GPa and 125 GPa respectively. The experimental result of Ni films agrees quite well with the bulk value. However, for Cu films, the measured Young's modulus is ~10% less. A concrete error analysis will be discussed later. It should be noted that the bulk values are taken from the measurements of isotropic polycrystalline materials. If a perfect {111} fiber texture exists, the bulk values would be higher using Neerfeld-Hill model (Appendix A), but even under this ideal condition, the texture effect is less than 10% (Faurie, Renault, Le Bourhis, and P. Goudeau 2006). Consequently, it is reasonable to compare with the bulk values above considering the imperfect texture in our case.

On the other hand, this novel technique may be attractive for amorphous materials, since no complex procedure is required, and many methods based on diffraction will be invalid. It is well known that a composite material can present excellent performance. For instance, the integration of Cu (high ductility, thermal conductivity) and W (high strength, low thermal expansion coefficient) can be applied in thermal management applications, and the microstructure of W can be controlled thanks to the introduction of Cu (Girault, Eyidi, Chauveau, et al. 2011). Herein, we also study the mechanical properties of W/Cu nanocomposite thin films. W (6 nm) and Cu (18 nm) have been sputtered alternatively twenty times on both sides and half surface of the Kapton® substrate with an Ar flow rate of 19 and 3 SCCM respectively. The thin films were deposited with 20 periods that resulted in a total thickness of $2 * 480$ nm (measured thickness: $2 * 359 \pm 3$ nm). As shown in Fig. 3.12, the elastic limit is ~ 0.9%, a value similar to the one of pure Cu films. In other words, this

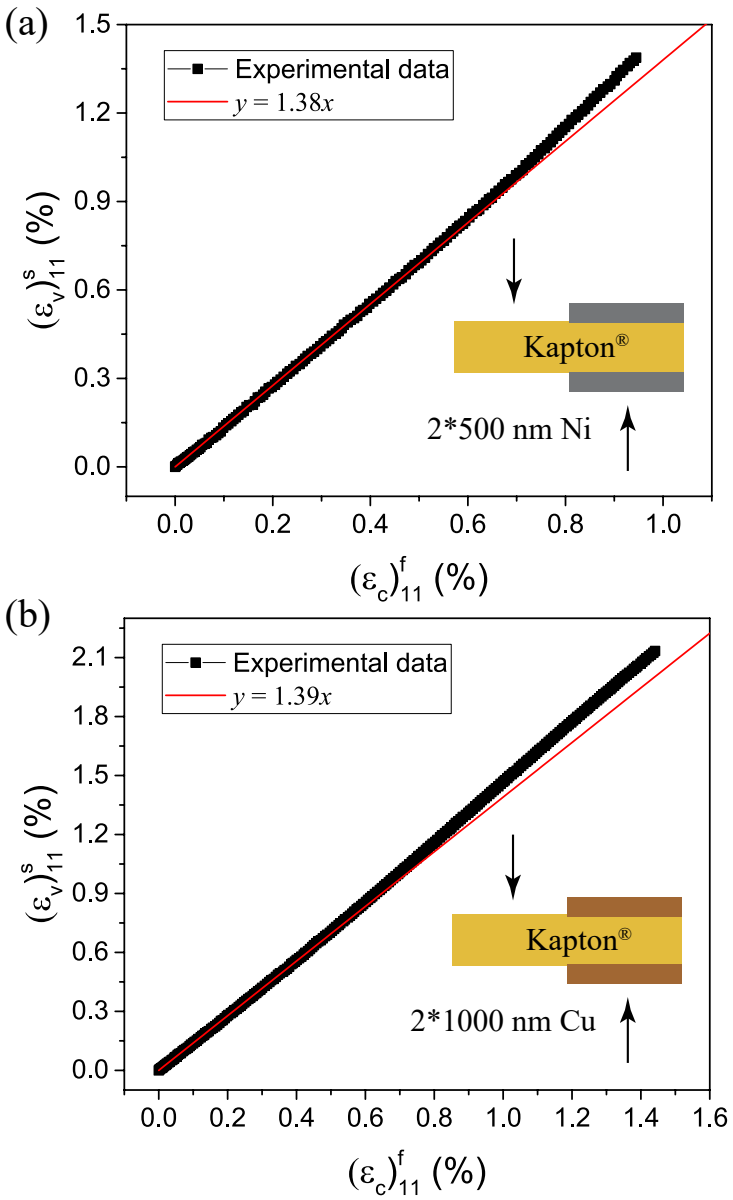

Figure 3.11: Determination of Young's modulus. (a) Longitudinal applied strain on virgin Kapton® as a function of the longitudinal applied strain on Ni-Kapton®-Ni composite. (b) Longitudinal applied strain on virgin Kapton® as a function of the longitudinal applied strain on Cu-Kapton®-Cu composite. Both red straight lines are the linear fits in the elastic regime.

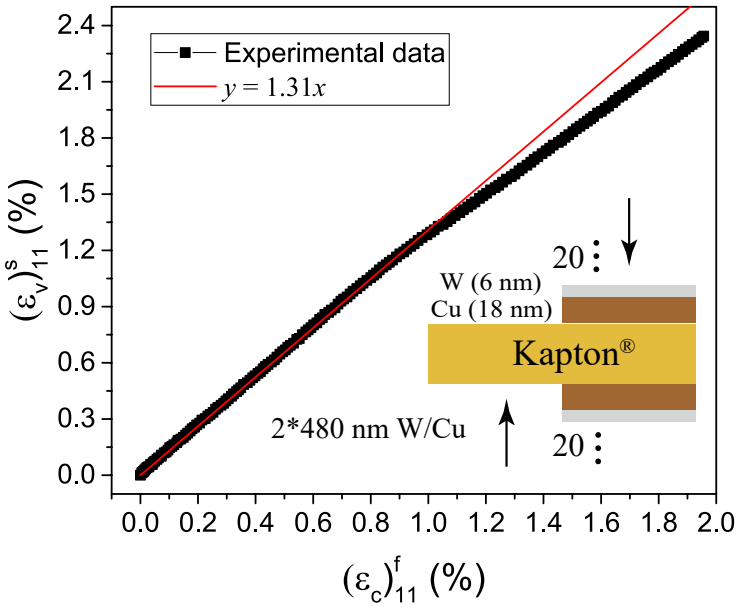

Figure 3.12: Young's modulus determination: longitudinal applied strain on virgin Kapton® as a function of the longitudinal applied strain on W/Cu-Kapton®-W/Cu composite. Thin W (6 nm) and Cu (18 nm) films are deposited alternatively on both sides and half of the Kapton® substrate with 20 periods. The red line is a linear regression in the elastic domain.

amount of W component does not play a significant role in the elastic limit. However, after applying Eq. (3.4), the Young's modulus is obtained as 216 ± 13 GPa, which is much larger than the one of pure Cu films. Unfortunately, we do not have a precise reference value. But with a coarse estimation, i.e. a weighted average, $E_{bulk} = (396 \times 1 + 125 \times 3)/4 = 193$ GPa, can be used. Evidently, they also agree well with each other taking account of the multiple interfaces of the multilayered structure.

ERROR ANALYSIS In order to discuss precisely the determination of thin films' Young's modulus, it is necessary to have an error analysis. Defining a non dimensional ratio $R = \frac{E_f t_f}{E_s t_s}$, the formula in Eq. (3.4) can be rewritten as:

$$\frac{E_f t_f}{E_s t_s} = \frac{(\varepsilon_v)^s_{11}}{(\varepsilon_c)^f_{11}} - 1 = R \tag{3.5}$$

After measuring all the quantities R, E_s, t_s and t_f with uncertainties δR, δE_s, δt_s and δt_f, the uncertainty in the Young's modulus determination can be calculated as follows:

$$\frac{\delta E_f}{E_f} = \sqrt{\left(\frac{\delta R}{R}\right)^2 + \left(\frac{\delta E_s}{E_s}\right)^2 + \left(\frac{\delta t_s}{t_s}\right)^2 + \left(\frac{\delta t_f}{t_f}\right)^2} \tag{3.6}$$

Taking W films as an example, the essential quantities are $E_f = 370$ GPa, $R = 0.60$, $E_s = 4.0$ GPa, $t_s = 125$ μm and $t_f = 405$ nm with uncertainties $\delta R = 0.01$, $\delta E_s = 0.2$ GPa, $\delta t_s = 0.5$ μm and $\delta t_f = 5$ nm. After substituting in Eq. (3.6), the uncertainty δE_f of W films can be easily obtained as 20 GPa.

3.6 CONCLUSIONS

A novel approach has been proposed to measure the Young's modulus of thin metal films. Based on the mechanical analysis of thin films coated on both sides of a substrate along half of the gauge length, the elastic modulus of thin films is found to be correlated with the applied longitudinal strains of films-substrate composite and uncoated substrate. A complete strain transfer through the film/substrate interface, and maintaining a flat specimen surface during the tensile testing are imperative assumptions in this analysis.

A new dual DIC system has been designed to verify the strain transfer and to measure the strains simultaneously. It is evidenced that the macroscopic strain is fully transferred from the substrate to the thin films whatever the residual stress, the film thickness and microstructure, i.e. no strain gradient was found along the thickness direction within an applied strain range of $\leqslant 2\%$. Interfacial adhesion can be regarded as the only factor which controls the strain transfer in our case, and this is unsurprising since a perfect adhesion compels the films to deform identically with the substrate and the film thicknesses are rather small. Thanks to our sputtering system, the established strong adhesion between the metal films and Kapton® substrates can be obtained without using a brittle intermediate layer which often fails before the films.

If films are coated on only one side of the substrate, a relatively large curvature has been observed in the transverse direction while being kept flat in longitudinal direction during the tensile testing. This is due to the compressive stress caused by Poisson's ratio mismatch between the film and the substrate. Films are then deposited on both sides to get a flat specimen and to increase the contribution of thin films.

Various thin metallic films including a multilayer have been measured to get their mechanical properties. The Young's modulus values agree well with the bulk values and the elastic limit of Ni and Cu films is much larger than W films as expected. In the inelastic domain, the brittle and ductile films present an opposite trend in the applied strain ratio, i.e. a decrease in W films while an increase in Ni and Cu films. For W/Cu multilayer, the Young's modulus is found to be close to the weighted average of the bulk elastic modulus of W and Cu films, and the elastic limit is similar to the one of pure Cu films. Moreover, a finite element method has been used which agrees well with the mechanical analysis and the experimental results. From both FEM and experiments, the effect of Poisson's ratio mismatch between thin films and substrates on the Young's modulus determination is found to be negligible.

BIBLIOGRAPHY

Barranger, Y. et al. "Strain measurement by digital image correlation: influence of two types of speckle patterns made from rigid or deformable marks". In: *Strain* 48.5 (2012), pp. 357–365 (cit. on pp. 52, 54, 72).

Belrhiti, Y. et al. "Application of optical methods to investigate the non-linear asymmetric behavior of ceramics exhibiting large strain to rupture by four-points bending test". In: *Journal of the European Ceramic Society* 32.16 (2012), pp. 4073–4081 (cit. on pp. 52, 53, 73).

Besnard, G., F. Hild, and S. Roux. ""Finite-element" displacement fields analysis from digital images: application to Portevin–Le Châtelier bands". In: *Experimental Mechanics* 46.6 (2006), pp. 789–803 (cit. on pp. 19, 72).

Conroy, M. and J. Armstrong. "A comparison of surface metrology techniques". In: *Journal of Physics: Conference Series*. Vol. 13. 1. IOP Publishing. 2005, p. 458 (cit. on p. 82).

Djaziri, S. et al. "Comparative study of the mechanical properties of nanostructured thin films on stretchable substrates". In: *Journal of Applied Physics* 116.9 (2014), p. 093504 (cit. on pp. 14, 66, 68, 80).

Faurie, D., P.-O. Renault, E. Le Bourhis, and P. Goudeau. "Study of texture effect on elastic properties of Au thin films by X-ray diffraction and in situ tensile testing". In: *Acta Materialia* 54.17 (2006), pp. 4503–4513 (cit. on pp. 17, 89, 125).

Faurie, D., P.-O. Renault, E. Le Bourhis, and Ph. Goudeau. "Determination of elastic constants of a fiber-textured gold film by combining synchrotron x-ray diffraction and in situ tensile testing". In: *Journal of applied physics* 98.9 (2005), p. 093511 (cit. on pp. 17, 66, 69).

Geandier, G. et al. "Elastic-strain distribution in metallic film-polymer substrate composites". In: *Applied Physics Letters* 96.4 (2010), p. 041905 (cit. on pp. 14, 66).

Girault, B., D. Eyidi, T. Chauveau, et al. "Copper coverage effect on tungsten crystallites texture development in W/Cu nanocomposite thin films". In: *Journal of Applied Physics* 109.1 (2011), p. 014305 (cit. on p. 89).

Hild, F. and S. Roux. "Digital image correlation: from displacement measurement to identification of elastic properties–a review". In: *Strain* 42.2 (2006), pp. 69–80 (cit. on pp. 19, 52, 55, 72).

Huang, H.B. and F. Spaepen. "Tensile testing of free-standing Cu, Ag and Al thin films and Ag/Cu multilayers". In: *Acta Materialia* 48.12 (2000), pp. 3261–3269 (cit. on p. 66).

Le Bourhis, E. et al. "Structural and mechanical studies of Fe-Cr thin films deposited by ion-beam sputtering". In: *The European Physical Journal Applied Physics* 30.01 (2005), pp. 33–39 (cit. on p. 88).

Marx, V.M., C. Kirchlechner, et al. "Adhesion measurement of a buried Cr interlayer on polyimide". In: *Philosophical Magazine* 95.16-18 (2015), pp. 1982–1991 (cit. on p. 88).

Noyan, I.C., T.C. Huang, and B.R. York. "Residual stress/strain analysis in thin films by X-ray diffraction". In: *Critical Reviews in Solid State and Material Sciences* 20.2 (1995), pp. 125–177 (cit. on pp. 11, 60, 66, 108).

Roland, T. et al. "Digital image correlation of metal nanofilms on SU-8 for flexible electronics and MEMS". In: *Journal of Micromechanics and Microengineering* 21.12 (2011), p. 125005 (cit. on p. 80).

Wojciechowski, P.H. and M.S. Mendolia. "Fracture and cracking phenomena in thin films adhering to high-elongation substrates". In: *Physics of thin films* 16 (1991), pp. 271–340 (cit. on pp. 15, 80).

Yang, Y. et al. "Deformation and fracture in micro-tensile tests of freestanding electrodeposited nickel thin films". In: *Scripta Materialia* 58.12 (2008), pp. 1062–1065 (cit. on p. 66).

Yin, H.M. and P.A. Prieto-Muñoz. "Stress transfer through fully bonded interface of layered materials". In: *Mechanics of Materials* 62 (2013), pp. 69–79 (cit. on pp. 15, 66).

4 CYCLIC TESTING OF THIN NANOMETRIC FILMS COMBINING XRD AND DIC ANALYSIS

Contents

In the first place, the methods for cyclic testing of thin metal films are reviewed. Relying on the Deben MICROTEST tensile/compression stage, we propose a novel pre-stretching technique which allows stretching and compressing the as-deposited films on both sides of a Kapton® substrate. Thanks to the XRD stress/strain and DIC strain measurements at each step of the cyclic testing, the relationship between thin films' intrinsic elastic stress/strain and true strain can be obtained within a relatively large applied strain domain, i.e. a positive or negative applied strain relative to the unloaded state. From these curves, we study the cyclic deformation behavior of thin Ni films with a nanometric grain size of ~ 20 nm. Particularly, the Bauschinger and work hardening effects are investigated.

4.1 DEVELOPMENT OF A PRE-STRETCHING TECHNIQUE COMBINED WITH XRD AND DIC MEASUREMENTS

4.1.1 Overview of the cyclic testing techniques for thin films

For bulk materials, the cyclic testing in tension and compression are well established to study various mechanical properties especially the plasticity, such as the yield strength and the Bauschinger effect. However, this is much more difficult for thin freestanding films or film-substrate composites owing to the large lateral dimension/thickness ratio which can cause buckling during the compression. Furthermore, tension and compression must be applied in the same experiment.

In the past, several specific methods have been proposed. For freestanding thin films, uniaxial micro-tensile load-unload testing is the most direct and interpretable way. Rajagopalan *et al.* (Rajagopalan, Han, and Saif 2008; Rajagopalan, Rentenberger, et al. 2010) performed a cyclic test in a series of steps[1] using a displacement controlled specimen straining holder in a transmission electron microscope. After recording the stress-strain data, a substantial Bauschinger effect in gold and aluminum films was observed and studied.

For thin films coated on substrates, a powerful technique combining X-ray diffraction and tension test was proposed to study the cyclic deformation of 700 nm thick and magnetron sputtered Cu films on Kapton® substrates (Hommel, Kraft, and Arzt 1999). The elastic strain of film was measured by X-ray diffraction and the total strain of substrate was measured thanks to a strain gauge on the substrate's backside. With the elastic strain as a function of the

1 Applied strain at each step: ~0.05-0.1%.

total strain, they found that the applied strain in the substrate was fully transferred to the film up to ~0.1% (linear relationship with a slope equals 1). A deviation from this linear behavior was attributed to the appearance of plastic deformation. Knowing the elastic constants of films, the yield strength, cyclic plastic deformation and strain hardening behavior can be well investigated (Hommel and Kraft 2001). However, if the interfacial adhesion is not strong enough, a deviation may occur even in the elastic domain and not be related to the introduction of plastic deformation; in other words, the strains correspond to each other in the early phase of elastic deformation, and diverge in the late elastic stage due to the failure of interface.

Plane-strain bulge test (Xiang and J. J. Vlassak 2006; Xiang and J. Vlassak 2005) and substrate curvature (Baker, Keller-Flaig, and Shu 2003) are also notable techniques to study the cyclic deformation of thin films on substrates and insightful research on the Bauschinger effect has been conducted. Furthermore, cyclic tests were carried out by Sim *et al.* (Sim et al. 2013) using a fatigue tester with in situ electrical resistance monitoring. In order to avoid buckling, the Ag film-substrate specimen was pre-stretched to given strains prior to fatigue testing. With the normalized resistance, the number of cycles and strain range, the effects of pre-straining (severe plastic deformation has already occurred) on the fatigue behavior were explored. Nevertheless, all these approaches associated with a tester have the same limitation: compressive strain cannot be applied when regarding the initial state of as-deposited thin films as a reference, *i.e.* the tensile/compressive deformation occurs in only one direction comparing to the initial state. For thermal cycles, the total strain is limited by the thermal expansion coefficient mismatch and the imposed temperature range. Undesirably, the applied strain and the temperature change cannot be decoupled so that other deformation mechanism may acts at a certain temperature.

Recently, we demonstrated that both compressive and tensile stresses can be applied to the films with a uniaxial tensile tester when using thin films deposited on pre-stretched compliant substrates (Renault et al. 2012). By virtue of this technique, Faurie et al. (Faurie, Renault, Le Bourhis, Drouet, et al. 2013) studied the X-ray elastic strain of a strongly {111} fiber textured Au film during the compression test.

4.1.2 Independent development of pre-stretching technique

Pre-stretching technique is widely popular in studying the buckling of thin films on compliant substrates and in the controlled formation of 3D functional structures (Song et al. 2008; Khang et al. 2006; Sun et al. 2006; Xu et al. 2015). The main principle is to bond 2D micro/nanostructures to the adhesion sites of uniaxial or biaxial pre-strained elastomeric substrates. Compressive stresses induced by relaxing the pre-strain in the substrate[2] lead to the buckling and the formation of 3D structures (mainly determined by the layout of adhesion sites and the pre-strain). Nevertheless, the fabrication procedure is quite complicated which includes photolithography and etching, and unfortunately, how to maintain the pre-strain in the processing steps is not presented.

As mentioned above, a new pre-stretching technique has been demonstrated in (Renault et al. 2012). The Kapton® substrate was mounted on a small Deben MICROTEST which can be adapted in our home-made vacuum sputtering chamber. Before pumping, the substrate was in situ pre-strained to ~2% which is smaller than its yield point (~4%). After deposition, the tensile and compressive load can be achieved in the same tester. However, only one deposition on one side can be performed with only one sample. In order to be efficient

2 Returning to its original shape.

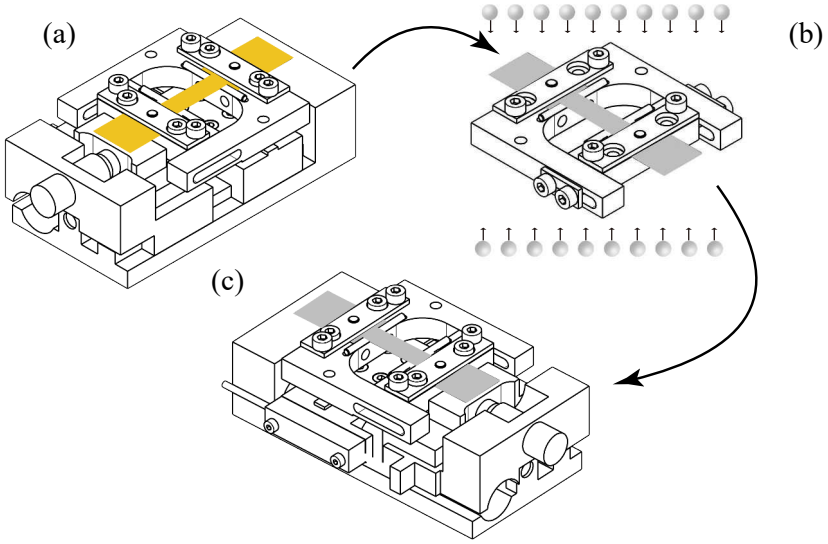

Figure 4.1: Synopsis of the pre-stretching technique. (a) Mounting and elastic stretching of a virgin substrate (pre-strain: ~ 2%). (b) Film deposition on both sides of the substrate thanks to the new grips removed from the tester (maintaining the substrate's pre-strain). (c) Grips' separating and reinstalling on Deben MICROTEST for further cyclic testing.

and to ensure consistency and repeatability, a novel grip system adapted to the Deben MICROTEST (Section 2.2) has been custom-designed.

The complete process of the pre-stretching technique is illustrated in Fig. 4.1. The procedure starts with the installation of virgin Kapton® and new grips on the Deben MICROTEST. The two grips are independent or not connected initially, then the substrate is pre-stretched up to 50 N corresponding to a pre-strain of ~ 2%. By virtue of four standard screws and cyanoacrylate glues, the grips are fixed together to be a rigid body. After removing from the tester, the grips with the pre-strained substrate can be taken into the deposition chamber. Thin metal films are deposited on both sides of the substrate after two depositions. It should be noted that four pre-tensile specimens can be sputtered simultaneously (Section 2.3.2). Ultimately, we reinstall the setup (Fig. 4.1(b))

on the Deben MICROTEST and separate the grips for further cyclic tensile/-compressive testing.

During the later testing, force control mode will be used considering its much higher precision compared with displacement control mode (resolution: 10 µm, corresponding strain: ~0.3%). Furthermore, after stretching up to 50 N, the force drops markedly when stopping the tensile load, and continuously tends to a steady state while the strain keeps constant as a result of the well-known stress relaxation. Therefore, the force recording is not reliable and it is exerted only for driving the samples which can achieve a strain resolution of $< 0.03\%$.

4.2 CYCLIC TESTING AND ELASTIC STRESS/TRUE STRAIN MEASUREMENTS OF THIN NI FILMS

Thanks to our new designs shown in Section 2.2, the DIC system combined with the Deben MICROTEST and pre-tensile specimen can be fitted to a 4-circles X-ray goniometer[3] from GE Seifert Group Company (Fig. 4.2). The 300 nm Ni films bonded to both sides of a Kapton® substrate were prepared and the deposition condition is shown in Section 2.3.2.

Fig. 4.3(a) shows the diffraction pattern using {111} diffracting planes. The measured diffraction peak position is shifted towards a lower diffraction angle with respect to the powder reference (ICDD-PDF, N°4-850). This is mainly due to the compressive residual stresses and the presence of auto-interstitials in the film, which lead to an increase of the stress-free lattice parameter.

3 Unfortunately, this diffractometer has been out of order for almost one year, and only one test can be carried out recently using another diffractometer (copper Kα X-ray source and 1 mm collimator).

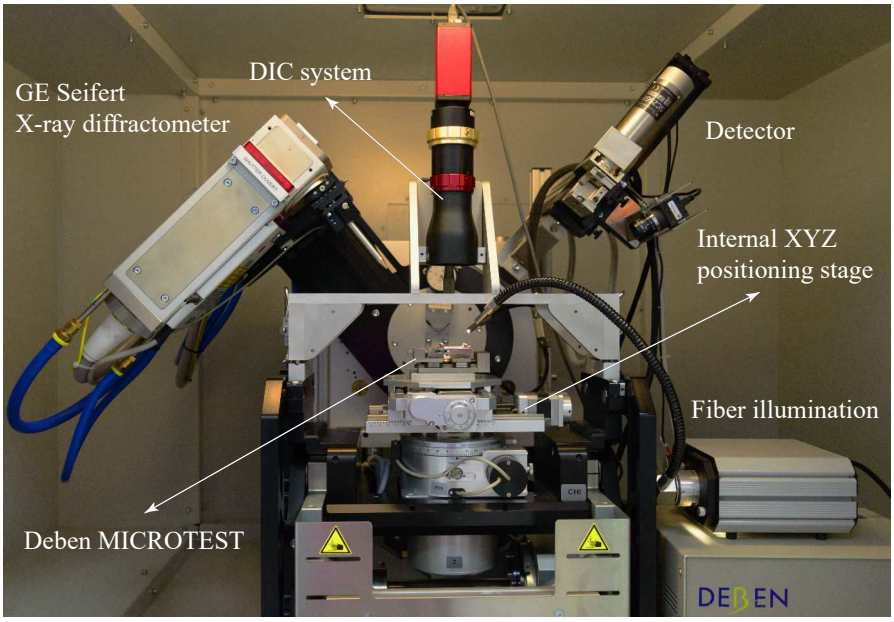

Figure 4.2: A DIC system combining the Deben MICROTEST and pre-stretched specimen adapted to the GE Seifert X-ray diffractometer. During each step of the cyclic testing, the DIC system is removed from the goniometer for the next XRD measurements after the optical acquisition.

Before releasing the grips, it is important to perform the texture analysis, residual stress measurement and to estimate the mean grain size. Owing to the fact that sputtered thin metal films usually present a fiber texture, the full pole figure measurement is dispensable. In this study, the intensity of {111} planes was measured as a function of ψ angles varying between 0° and 85° with the in-plane angle φ held constant at 0°. Moreover, the diffraction angle was fixed at 44.5°, and two extra rocking curves were performed at contiguous angles of 40° and 48°. Then the ultimate rocking curve was obtained by subtracting the average of them to get rid of the background effects. As shown in Fig. 4.3(b), the high intensity of the {111} reflections in pole directions is obvious which indicates a strong {111} fiber texture.

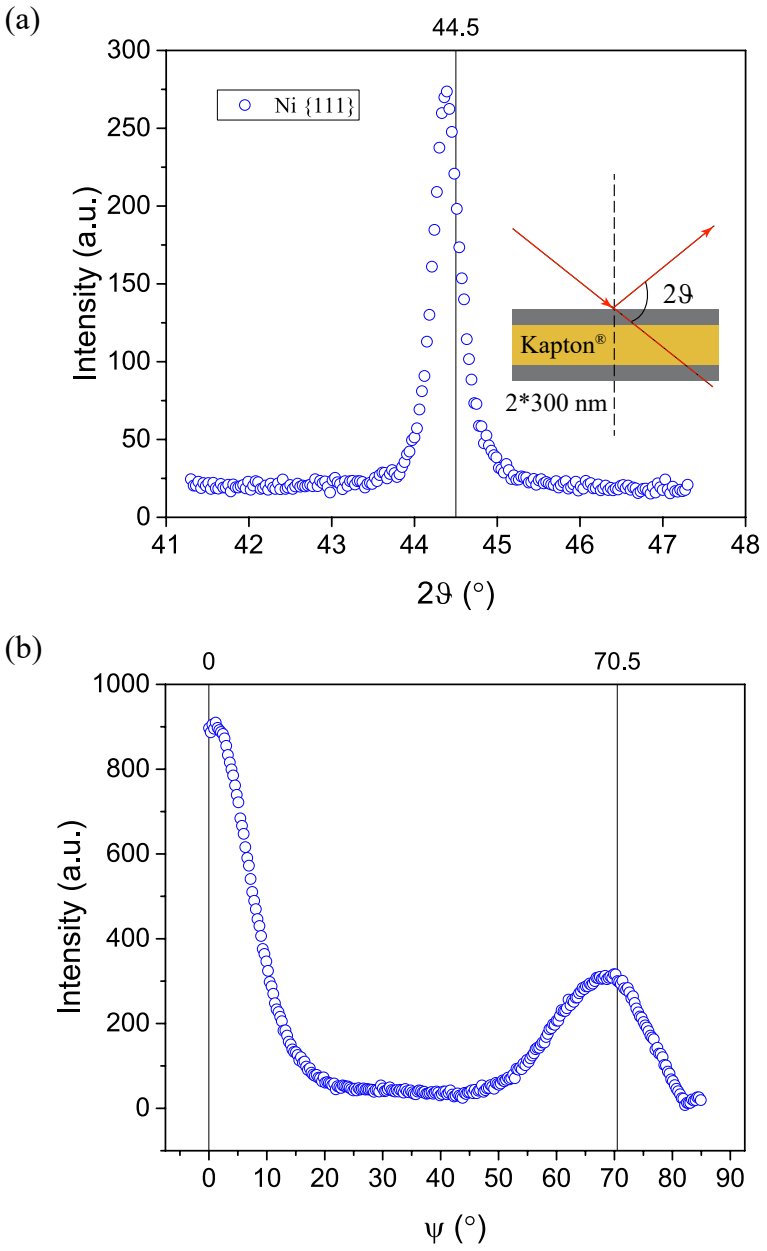

Figure 4.3: XRD patterns of the studied Ni film. (a) Diffraction pattern of the {111} diffracting planes recorded in the ϑ-2ϑ mode. The vertical line shows the diffraction angle taking from the Ni powder diffraction file (ICDD-PDF, N° 4-850). The XRD measurement on the specimen is illustrated in the insert. (b) Variation of the {111} diffraction peak intensity as a function of ψ angle. The $\vartheta - 2\vartheta$ angles are fixed at the maximum of the {111} diffraction peak, $2\vartheta = 44.5°$. The scan is done with a step size of 0.3° and a recording time of 30 seconds. The pole directions are indicated by the vertical lines.

When the diffraction pattern is restricted to the main diffraction peak ({111} for nickel), a simple method to estimate the mean grain size is to apply the Scherrer formula (A. Monshi, Foroughi, and M. Monshi 2012):

$$D = \frac{0.89\lambda}{\beta \cos\vartheta} \tag{4.1}$$

where λ is the wavelength of X-ray, β the full width at half maximum expressed in radians, and ϑ the Bragg's angle. The value of 0.89 is a constant related to the crystallite shape which is assumed to be spherical with cubic unit cells. In the case of nickel, we find $\beta = 0.43°$ and $2\vartheta = 44.34°$ for the copper $K\alpha_1$ wavelength which equals 0.15406 nm. Then the grain size is calculated as ~ 20 nm, a value which is certainly underestimated (microstrains are neglected) but still remains very small.

For the determination of residual stress and applied lattice stress/strain, the diffraction of the {111} planes were employed. Typically, the stress analysis based on the X-ray diffraction should not be performed using low Bragg angle reflections due to the relatively large uncertainties which result in statistical errors on the calculated stresses. However, the X-ray tube and the detector we used are not powerful enough to capture the diffractions of other planes, and we will show that this effect is negligible.

With the assumption of equibiaxial residual stress state, Eq. (2.9) is used to get $\sigma^{Res.}$ and $\ln(1/\sin\vartheta_0)$, where the stiffness is selected from Eq. (A.12). The calculated values are: $\sigma_{11}^{Res.} = -1.03\text{GPa}$, $\ln(1/\sin\vartheta_0) = 1.4944$ and $\varepsilon_{11}^{Res.} = -0.33\%$ (Eq. (2.7)). After releasing the grips, the same measurements were performed to check the effects of specimen manipulation. It is interesting to find that the values agree excellently well with the above ones which means the grips releasing does not play a role in this experiment, and all the subsequent X-ray stress/strain measurements will use them as the reference state.

During the cyclic test, the specimen was strained in steps of ~ 3 N (~ 0.06% in strain). Before each step, five images were taken to be a reference for the DIC analysis. After a step, another five images were acquired and the film stress/strain was measured by the X-ray diffraction[4]. It should be noted that the white paints were sprayed on the film surface in order to get its strain directly. Since the paint spots are extremely tiny and soft with a random discrete distribution, their effects on films can be omitted. In this way, the true stain and the elastic stress/strain at each loading step can be obtained.

For all the XRD measurements, due to the strong fiber texture of Ni films, the pole directions (ψ= 0°, 70.5°) are preferred. At the initial steps, three data points near the two angles were taken. However, we find that the precision does not differ significantly when using less points. Accordingly, only three points (ψ= 0°, 68.5° and 70.5°) in total were determined to reduce the measuring time (about one hour for each step). The 2ϑ range is from 41.5° to 47.5° with a step size of 0.03° and a counting time of 6 seconds. The classic "$\ln(1/\sin\vartheta)$ versus $\sin^2\psi$" curves during the cyclic testing are demonstrated in Fig. 4.4. As can be clearly seen, all the linear lines intersect at one point as expected indicating a high precision. Furthermore, a positive slope corresponds to a tensile stress and a negative slope at a compressive stress.

As expected, the stress state of the Ni film is no longer equibiaxial during the uniaxial tension/compression tests, the stress cannot be determined as done formerly for the residual stress analysis. However, the applied stress can be obtained if we consider the fact that the stress component normal to the film

4 The DIC setup was already removed from the goniometer before the X-ray measurement.

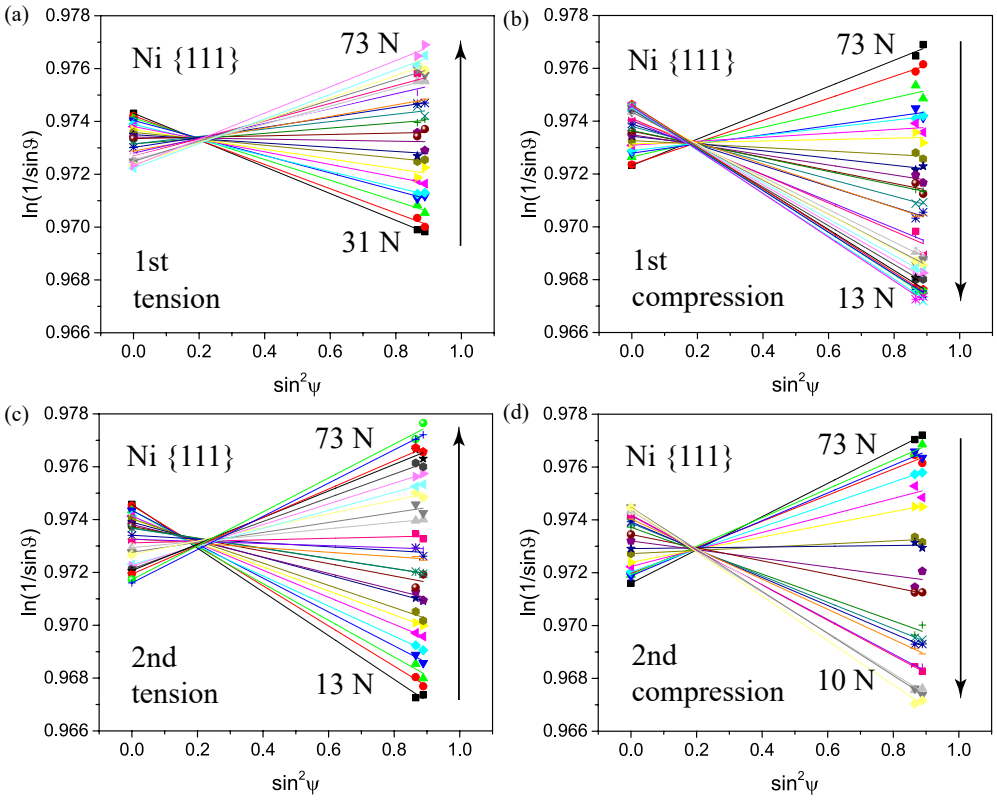

Figure 4.4: $\ln(1/\sin\vartheta)$ versus $\sin^2\psi$ plots for {111} planes of the Ni film. (a) The first uniaxial loading from 31 to 73 N. (b) The first unloading from 73 to 13 N. (c) The second tension from 13 to 73 N. (d) The second compression from 73 to 10 N. All the color lines correspond to the linear fits and are plotted to the same scale.

surface is nil (Hommel, Kraft, and Arzt 1999; I. Noyan, T. Huang, and York 1995). With the Hooke's law, we get the stress/strain relationships:

$$\begin{bmatrix} \sigma_{11} \\ \sigma_{22} \\ 0 \\ 0 \\ 0 \\ 0 \end{bmatrix} = \begin{bmatrix} c_{11} & c_{12} & c_{13} & 0 & 0 & 0 \\ c_{21} & c_{22} & c_{23} & 0 & 0 & 0 \\ c_{31} & c_{32} & c_{33} & 0 & 0 & 0 \\ 0 & 0 & 0 & c_{44} & 0 & 0 \\ 0 & 0 & 0 & 0 & c_{55} & 0 \\ 0 & 0 & 0 & 0 & 0 & c_{66} \end{bmatrix} \begin{bmatrix} \varepsilon_{11} \\ \varepsilon_{22} \\ \varepsilon_{33} \\ 0 \\ 0 \\ 0 \end{bmatrix} \tag{4.2}$$

where $[c_{ij}]$ is the stiffness matrix, "11" and "22" corresponds to the in-plane loading direction and the transverse direction respectively. After knowing the elastic stiffness (Eq. (A.12)) and ε_{11}, ε_{33} (Eq. (2.7)), the in-plane elastic stresses can be obtained:

$$\begin{cases} \sigma_{11} = c_{11}\varepsilon_{11} + c_{12}\varepsilon_{22} + c_{13}\varepsilon_{33} \\ \sigma_{22} = c_{21}\varepsilon_{11} + c_{22}\varepsilon_{22} + c_{23}\varepsilon_{33} \\ \sigma_{33} = c_{31}\varepsilon_{11} + c_{32}\varepsilon_{22} + c_{33}\varepsilon_{33} = 0 \end{cases} \tag{4.3}$$

4.3 BAUSCHINGER EFFECT AND STRAIN HARDENING INVESTIGATIONS IN THIN NICKEL FILMS ON A KAPTON® SUBSTRATE

In this section, the cyclic deformation especially the Bauschinger effect of thin Ni films will be studied. Before going further, it is important to point out that the XRD technique can only measure the elastic component of full deformation,

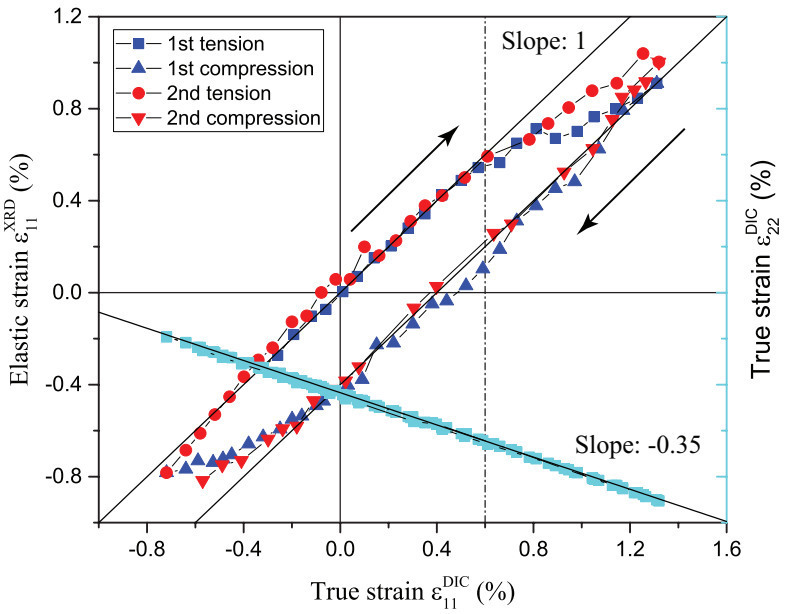

Figure 4.5: Nickel film's elastic strain ε_{11}^{XRD} in the longitudinal direction and true strain ε_{22}^{DIC} (cyan) in the transverse direction as a function of longitudinal true strain ε_{11}^{DIC} during the cyclic testing. The arrows indicate the strain evolution and the dashed line intersects the elastic limit in tension.

while DIC method can acquire both elastic and plastic behavior. Moreover, the Deben MICROTEST must be well aligned in the goniometer for the measurement of applied longitudinal strains, in other words, the φ angle in Fig. 2.15 must be exactly or approximately zero.

Fig. 4.5 presents the evolution of longitudinal lattice strain and the transverse true strain during the cyclic testing. The initial point represents the compressive biaxial residual strains in the films. In the first tension, up to ~0.6%, the longitudinal strains measured by XRD and DIC correspond to each other. This shows that the precision of XRD and DIC measurements is enough and the effects of the soft paints can be neglected, since the applied strain is unique. For strains larger than 0.6%, an obvious deviation from this linear behavior indicates the introduction of a plastic deformation. After stretching up to 1.31%, the specimen is unloaded with the same slope as the initial loading. When the strain reaches zero, the film begins to yield in the compressive direction. Upon

reloading, the similar behavior is observed except that the maximum strain is slightly higher. Fig. 4.5 also shows that the poison's ratio (0.35) of the film-substrate composite is constant even when film behaves plastically. This is not surprising since the substrate is still fully elastic and constrains the transverse deformation of the film.

As observed, strain hardening is not detected here contrary to the observations of Hommel et al. (Hommel and Kraft 2001; Hommel, Kraft, and Arzt 1999). Noteworthy, the grain size reported by the authors is much more elevated ($\geqslant$ 180 nm) than the coherent domain size determined in our films (~20 nm). In the present case, the length scale hinders the phenomenon like the dislocation pileups responsible for the Hall-Petch hardening mechanism. In other words, the grains are too small to have a dislocation accumulation inside.

Interestingly, Fig. 4.5 shows a Bauschinger effect on unloading. This may be due to the grain boundaries and the strong interface. However, the intrinsic mechanism is not clear with only this experiment, a micrograph of grain structures and subsequent tests with larger applied strain domain are necessary. Furthermore, the elaboration by Xiang and Vlassak (Xiang and J. Vlassak 2005; Xiang and J. J. Vlassak 2006) cannot be applied in our case, since their films present columnar grain structures with grain size $\geqslant$ 330 nm.

As a typical means to study the cyclic deformation of the sputtered Ni films, the stress-strain curves are presented in Fig. 4.6. Fig. 4.6(a) shows the development of the longitudinal and transverse XRD stresses of the film during the first cycle. From the longitudinal stress-strain curves, as expected, the film starts to behave elastically from the compressive residual stress state to a tensile stress state. Then, at ~1.2 GPa, the film yields which is indicated by the deviation from the linear behavior and a dashed line shows the corresponding strain. Subsequently, the tensile stress increases up to ~2.2 GPa at a true strain of 1.31%.

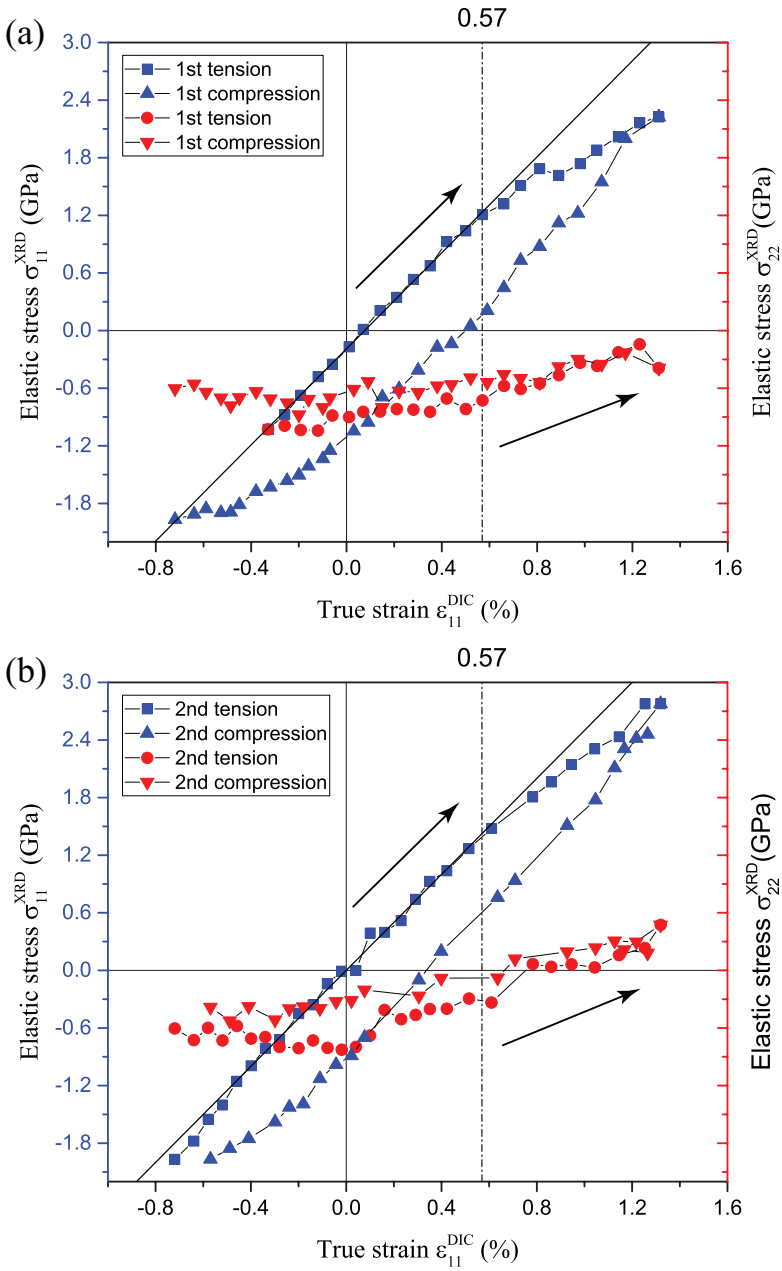

Figure 4.6: Longitudinal and transverse XRD stresses as a function of the longitudinal DIC strain. (a) The first cycle. (b) The second cycle. The dashed line indicates the elastic limit. All the curves are plotted to the same scale.

In Fig. 4.6(b), an analogous deformation trend is observed. However, there has been a subtle shift of the applied longitudinal stresses. This is because of the slight rigid body motion of the specimen along "33" direction during the cyclic testing, causing the experimental errors of ε_{33} measurements. Those errors can be calibrated out with reference to the XRD measurements of the soft paints on the film surface, but herein, this is impossible since we suffered from the low X-ray intensity as shown in Fig. 4.3. Moreover, it is important to point out that this does not affect markedly the measurements of ε_{11} if we consider the fact that ε_{11} is much larger than ε_{33}. Accordingly, the measured stresses are shown to give a perception, and the crucial analyses should be based on the measurements in Fig. 4.5.

For the transverse stress evolution, it climbs slightly in the elastic regime and increases more strongly in the plastic domain. From comparing the in-plane Poisson's ratios, 0.38 (Table 3.1) and 0.34 for the Ni film and Kapton® respectively, the film undergoes applied tensile transverse stress due to the mismatch. It should be noted that the in-plane Poisson's ratio of a {111} fiber-textured Ni film is higher than the bulk isotropic one (0.31). Moreover, when the metallic Ni film behaves plastically, the trend of Poisson's ratio may be towards 0.5 (incompressible properties in plastic domain) which rises the transverse stress.

4.4 CONCLUSIONS

Uniaxial tensile/compressive testing is extremely suitable for the Bauschinger effect study. A novel pre-stretching technique has been developed to exert both positive and negative applied strain, relative to the initial or unloaded state, on thin films in a relatively large strain domain. In the case of 300 nm Ni films deposited on both sides of a Kapton® substrate, the elastic stress/strain

and true strain of Ni films are measured by XRD and DIC techniques respectively during each step of the cyclic testing. Two deformation cycles have been performed. From the first one, a Bauschinger effect is observed even with such a tiny grain size (~20 nm). The second deformation cycle overlaps the first one, which demonstrates little or no strain hardening. This unusual mechanical behavior is certainly due to the tiny grain size (~20 nm) where no dislocation pile-ups are allowed to form inside the grains. Furthermore, grain boundaries and interfaces certainly play a crucial role on the mechanisms of the Bauschinger and strain hardening effects in nanocrystalline materials.

Considering the transversal direction, we observe that the Poisson's ratio of the film-substrate composite remains unvarying even when the films undergo plastic deformations. This behavior is mainly owing to the fact that the substrate is still fully elastic and much thicker than the films.

BIBLIOGRAPHY

Baker, S.P., R.-M. Keller-Flaig, and J.B. Shu. "Bauschinger effect and anomalous thermomechanical deformation induced by oxygen in passivated thin Cu films on substrates". In: *Acta materialia* 51.10 (2003), pp. 3019–3036 (cit. on pp. 21, 99).

Faurie, D., P.-O. Renault, E. Le Bourhis, M. Drouet, et al. "X-ray elastic strain analysis of compressed Au thin film on polymer substrate". In: *Surface and Coatings Technology* 215 (2013), pp. 322–326 (cit. on p. 100).

Hommel, M. and O. Kraft. "Deformation behavior of thin copper films on deformable substrates". In: *Acta Materialia* 49.19 (2001), pp. 3935–3947. ISSN: 1359-6454 (cit. on pp. 99, 110).

Hommel, M., O. Kraft, and E. Arzt. "A new method to study cyclic deformation of thin films in tension and compression". In: *Journal of materials research* 14.06 (1999), pp. 2373–2376 (cit. on pp. 14, 98, 108, 110).

Khang, D.-Y. et al. "A stretchable form of single-crystal silicon for high-performance electronics on rubber substrates". In: *Science* 311.5758 (2006), pp. 208–212 (cit. on p. 100).

Monshi, A., M.R. Foroughi, and M.R. Monshi. "Modified Scherrer equation to estimate more accurately nano-crystallite size using XRD". In: *World Journal of Nano Science and Engineering* 2.03 (2012), p. 154 (cit. on p. 105).

Noyan, I.C., T.C. Huang, and B.R. York. "Residual stress/strain analysis in thin films by X-ray diffraction". In: *Critical Reviews in Solid State and Material Sciences* 20.2 (1995), pp. 125–177 (cit. on pp. 11, 60, 66, 108).

Rajagopalan, J., J.H. Han, and M.T.A. Saif. "Bauschinger effect in unpassivated freestanding nanoscale metal films". In: *Scripta Materialia* 59.7 (2008), pp. 734–737 (cit. on pp. 23, 98).

Rajagopalan, J., C. Rentenberger, et al. "In situ TEM study of microplasticity and Bauschinger effect in nanocrystalline metals". In: *Acta Materialia* 58.14 (2010), pp. 4772–4782 (cit. on pp. 23, 98).

Renault, P.-O. et al. "Deposition of ultra-thin gold film on in situ loaded polymeric substrate for compression tests". In: *Materials Letters* 73 (2012), pp. 99–102 (cit. on pp. 41, 100).

Sim, G.-D. et al. "Effects of stretching and cycling on the fatigue behavior of polymer-supported Ag thin films". In: *Materials Science and Engineering: A* 575 (2013), pp. 86–93 (cit. on p. 99).

Song, J. et al. "Buckling of a stiff thin film on a compliant substrate in large deformation". In: *International Journal of Solids and Structures* 45.10 (2008), pp. 3107–3121 (cit. on p. 100).

Sun, Y.G. et al. "Controlled buckling of semiconductor nanoribbons for stretchable electronics". In: *Nature nanotechnology* 1.3 (2006), pp. 201–207 (cit. on p. 100).

Xiang, Y. and J.J. Vlassak. "Bauschinger effect in thin metal films". In: *Scripta Materialia* 53.2 (2005), pp. 177–182. ISSN: 1359-6462 (cit. on pp. 22, 23, 99, 110).

Xiang, Y. and Joost J. Vlassak. "Bauschinger and size effects in thin-film plasticity". In: *Acta Materialia* 54.20 (2006), pp. 5449–5460. ISSN: 1359-6454 (cit. on pp. 22, 23, 99, 110).

Xu, S. et al. "Assembly of micro/nanomaterials into complex, three-dimensional architectures by compressive buckling". In: *Science* 347.6218 (2015), pp. 154–159 (cit. on p. 100).

GENERAL CONCLUSIONS AND PERSPECTIVES

ON the basis of this thesis work, it is indispensable to give a summary or a general conclusion, and to provide several meaningful perspectives for the future investigation.

GENERAL CONCLUSIONS The mechanical properties, particularly the Young's modulus and the Bauschinger effect, of thin metal films on Kapton® substrates have been researched. The uniaxial tensile/compressive testing, DIC true strain measurement and XRD elastic stress/strain determination, which run through this study, are of crucial importance. These techniques have been introduced and discussed in detail in Chapter 2. Adapting to the Deben MICROTEST and the X-ray diffractometer, many setups have been custom-designed. Moreover, the residual stresses, texture and phases of thin films can be controlled thanks to our sputtering system.

A novel approach has been proposed to measure the Young's modulus of thin metal films. Based on the mechanical analysis of thin films coated on both sides of a substrate along half of the gauge length, the elastic modulus of thin films is found to be correlated with the applied longitudinal strains of films-substrate composite and uncoated substrate.

In order to verify the strain transfer through film-substrate interface, which is key to the Young's modulus determination, a novel dual DIC system is developed. It is evidenced that the macroscopic strain is fully transferred from the substrate to the thin films whatever the residual stress, the film thickness and microstructure, i.e. no strain gradient was found along the thickness direction within an applied strain range of $\leqslant 2\%$. Interfacial adhesion can be regarded

as the only factor which controls the strain transfer in our case, and this is unsurprising since a perfect adhesion compels the films to deform identically with the substrate and the film thicknesses are rather small. Thanks to our sputtering system, the established strong adhesion between the metal films and Kapton® substrates can be obtained without using a brittle intermediate layer which often fails before the films.

If films are coated on only one side of the substrate, a relatively large curvature has been observed in the transverse direction while being kept flat in longitudinal direction during the tensile testing. This is due to the compressive stress caused by Poisson's ratio mismatch between the film and the substrate. Films are then deposited on both sides to get a flat specimen and to increase the contribution of thin films.

Various thin metallic films including a multilayer have been measured to get their mechanical properties. The Young's modulus values agree well with the bulk values and the elastic limit of Ni and Cu films is much larger than W films as expected. In the inelastic domain, the brittle and ductile films present an opposite trend in the applied strain ratio, i.e. a decrease in W films while an increase in Ni and Cu films. For W/Cu multilayer, the Young's modulus is found to be close to the weighted average of the bulk elastic modulus of W and Cu films, and the elastic limit is similar to the one of pure Cu films. Moreover, a finite element method has been used which agrees well with the mechanical analysis and the experimental results. From both FEM and experiments, the effect of Poisson's ratio mismatch on the Young's modulus determination is found to be negligible.

On the other hand, Uniaxial tensile/compressive testing is extremely suitable for the Bauschinger effect study. A novel pre-stretching technique has been developed to exert both positive and negative applied strain, relative to the initial or unloaded state, on thin films in a relatively large strain domain. In the case of 300 nm Ni films deposited on both sides of a Kapton® substrate,

the elastic stress/strain and true strain of Ni films are measured by XRD and DIC techniques respectively during each step of the cyclic testing. Two deformation cycles have been performed. From the first one, a Bauschinger effect is observed even with such a tiny grain size (~20 nm). The second deformation cycle overlaps the first one, which demonstrates little or no strain hardening. This unusual mechanical behavior is certainly due to the tiny grain size (~20 nm) where no dislocation pile-ups are allowed to form inside the grains. Furthermore, grain boundaries and interfaces certainly play a crucial role on the mechanisms of the Bauschinger and strain hardening effects in nanocrystalline materials.

PERSPECTIVES

I Tensile testing of pure α-W and β-W films combined with XRD and DIC techniques.

To the best of our knowledge, the elastic modulus of pure β-W films on soft substrates has never been measured due to the complexity of fabrication[1] and the limitation from soft substrates. After achieving the pure α-W and β-W films, we propose a novel approach to measure and compare their mechanical properties during a tensile testing.

Films will be deposited on both sides of the half specimen surface. In order to stretch the elongated sample in a large strain regime, a new grip adapted to the Deben MICROTEST has already been developed as shown in Fig. 4.7. This setup can be shifted in 3D space thanks to the internal XYZ positioning stage (Fig. 4.2). Similar to the procedure in Section 4.2, the tensile testing will be carried out step by step with the XRD and DIC measurements. The new idea is to add in the true strain measurement of the uncoated substrate, i.e. immediately after the image capture of the film,

1 As can be seen in Fig. 2.9, β-W phase always exists with a presence of α-W phase even when the deposition condition alters precisely.

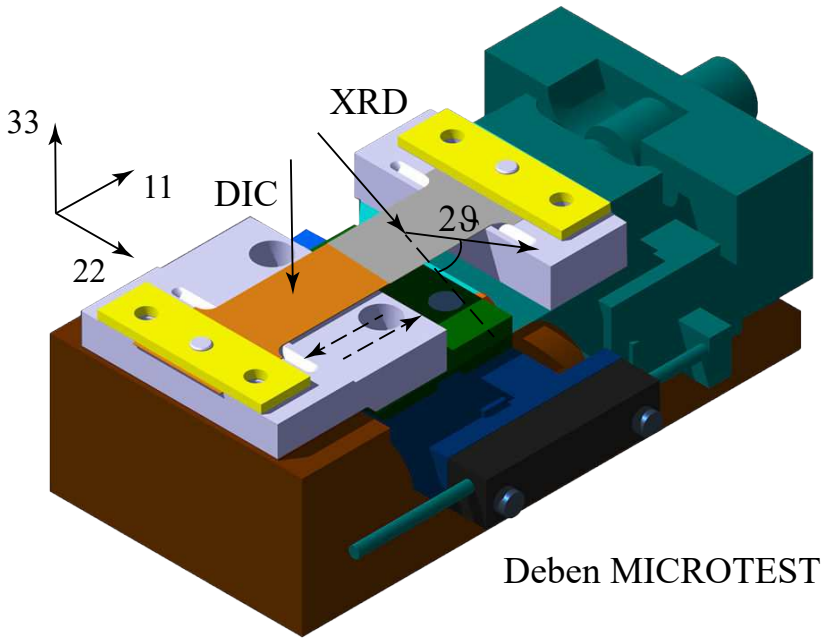

Figure 4.7: Horizontal grips with elongated specimen for XRD and DIC analysis. Thanks to the XYZ positioning stage inside the goniometer, this setup can undergo translation along "11" direction as indicated by the dashed arrows. At each step during the tensile testing, the elastic strain of thin films and the true strain of both thin films and the virgin substrate can be measured by XRD and DIC techniques, respectively. The Deben MICROTEST is darkened to highlight the design of new grips.

the specimen will be translated along "11" direction for a capture of the virgin substrate. With the combination of the techniques in Chapter 3 and Chapter 4, a very powerful method will be born to study the mechanical properties of thin films on substrates in both elastic and inelastic regime, such as the Young's modulus and the strain hardening behavior.

II Bauschinger and size effects in thin metal films on Kapton® substrates.

Based on the literature review, no other groups have experimentally investigated the Bauschinger effect of thin films on a Kapton® substrate. It is important to go further by means of our pre-stretching technique. A

similar experiment, as shown in Section 4.2, will be done[2] for 300 nm Ni and Cu films coated on the pre-tensile substrates' both sides. Moreover, a larger applied tensile strain will be applied in the second cycle to better study the strain hardening and the Bauschinger effect.

It is believed that the Bauschinger effect is strongly related to the microstresses induced by dislocations, so that the grain size/boundary, microstructural heterogeneity, film thickness, and interface should play a significant role. Therefore, thin Ni films with different thickness and grain size deposited on pre-tensile Kapton® substrates will be prepared. In order to improve the testing precision, a soft material with powders inside will be attached to the back side of Kapton®.

P.S. All the designed experiments above will be performed in the next few months, but it depends strongly on the availability and performance of the X-ray diffractometer.

2 Scheduled before my Ph.D. defense.

Appendices

A X-RAY ELASTIC CONSTANTS AND STRESS-STRAIN RELATIONSHIPS

This appendix details the elastic constants of polycrystalline thin metal films with single phase and the theoretical models for our X-ray stress analysis. (Nye 1985; Hauk 1997; Tanaka, Akiniwa, and Ito 1999; Faurie, Renault, Le Bourhis, and P. Goudeau 2006) are strongly recommended for the readers. It is well known that the anisotropy and orientations of constituting crystallites and the grain interactions can significantly affect the mechanical behavior of polycrystalline materials. In our study, W films are locally isotropic materials, therefore, macroscopically isotropic regardless of texture, while a sharp {111} fiber texture exists in all the other locally anisotropic thin metal films. Herein, Neerfeld-Hill elastic grain interaction model is selected as the best approximation to reality, which corresponds to the arithmetic averages of elastic constants calculated according to the models of Reuss and of Voigt. All the subsequent analysis is based on an ideal {111} fiber texture. In this case, thin films are transversely isotropic in the (S_1, S_2) plane, and S_3 the fiber axis (Fig. 2.15). Moreover, the system of principal stresses/strains P is set to coincide with the specimen coordinate system S.

REUSS MODEL

COMPLIANCE AND TRANSVERSE ISOTROPY In Reuss model, each crystallite is assumed to be subjected to the same stress and the same value as the polycrystalline thin film. Then the compliance of the film (system of principal stresses/strains P) is the average of all the crystallites (crystal system C) in the considered volume after the coordinate transformation:

$$\tilde{s}^{P}_{ij} = \begin{bmatrix} \tilde{s}^{P}_{11} & \tilde{s}^{P}_{12} & \tilde{s}^{P}_{13} & 0 & 0 & 0 \\ \tilde{s}^{P}_{12} & \tilde{s}^{P}_{11} & \tilde{s}^{P}_{13} & 0 & 0 & 0 \\ \tilde{s}^{P}_{13} & \tilde{s}^{P}_{13} & \tilde{s}^{P}_{33} & 0 & 0 & 0 \\ 0 & 0 & 0 & \tilde{s}^{P}_{44} & 0 & 0 \\ 0 & 0 & 0 & 0 & \tilde{s}^{P}_{44} & 0 \\ 0 & 0 & 0 & 0 & 0 & 2\left(\tilde{s}^{P}_{11} - \tilde{s}^{P}_{12}\right) \end{bmatrix} \tag{A.1}$$

where

$$\begin{cases} \tilde{s}^{P}_{11} = s_{11} - s_0/2 \\ \tilde{s}^{P}_{12} = s_{12} + s_0/6 \\ \tilde{s}^{P}_{13} = s_{12} + s_0/3 \\ \tilde{s}^{P}_{33} = s_{11} - 2s_0/3 \\ \tilde{s}^{P}_{44} = s_{44} + 4s_0/3 \end{cases} \tag{A.2}$$

Moreover, "$\sim$" denote average (all crystallites), s_{ij} is the single crystal compliance and s_0 is the anisotropy index defined by

$$s_0 = s_{11} - s_{12} - s_{44}/2 \tag{A.3}$$

In order to indicate the transverse isotropy, the Young's modulus in <hkl> directions is obtained:

$$\begin{aligned}\left(\tilde{s}_{11}^{p}\right)_{hkl} = &\left(\frac{h^2+k^2}{h^2+k^2+l^2}\right)^2 \tilde{s}_{11}^{p} + \left(\frac{l^2}{h^2+k^2+l^2}\right)^2 \tilde{s}_{33}^{p} \\ &+ \frac{\left(h^2+k^2\right)l^2}{\left(h^2+k^2+l^2\right)^2}\left(2\tilde{s}_{13}^{p} + \tilde{s}_{44}^{p}\right)\end{aligned} \tag{A.4}$$

where $E_{hkl} = 1/\left(\tilde{s}_{11}^{p}\right)_{hkl}$. Evidently, The Young's modulus is constant in the (S_1, S_2) plane ($l = 0$) but varies in the other directions. In this study, single crystal constants $S_{11} = 0.7674\ \mathrm{Mb}^{-1}$, $S_{12} = -0.2953\ \mathrm{Mb}^{-1}$ and $S_{44} = 0.8244\ \mathrm{Mb}^{-1}$ are selected for polycrystalline Ni films (Simmons and H. Wang 1971). Then the in-plane Young's modulus can be easily calculated as 226.2 GPa.

STRESS DETERMINATION FROM X-RAY STRAIN For a biaxial stress state, the average strain $\left(\bar{\varepsilon}_{33}^{L}\right)_{\varphi\psi}$ (laboratory system L) of all the crystallites diffracting in the considered volume is related to the macrostress σ_{ij} (system of principal stresses/strains P):

$$\begin{aligned}\left(\bar{\varepsilon}_{33}^{L}\right)_{\varphi\psi} = &(\sigma_{11}-\sigma_{22})\left[\frac{s_{11}-s_{12}+s_{44}}{6}\cos(2\varphi)\sin^2\psi\right. \\ &+ \left.\left(-s_{11}+s_{12}+\frac{s_{44}}{2}\right)\frac{\sin(3\beta+\varphi)\sin(2\psi)}{3\sqrt{2}}\right] \\ &+ (\sigma_{11}+\sigma_{22})\left[\frac{2s_{11}+4s_{12}-s_{44}}{6} + \frac{s_{44}}{4}\sin^2\psi\right]\end{aligned} \tag{A.5}$$

where "−" denote average (all crystallites with diffraction), β defines the rotation of crystallites around S_3.

VOIGT MODEL

In Voigt model, homogeneous strain of each crystallite which equals to the macrostrain is assumed. Then the compliance of film (system of principal stresses/strains P) is the average of all the crystallites (crystal system C) in the considered volume after the coordinate transformation:

$$\tilde{c}^{P}_{ij} = \begin{bmatrix} \tilde{c}^{P}_{11} & \tilde{c}^{P}_{12} & \tilde{c}^{P}_{13} & 0 & 0 & 0 \\ \tilde{c}^{P}_{12} & \tilde{c}^{P}_{11} & \tilde{c}^{P}_{13} & 0 & 0 & 0 \\ \tilde{c}^{P}_{13} & \tilde{c}^{P}_{13} & \tilde{c}^{P}_{33} & 0 & 0 & 0 \\ 0 & 0 & 0 & \tilde{c}^{P}_{44} & 0 & 0 \\ 0 & 0 & 0 & 0 & \tilde{c}^{P}_{44} & 0 \\ 0 & 0 & 0 & 0 & 0 & \left(\tilde{c}^{P}_{11} - \tilde{c}^{P}_{12}\right)/2 \end{bmatrix} \tag{A.6}$$

where

$$\begin{cases} \tilde{c}^{P}_{11} = c_{11} - c_0/2 \\ \tilde{c}^{P}_{12} = c_{12} + c_0/6 \\ \tilde{c}^{P}_{13} = c_{12} + c_0/3 \\ \tilde{c}^{P}_{33} = c_{11} - 2c_0/3 \\ \tilde{c}^{P}_{44} = c_{44} + c_0/3 \end{cases} \tag{A.7}$$

Moreover, c_{ij} is the single crystal stiffness and c_0 is the anisotropy index defined by

$$c_0 = c_{11} - c_{12} - 2c_{44} \tag{A.8}$$

The mechanical compliance of thin films can be obtained using the inverse of the mechanical stiffness:

$$\begin{cases} \left(\tilde{c}^{p}_{11}\right)^{-1} = \frac{1}{3}s_{11} + \frac{2}{3}s_{12} + \frac{11}{24}s_{44} - \frac{3s_{44}^2}{8(4s_0+3s_{44})} \\ \left(\tilde{c}^{p}_{12}\right)^{-1} = \frac{1}{3}s_{11} + \frac{2}{3}s_{12} - \frac{7}{24}s_{44} + \frac{3s_{44}^2}{8(4s_0+3s_{44})} \\ \left(\tilde{c}^{p}_{13}\right)^{-1} = s_{12} + \frac{1}{3}s_0 \\ \left(\tilde{c}^{p}_{33}\right)^{-1} = s_{11} - \frac{2}{3}s_0 \\ \left(\tilde{c}^{p}_{44}\right)^{-1} = \frac{6s_{44}(s_{11}-s_{12})}{2s_0+3s_{44}} \end{cases} \tag{A.9}$$

In order to indicate the transverse isotropy, the Young's modulus in <hkl> directions is obtained as:

$$\begin{aligned} \left(\tilde{c}^{p}_{11}\right)^{-1}_{hkl} = &\left(\frac{h^2+k^2}{h^2+k^2+l^2}\right)^2 (\tilde{c}^{p}_{11})^{-1} + \left(\frac{l^2}{h^2+k^2+l^2}\right)^2 (\tilde{c}^{p}_{33})^{-1} \\ &+ \frac{\left(h^2+k^2\right)l^2}{(h^2+k^2+l^2)^2}\left[2(\tilde{c}^{p}_{13})^{-1} + (\tilde{c}^{p}_{44})^{-1}\right] \end{aligned} \tag{A.10}$$

where $E_{hkl} = 1/\left(\tilde{c}^{p}_{11}\right)^{-1}_{hkl}$. Evidently, The Young's modulus is constant in the (S_1, S_2) plane ($l = 0$) but varies in the other directions. With the same single crystal constants, the in-plane Young's modulus of polycrystalline Ni films is 258.7 GPa.

STRESS DETERMINATION FROM X-RAY STRAIN For a biaxial stress state, the average strain $\left(\bar{\varepsilon}^{L}_{33}\right)_{\varphi\psi}$ (laboratory system L) of all the crystallites with diffraction in the considered volume is related to the macrostress σ_{ij} (system of principal stresses/strains P):

$$\begin{aligned} \left(\bar{\varepsilon}^{L}_{33}\right)_{\varphi\psi} = &(\sigma_{11}-\sigma_{22})[\frac{3(s_{11}-s_{12})s_{44}}{2(4s_{11}-4s_{12}+s_{44})}\cos(2\varphi)\sin^2\psi] \\ &+ (\sigma_{11}+\sigma_{22})[\frac{2s_{11}+4s_{12}-s_{44}}{6} + \frac{s_{44}}{4}\sin^2\psi] \end{aligned} \tag{A.11}$$

NEERFELD-HILL MODEL

Neerfeld and Hill suppose the elastic constants are the arithmetic averages of the ones calculated with Reuss model and Voigt model. This is known as Neerfeld-Hill model which has been well supported by empirical data. From the calculations above, the in-plane Young's modulus of a perfect {111} fiber-textured Ni film will be 242.4 GPa, and this ideal value is used for the numerical simulation in Section 3.2[1]. For the X-ray stress measurements in Chapter 4, the principal lattice strains are measured by $\sin^2\psi$ method, then the mechanical stiffness here is used for stress determination. After applying the average value of stiffness according to the models of Reuss and of Voigt, the stiffness matrix of the {111} fiber-textured polycrystalline Ni films is:

$$\tilde{c}_{ij}^{p} = \begin{bmatrix} 317.0 & 141.0 & 107.7 & 0 & 0 & 0 \\ 141.0 & 317.0 & 107.7 & 0 & 0 & 0 \\ 107.7 & 107.7 & 350.3 & 0 & 0 & 0 \\ 0 & 0 & 0 & 65.5 & 0 & 0 \\ 0 & 0 & 0 & 0 & 65.5 & 0 \\ 0 & 0 & 0 & 0 & 0 & 88.0 \end{bmatrix} \text{GPa} \qquad \text{(A.12)}$$

Similarly, for a polycrystalline Cu film, single crystal constants $S_{11} = 1.4995\ \text{Mb}^{-1}$, $S_{12} = -0.6282\ \text{Mb}^{-1}$ and $S_{44} = 1.3263\ \text{Mb}^{-1}$ are taken, and the elastic stiffness is:

1 A tiny difference between the values comes from the data precision or significant figures.

$$\tilde{c}_{ij}^{p} = \begin{bmatrix} 213.0 & 111.5 & 86.9 & 0 & 0 & 0 \\ 111.5 & 213.0 & 86.9 & 0 & 0 & 0 \\ 86.9 & 86.9 & 237.6 & 0 & 0 & 0 \\ 0 & 0 & 0 & 35.6 & 0 & 0 \\ 0 & 0 & 0 & 0 & 35.6 & 0 \\ 0 & 0 & 0 & 0 & 0 & 50.8 \end{bmatrix} \text{GPa} \tag{A.13}$$

It is worth mentioning that Eqs. (A.5) and (A.11) are not applied for stress determination, because the nonlinearity of the $\varepsilon - \sin^2\psi$ curve predicted by the Neerfeld-Hill model is not true in our case. However, they could be used for residual stress measurements (Section 2.5.3), and most significantly, the calculated elastic constants of polycrystalline thin films with a very strong {111} fiber texture are generally reliable and in good agreement with experimental data.

BIBLIOGRAPHY

BOOK REFERENCES

Crawford, G. *Flexible flat panel displays*. John Wiley & Sons, 2005 (cit. on p. 2).

Freund, L.B. and S. Suresh. *Thin film materials: stress, defect formation and surface evolution*. Cambridge University Press, 2004 (cit. on pp. 5, 11, 17).

Hauk, V. *Structural and residual stress analysis by nondestructive methods: Evaluation-Application-Assessment*. Elsevier, 1997 (cit. on pp. 8, 12, 58, 61, 125).

Kocks, U.F., C.N. Tomé, and H.-R. Wenk. *Texture and anisotropy: preferred orientations in polycrystals and their effect on materials properties*. Cambridge university press, 2000 (cit. on p. 8).

Noyan, I.C. and J.B. Cohen. *Residual stress: measurement by diffraction and interpretation*. Springer, 1987 (cit. on pp. 7, 12).

Nye, J.F. *Physical properties of crystals: their representation by tensors and matrices*. Oxford university press, 1985 (cit. on p. 125).

ARTICLE REFERENCES

Akogwu, O. et al. "Large strain deformation and cracking of nano-scale gold films on PDMS substrate". In: *Materials Science and Engineering: B* 170.1 (2010), pp. 32–40 (cit. on p. 18).

Arzt, E. et al. "Interface controlled plasticity in metals: dispersion hardening and thin film deformation". In: *Progress in Materials science* 46.3 (2001), pp. 283–307 (cit. on p. 17).

Baker, S.P., R.-M. Keller-Flaig, and J.B. Shu. "Bauschinger effect and anomalous thermomechanical deformation induced by oxygen in passivated thin Cu films on substrates". In: *Acta materialia* 51.10 (2003), pp. 3019–3036 (cit. on pp. 21, 99).

Balakrishnan, G. et al. "Effect of substrate temperature on microstructure and optical properties of nanocrystalline alumina thin films". In: *Ceramics International* 39.8 (2013), pp. 9017–9023 (cit. on p. 17).

Bamberg, E. et al. "A tensile test device for in situ atomic force microscope mechanical testing". In: *Precision engineering* 30.1 (2006), pp. 71–84 (cit. on p. 40).

Barranger, Y. et al. "Strain measurement by digital image correlation: influence of two types of speckle patterns made from rigid or deformable marks". In: *Strain* 48.5 (2012), pp. 357–365 (cit. on pp. 52, 54, 72).

Bauschinger, J. "Ueber die Veranderung der Elasticitatagrenze und dea Elasticitatamoduls verschiadener Metalle". In: *zivilingenieur* 27 (1881), pp. 289–348 (cit. on p. 19).

Belrhiti, Y. et al. "Application of optical methods to investigate the non-linear asymmetric behavior of ceramics exhibiting large strain to rupture by four-points bending test". In: *Journal of the European Ceramic Society* 32.16 (2012), pp. 4073–4081 (cit. on pp. 52, 53, 73).

Bemporad, E. et al. "A critical comparison between XRD and FIB residual stress measurement techniques in thin films". In: *Thin Solid Films* 572 (2014), pp. 224–231 (cit. on pp. 12, 13).

Besnard, G., F. Hild, and S. Roux. ""Finite-element" displacement fields analysis from digital images: application to Portevin–Le Châtelier bands". In: *Experimental Mechanics* 46.6 (2006), pp. 789–803 (cit. on pp. 19, 72).

Böhm, J. et al. "Tensile testing of ultrathin polycrystalline films: a synchrotron-based technique". In: *Review of Scientific Instruments* 75.4 (2004), pp. 1110–1119 (cit. on p. 17).

Bornert, M. et al. "Assessment of digital image correlation measurement errors: methodology and results". In: *Experimental mechanics* 49.3 (2009), pp. 353–370 (cit. on pp. 52, 57).

Brand, J. van den et al. "Flexible and stretchable electronics for wearable health devices". In: *Solid-State Electronics* 113 (2015), pp. 116–120 (cit. on pp. 2, 3).

Brugger, C. et al. "Strain gradient plasticity analysis of the strength and ductility of thin metallic films using an enriched interface model". In: *Acta materialia* 58.15 (2010), pp. 4940–4949 (cit. on p. 22).

Chapman, B.N. "Thin-film adhesion". In: *Journal of Vacuum Science & Technology* 11.1 (1974), pp. 106–113 (cit. on p. 14).

Chasiotis, I. "Mechanics of thin films and microdevices". In: *Device and Materials Reliability, IEEE Transactions on* 4.2 (2004), pp. 176–188 (cit. on p. 18).

Chen, J. and S.J. Bull. "Indentation fracture and toughness assessment for thin optical coatings on glass". In: *Journal of Physics D: Applied Physics* 40.18 (2007), p. 5401 (cit. on p. 14).

Chen, X. et al. "Tensile testing of thin films supported on compliant substrates". In: *Mechanics of Materials* 41.7 (2009), pp. 839–848 (cit. on p. 19).

Cho, S. et al. "Young's modulus, Poisson's ratio and failure properties of tetrahedral amorphous diamond-like carbon for MEMS devices". In: *Journal of Micromechanics and Microengineering* 15.4 (2005), p. 728 (cit. on p. 17).

Choi, Y.J. and Y.-K. Lee. "Elastic modulus of amorphous Ge2Sb2Te5 thin film measured by uniaxial microtensile test". In: *Electronic Materials Letters* 6.1 (2010), pp. 23–26 (cit. on p. 19).

Chou, T.-L., S.-Y. Yang, and K.-N. Chiang. "Overview and applicability of residual stress estimation of film–substrate structure". In: *Thin Solid Films* 519.22 (2011), pp. 7883–7894 (cit. on p. 11).

Clemens, B.M. and J.A. Bain. "Stress determination in textured thin films using X-ray diffraction". In: *MRS bulletin* 17.07 (1992), pp. 46–51 (cit. on p. 12).

Conroy, M. and J. Armstrong. "A comparison of surface metrology techniques". In: *Journal of Physics: Conference Series*. Vol. 13. 1. IOP Publishing. 2005, p. 458 (cit. on p. 82).

Cordill, M.J. et al. "Adhesion energies of Cr thin films on polyimide determined from buckling: Experiment and model". In: *Acta Materialia* 58.16 (2010), pp. 5520–5531 (cit. on p. 14).

Culity, B.D. "Elements of X-ray Diffraction". In: *2nd, Addition-Wesley, MA, London* (1978) (cit. on pp. 12, 58).

Davoudi, K.M., L. Nicola, and Joost J. Vlassak. "Bauschinger effect in thin metal films: Discrete dislocation dynamics study". In: *Journal of Applied Physics* 115.1 (2014), p. 013507 (cit. on pp. 21, 23).

Denis, Y.W. and F. Spaepen. "The yield strength of thin copper films on Kapton". In: *Journal of Applied Physics* 95.6 (2004), pp. 2991–2997 (cit. on p. 19).

Djaziri, S. et al. "Comparative study of the mechanical properties of nanostructured thin films on stretchable substrates". In: *Journal of Applied Physics* 116.9 (2014), p. 093504 (cit. on pp. 14, 66, 68, 80).

Dupré, J.C. et al. "Displacement Discontinuity or Complex Shape of Sample: Assessment of Accuracy and Adaptation of Local DIC Approach". In: *Strain* 51.5 (2015), pp. 391–404 (cit. on pp. 52, 54).

Eiper, E. et al. "Size-independent stresses in Al thin films thermally strained down to- 100 C". In: *Acta materialia* 55.6 (2007), pp. 1941–1946 (cit. on p. 17).

Faurie, D., O. Castelnau, et al. "In situ diffraction strain analysis of elastically deformed polycrystalline thin films, and micromechanical interpretation". In: *Journal of Applied Crystallography* 42.6 (2009), pp. 1073–1084 (cit. on p. 12).

Faurie, D., P. Djemia, et al. "Elastic anisotropy of polycrystalline Au films: Modeling and respective contributions of X-ray diffraction, nanoindentation and Brillouin light scattering". In: *Acta Materialia* 58.15 (2010), pp. 4998–5008 (cit. on p. 17).

Faurie, D., P.-O. Renault, E. Le Bourhis, T. Chauveau, et al. "X-ray strain analysis of 111 fiber-textured thin films independent of grain-interaction models". In: *Journal of Applied Crystallography* 44.2 (2011), pp. 409–413 (cit. on pp. 8, 9).

Faurie, D., P.-O. Renault, E. Le Bourhis, M. Drouet, et al. "X-ray elastic strain analysis of compressed Au thin film on polymer substrate". In: *Surface and Coatings Technology* 215 (2013), pp. 322–326 (cit. on p. 100).

Faurie, D., P.-O. Renault, E. Le Bourhis, and P. Goudeau. "Study of texture effect on elastic properties of Au thin films by X-ray diffraction and in situ tensile testing". In: *Acta Materialia* 54.17 (2006), pp. 4503–4513 (cit. on pp. 17, 89, 125).

Faurie, D., P.-O. Renault, E. Le Bourhis, and Ph. Goudeau. "Determination of elastic constants of a fiber-textured gold film by combining synchrotron x-ray diffraction and in situ tensile testing". In: *Journal of applied physics* 98.9 (2005), p. 093511 (cit. on pp. 17, 66, 69).

Fewster, P.F. "X-ray analysis of thin films and multilayers". In: *Reports on Progress in Physics* 59.11 (1996), p. 1339 (cit. on p. 1).

Forrest, S.R. "The path to ubiquitous and low-cost organic electronic appliances on plastic". In: *Nature* 428.6986 (2004), pp. 911–918 (cit. on pp. 3, 4).

Geandier, G. et al. "Elastic-strain distribution in metallic film-polymer substrate composites". In: *Applied Physics Letters* 96.4 (2010), p. 041905 (cit. on pp. 14, 66).

Gerberich, W.W. and M.J. Cordill. "Physics of adhesion". In: *Reports on Progress in Physics* 69.7 (2006), p. 2157 (cit. on p. 14).

Gianola, D.S. and C. Eberl. "Micro-and nanoscale tensile testing of materials". In: *JOM* 61.3 (2009), pp. 24–35 (cit. on p. 19).

Girault, B., D. Eyidi, T. Chauveau, et al. "Copper coverage effect on tungsten crystallites texture development in W/Cu nanocomposite thin films". In: *Journal of Applied Physics* 109.1 (2011), p. 014305 (cit. on p. 89).

Girault, B., D. Eyidi, Ph. Goudeau, et al. "Controlled nanostructuration of polycrystalline tungsten thin films". In: *Journal of Applied Physics* 113.17 (2013), p. 174310 (cit. on p. 49).

Guruprasad, P.J., W.J. Carter, and A.A. Benzerga. "A discrete dislocation analysis of the Bauschinger effect in microcrystals". In: *Acta Materialia* 56.19 (2008), pp. 5477–5491 (cit. on p. 23).

Helm, J.D. and J.R. Deanner. "Off-axis two-dimensional digital image correlation". In: *Proceedings of 2004 SEM X international congress & exposition on experimental and applied mechanics, Costa Mesa*. 2004, pp. 06–01 (cit. on p. 57).

Hild, F. and S. Roux. "Digital image correlation: from displacement measurement to identification of elastic properties–a review". In: *Strain* 42.2 (2006), pp. 69–80 (cit. on pp. 19, 52, 55, 72).

Hommel, M. and O. Kraft. "Deformation behavior of thin copper films on deformable substrates". In: *Acta Materialia* 49.19 (2001), pp. 3935–3947. ISSN: 1359-6454 (cit. on pp. 99, 110).

Hommel, M., O. Kraft, and E. Arzt. "A new method to study cyclic deformation of thin films in tension and compression". In: *Journal of materials research* 14.06 (1999), pp. 2373–2376 (cit. on pp. 14, 98, 108, 110).

Huang, H.B. and F. Spaepen. "Tensile testing of free-standing Cu, Ag and Al thin films and Ag/Cu multilayers". In: *Acta Materialia* 48.12 (2000), pp. 3261–3269 (cit. on p. 66).

Janssen, G.C.A.M. et al. "Celebrating the 100th anniversary of the Stoney equation for film stress: Developments from polycrystalline steel strips to single crystal silicon wafers". In: *Thin Solid Films* 517.6 (2009), pp. 1858–1867 (cit. on p. 11).

Jordan-Sweet, J.L. et al. "Characterization of strain in thin-film structures with microdiffraction". In: *Adv. X-Ray Anal* 42 (2000) (cit. on p. 16).

Kelly, P.J. and R.D. Arnell. "Magnetron sputtering: a review of recent developments and applications". In: *Vacuum* 56.3 (2000), pp. 159–172 (cit. on p. 5).

Khang, D.-Y. et al. "A stretchable form of single-crystal silicon for high-performance electronics on rubber substrates". In: *Science* 311.5758 (2006), pp. 208–212 (cit. on p. 100).

Kim, C. et al. "Warpage Analysis of Electroplated Cu Films on Fiber-Reinforced Polymer Packaging Substrates". In: *Polymers* 7.6 (2015), pp. 985–1004 (cit. on p. 12).

Kim, D.-H et al. "Materials and noncoplanar mesh designs for integrated circuits with linear elastic responses to extreme mechanical deformations". In: *Proceedings of the National Academy of Sciences* 105.48 (2008), pp. 18675–18680 (cit. on p. 4).

Kim, D.-H. et al. "Stretchable, curvilinear electronics based on inorganic materials". In: *Advanced Materials* 22.19 (2010), pp. 2108–2124 (cit. on p. 2).

Kirsch, B.L. et al. "Probing the effects of nanoscale architecture on the mechanical properties of hexagonal silica/polymer composite thin films". In: *Advanced Functional Materials* 15.8 (2005), pp. 1319–1327 (cit. on p. 14).

Korsunsky, A.M., M. Sebastiani, and E. Bemporad. "Focused ion beam ring drilling for residual stress evaluation". In: *Materials Letters* 63.22 (2009), pp. 1961–1963 (cit. on p. 12).

Kraft, O. and C.A. Volkert. "Mechanical testing of thin films and small structures". In: *Advanced Engineering Materials* 3.3 (2001), pp. 99–110 (cit. on p. 18).

Krottenthaler, M. et al. "A simple method for residual stress measurements in thin films by means of focused ion beam milling and digital image correlation". In: *Surface and Coatings Technology* 215 (2013), pp. 247–252 (cit. on p. 12).

Le Bourhis, E. et al. "Structural and mechanical studies of Fe-Cr thin films deposited by ion-beam sputtering". In: *The European Physical Journal Applied Physics* 30.01 (2005), pp. 33–39 (cit. on p. 88).

Leterrier, Y. "Durability of nanosized oxygen-barrier coatings on polymers". In: *Progress in Materials Science* 48.1 (2003), pp. 1–55 (cit. on p. 14).

Li, T. and Z.G. Suo. "Ductility of thin metal films on polymer substrates modulated by interfacial adhesion". In: *International Journal of Solids and Structures* 44.6 (2007), pp. 1696–1705 (cit. on p. 14).

Liu, Z.-L. et al. "Bauschinger and size effects in thin-film plasticity due to defect-energy of geometrical necessary dislocations". In: *Acta Mechanica Sinica* 27.2 (2011), pp. 266–276 (cit. on p. 23).

Lu, N.S., Z.G. Suo, and Joost J. Vlassak. "The effect of film thickness on the failure strain of polymer-supported metal films". In: *Acta Materialia* 58.5 (2010), pp. 1679–1687 (cit. on pp. 17, 18).

Lu, N.S., X. Wang, et al. "Metal films on polymer substrates stretched beyond 50%". In: *Applied Physics Letters* 91.22 (2007), p. 221909 (cit. on p. 4).

M., Maryam et al. "Evaluation of structure and mechanical properties of Ni-rich NiTi/Kapton composite film". In: *Materials Science and Engineering: A* 668 (2016), pp. 13–19 (cit. on p. 14).

Macionczyk, F. et al. "Young's modulus and tensile strength of CuNi (Mn) thin films on polyimide foils by tensile testing". In: *Journal of materials research* 13.10 (1998), pp. 2852–2858 (cit. on p. 19).

Maeder, G. "X-Ray Diffraction and Stress Measurement". In: *Chemica Scripta* 26A (1986), pp. 23–31 (cit. on p. 59).

Martinschitz, K.J. et al. "Elastic constants of fibre-textured thin films determined by X-ray diffraction". In: *Journal of applied crystallography* 42.3 (2009), pp. 416–428 (cit. on p. 12).

Marx, V.M., C. Kirchlechner, et al. "Adhesion measurement of a buried Cr interlayer on polyimide". In: *Philosophical Magazine* 95.16-18 (2015), pp. 1982–1991 (cit. on p. 88).

Marx, V.M., F. Toth, et al. "The influence of a brittle Cr interlayer on the deformation behavior of thin Cu films on flexible substrates: Experiment and model". In: *Acta materialia* 89 (2015), pp. 278–289 (cit. on p. 14).

Misra, A., J.P. Hirth, and R.G. Hoagland. "Length-scale-dependent deformation mechanisms in incoherent metallic multilayered composites". In: *Acta materialia* 53.18 (2005), pp. 4817–4824 (cit. on p. 17).

Mittal, K.L. "Adhesion measurement of thin films". In: *Active and Passive Electronic Components* 3.1 (1976), pp. 21–42 (cit. on p. 14).

Mompiou, F., M. Legros, A. Boé, et al. "Inter-and intragranular plasticity mechanisms in ultrafine-grained Al thin films: an in situ TEM study". In: *Acta Materialia* 61.1 (2013), pp. 205–216 (cit. on p. 18).

Mompiou, F., M. Legros, T. Radetic, et al. "In situ TEM observation of grain annihilation in tricrystalline aluminum films". In: *Acta Materialia* 60.5 (2012), pp. 2209–2218 (cit. on p. 18).

Monshi, A., M.R. Foroughi, and M.R. Monshi. "Modified Scherrer equation to estimate more accurately nano-crystallite size using XRD". In: *World Journal of Nano Science and Engineering* 2.03 (2012), p. 154 (cit. on p. 105).

Noyan, I.C., T.C. Huang, and B.R. York. "Residual stress/strain analysis in thin films by X-ray diffraction". In: *Critical Reviews in Solid State and Material Sciences* 20.2 (1995), pp. 125–177 (cit. on pp. 11, 60, 66, 108).

Oliver, W.C. and G.M. Pharr. "Measurement of hardness and elastic modulus by instrumented indentation: Advances in understanding and refinements to methodology". In: *Journal of materials research* 19.01 (2004), pp. 3–20 (cit. on p. 17).

Rajagopalan, J., J.H. Han, and M.T.A. Saif. "Bauschinger effect in unpassivated freestanding nanoscale metal films". In: *Scripta Materialia* 59.7 (2008), pp. 734–737 (cit. on pp. 23, 98).

Rajagopalan, J., C. Rentenberger, et al. "In situ TEM study of microplasticity and Bauschinger effect in nanocrystalline metals". In: *Acta Materialia* 58.14 (2010), pp. 4772–4782 (cit. on pp. 23, 98).

Renault, P.-O. et al. "Deposition of ultra-thin gold film on in situ loaded polymeric substrate for compression tests". In: *Materials Letters* 73 (2012), pp. 99–102 (cit. on pp. 41, 100).

Rogers, J.A., T. Someya, and Y.G. Huang. "Materials and mechanics for stretchable electronics". In: *Science* 327.5973 (2010), pp. 1603–1607 (cit. on pp. 2, 3).

Roland, T. et al. "Digital image correlation of metal nanofilms on SU-8 for flexible electronics and MEMS". In: *Journal of Micromechanics and Microengineering* 21.12 (2011), p. 125005 (cit. on p. 80).

Schadler, L.S. and I. Cevdet Noyan. "Experimental Determination of the Strain Transfer Across a Flexible Intermediate Layer in Thin Film Structures as a Function of Flexible Layer Thickness". In: *MRS Proceedings*. Vol. 239. Cambridge Univ Press. 1991, p. 151 (cit. on p. 15).

Schadler, L.S. and I.C. Noyan. "Experimental determination of the strain transfer across a flexible intermediate layer in thin-film structures". In: *Journal of Materials Science Letters* 11.15 (1992), pp. 1067–1069. ISSN: 1573-4811 (cit. on p. 15).

Schmidt, T.K. et al. "Influence of tantalum and silver interlayers on thermal stress evolution in copper thin films on silicon substrates". In: *Scripta materialia* 50.6 (2004), pp. 733–737 (cit. on p. 17).

Sebastiani, M. et al. "Depth-resolved residual stress analysis of thin coatings by a new FIB–DIC method". In: *Materials Science and Engineering: A* 528.27 (2011), pp. 7901–7908 (cit. on p. 12).

Shishvan, S.S., L. Nicola, and E. Van der Giessen. "Bauschinger effect in unpassivated freestanding thin films". In: *Journal of Applied Physics* 107.9 (2010), p. 093529 (cit. on p. 23).

Sim, G.-D. et al. "Effects of stretching and cycling on the fatigue behavior of polymer-supported Ag thin films". In: *Materials Science and Engineering: A* 575 (2013), pp. 86–93 (cit. on p. 99).

Simmons, G. and H. Wang. *Single crystal elastic constants and calculated aggregate properties: a handbook*. Tech. rep. The M.I.T.press, 1971 (cit. on pp. 8, 127).

Song, J. et al. "Buckling of a stiff thin film on a compliant substrate in large deformation". In: *International Journal of Solids and Structures* 45.10 (2008), pp. 3107–3121 (cit. on p. 100).

Stoney, G.G. "The tension of metallic films deposited by electrolysis". In: *Proceedings of the Royal Society of London. Series A, Containing Papers of a Mathematical and Physical Character* 82.553 (1909), pp. 172–175 (cit. on p. 11).

Sun, Y.G. et al. "Controlled buckling of semiconductor nanoribbons for stretchable electronics". In: *Nature nanotechnology* 1.3 (2006), pp. 201–207 (cit. on p. 100).

Suo, Z.G., Joost J. Vlassak, and S. Wagner. "Micromechanics of macroelectronics". In: *China Particuology* 3.06 (2005), pp. 321–328 (cit. on p. 4).

Tanaka, K., Y. Akiniwa, and K. Ito T.and Inoue. "Elastic Constants and X-Ray Stress Measurement of Cubic Thin Films with Fiber Texture." In: *JSME Inter-*

national Journal Series A Solid Mechanics and Material Engineering 42.2 (1999), pp. 224–234 (cit. on p. 125).
Villain, P. et al. "Atomistic calculation of size effects on elastic coefficients in nanometre-sized tungsten layers and wires". In: *Scripta materialia* 50.9 (2004), pp. 1247–1251 (cit. on p. 17).
Vlassak, Joost J. and W.D. Nix. "A new bulge test technique for the determination of Young's modulus and Poisson's ratio of thin films". In: *Journal of Materials Research* 7.12 (1992), pp. 3242–3249 (cit. on p. 18).
Wang, D. et al. "Influences of Ta passivation layers on the fatigue behavior of thin Cu films". In: *Materials Science and Engineering: A* 610 (2014), pp. 33–38 (cit. on p. 18).
Welzel, U. et al. "Stress analysis of polycrystalline thin films and surface regions by X-ray diffraction". In: *Journal of Applied Crystallography* 38.1 (2005), pp. 1–29 (cit. on pp. 6, 7).
Wojciechowski, P.H. and M.S. Mendolia. "Fracture and cracking phenomena in thin films adhering to high-elongation substrates". In: *Physics of thin films* 16 (1991), pp. 271–340 (cit. on pp. 15, 80).
Xiang, Y., X. Chen, and Joost J. Vlassak. "Plane-strain bulge test for thin films". In: *Journal of materials research* 20.09 (2005), pp. 2360–2370 (cit. on p. 18).
Xiang, Y., T. Li, et al. "High ductility of a metal film adherent on a polymer substrate". In: *Applied Physics Letters* 87.16 (2005), p. 161910 (cit. on p. 14).
Xiang, Y. and J.J. Vlassak. "Bauschinger effect in thin metal films". In: *Scripta Materialia* 53.2 (2005), pp. 177–182. ISSN: 1359-6462 (cit. on pp. 22, 23, 99, 110).
Xiang, Y. and Joost J. Vlassak. "Bauschinger and size effects in thin-film plasticity". In: *Acta Materialia* 54.20 (2006), pp. 5449–5460. ISSN: 1359-6454 (cit. on pp. 22, 23, 99, 110).
Xu, S. et al. "Assembly of micro/nanomaterials into complex, three-dimensional architectures by compressive buckling". In: *Science* 347.6218 (2015), pp. 154–159 (cit. on p. 100).
Yanaka, M. et al. "Cracking phenomena of brittle films in nanostructure composites analysed by a modified shear lag model with residual strain". In: *Journal of Materials Science* 33.8 (1998), pp. 2111–2119 (cit. on p. 15).
Yang, Y. et al. "Deformation and fracture in micro-tensile tests of freestanding electrodeposited nickel thin films". In: *Scripta Materialia* 58.12 (2008), pp. 1062–1065 (cit. on p. 66).
Yin, H.M. and P.A. Prieto-Muñoz. "Stress transfer through fully bonded interface of layered materials". In: *Mechanics of Materials* 62 (2013), pp. 69–79 (cit. on pp. 15, 66).

Zhang, G.P. et al. “Fatigue and thermal fatigue damage analysis of thin metal films”. In: *Microelectronics Reliability* 47.12 (2007) (cit. on p. 18).

Zhou, C.Z. and R. LeSar. “Dislocation dynamics simulations of the Bauschinger effect in metallic thin films”. In: *Computational Materials Science* 54 (2012), pp. 350–355 (cit. on p. 22).

Résumé

Ce travail est dédié aux propriétés d'élasticités et au comportement cyclique de films minces sur substrats souples. En utilisant deux revêtements déposés symétriquement et sur la moitié de substrats polyimides, un système dual de corrélation d'images numériques (CIN) a été développé pour mesurer les déformations macroscopiques du composite film-substrat et du substrat non revêtu simultanément pendant un essai de traction. La différence des déformations observée permet d'extraire les propriétés d'élasticité du film dont les résultats sont en accord avec ceux issus d »une analyse numérique. De plus, un transfert total de la déformation du substrat vers le film est observé indiquant une adhésion parfaite à l'interface. Grâce à notre nouvelle technique de pré tension, les films minces sont déposés sur des substrats pré tendus et peuvent ainsi être déformés alternativement en tension et en compression respectivement par rapport à l'état non chargé. Les déformations élastiques et macroscopiques des films minces polycristallins sont mesurées par diffraction des rayons X (DRX) et CIN respectivement. A partir des courbes de déformation cristalline/déformation macroscopique, la réponse mécanique du film de nickel est analysée aux vus de l'histoire complète de chargement et de la présence de contraintes résiduelles et d'une texture cristallographique. L'effet Bauschniger est observé dans le film alors qu'il ne présente que très peu ou pas du tout de durcissement après déformation plastique.

Mots-clés: Films minces polycristallins; Système CIN dual; Propriétés d'élasticité; Essais cycliques; Effet Bauschinger; nanocristallites

Abstract

This work is devoted to the elastic properties and cyclic behavior of thin films on soft substrates. With two coating layers bonded symmetrically to half polyimide substrates, a dual digital image correlation (DIC) system has been developed to measure the macroscopic strains of the film-substrate composite and the uncoated substrate simultaneously during a tensile testing. The strain difference allows extracting the elastic properties of thin films, and it agrees well with our numerical analysis. Moreover, we observe that the strain is transferred fully from a substrate to a film indicating a perfect interfacial adhesion. Thanks to our new pre-stretching technique, the thin films are deposited on pre-tensile substrates and thus can be deformed alternately in tension and compression relative to the unloaded state. The elastic and true strains of polycrystalline thin films are measured by X-ray diffraction (XRD) and DIC respectively. From the lattice stress/strain-true strain curves, the mechanical response of the Ni film is analyzed in view of the complete loading history and the presence of residual stresses and crystallographic texture. The Bauschinger effect is observed in the film, while it shows little or no work hardening during the plastic deformation.

Keywords: Polycrystalline thin films; Dual DIC system; Elastic properties; Cyclic testing; Bauschinger effect; Nanocrystallites